NAT'L INST. OF STAND & TECH R.I.C.
A11104 232798

NATIONAL INSTITUTE OF STANDARDS &
TECHNOLOGY
Research Information Center
Gaithersburg, MD 20899

NISTIR 88-3898

NBS' Industry - Government Consortium Research Program on Flowmeter Installation Effects:

Summary Report with Emphasis on Research Period July - December 1987

G. E. Mattingly and T. T. Yeh

U.S. DEPARTMENT OF COMMERCE
National Institute of Standards and Technology
(Formerly National Bureau of Standards)
National Engineering Laboratory
Center for Chemical Engineering
Fluid Flow Group
Chemical Process Metrology Division
Gaithersburg, MD 20899

May 1988

Issued November 1988

NISTIR 88-3898

NBS' Industry - Government Consortium Research Program on Flowmeter Installation Effects:

Summary Report with Emphasis on Research Period July - December 1987

G. E. Mattingly and T. T. Yeh

U.S. DEPARTMENT OF COMMERCE
National Institute of Standards and Technology
(Formerly National Bureau of Standards)
National Engineering Laboratory
Center for Chemical Engineering
Fluid Flow Group
Chemical Process Metrology Division
Gaithersburg, MD 20899

May 1988

Issued November 1988



National Bureau of Standards became the National Institute of Standards and Technology on August 23, 1988, when the Omnibus Trade and Competitiveness Act was signed. NIST retains all NBS functions. Its new programs will encourage improved use of technology by U.S. industry.

U.S. DEPARTMENT OF COMMERCE
C. William Verity, Secretary

NATIONAL INSTITUTE OF STANDARDS
AND TECHNOLOGY
Ernest Ambler, Director

PREFACE

The research results reported in this document were produced at the support of an NBS initiated industry-government consortium. In this mode of operation, there is a high degree of interaction between the representatives of the consortium member companies and the NBS researchers. These interactions include: (1) the planning of the specific focus of the NBS research efforts, (2) the analyses of the results obtained, and (3) the conclusions drawn for the particular phase of the work. For this reason, it is pertinent to acknowledge both the support given to this phase of the research program and the technical contributions made by the representatives of the consortium members.

The current consortium members are alphabetically:

1. Ametek-McCrometer
2. Chevron Oil
3. Daniel Industries
4. Department of Energy
5. Dow Chemical Co.
6. E.I. Dupont de Nemours
7. Fischer & Porter
8. Ford Motor Co.
9. Gas Research Institute*
10. Gas Unie (The Netherlands)
11. Instrument Testing Service
12. ITT Barton
13. Kimmon Mfg. Ltd. (Japan)
14. NBS-B
15. Rockwell International
16. Rosemount

*Specific acknowledgment is due to Dr. Kiran Kothari of GRI. Both his support for this program and his technical inputs in the analyses of results and in the conclusions drawn are gratefully acknowledged.

TABLE OF CONTENTS

	Page
PREFACE	ii
ABSTRACT	1
INTRODUCTION	1
EXPERIMENTAL RESULTS	2
CONCLUSIONS	9
REFERENCES	10
TABLE	11
FIGURES	12

NBS' Industry - Government Consortium Research Program on Flowmeter Installation Effects: Summary Report with Emphasis on Six Month Period July - December, 1987.

G.E. Mattingly
T.T. Yeh

Fluid Flow Group
Chemical Process Metrology Division
Center for Chemical Engineering
National Bureau of Standards
Gaithersburg, Maryland 20899

ABSTRACT

This report presents results produced in a consortium-sponsored research program on Flowmeter Installation Effects. This project is a collaborative one that has been underway for three years; it is supported by an industry-government consortium that meets twice yearly to review and discuss results and to plan subsequent phases of the work. This report contains the results and conclusions of the recent meeting of this consortium at NBS-G on Feb. 17, 1988. At this meeting it was voted that results should be disseminated not in meeting minutes format but rather in self-standing reports. Hence, we adopt this format.

The objective of this research program is to produce improved flowmeter performance when meters are installed in "non-ideal" conditions. This objective is being attained via a strategy to (A) measure, understand, and quantify the "non-ideal" pipe flows from such pipeline elements as elbows, reducers, valves, or combinations of these, (B) for selected types of flowmeters, correlate meter factor "shifts" relative to the features of these "non-ideal" pipe flows so as to be able to accurately predict meter performance in "non-ideal" installations, and (C) disseminate the resulting technology through appropriate channels such as publishing our results in pertinent journals and upgrading "paper" standards for flow measurement.

Specific results included in this report include:

1. the distributions of the mean and the turbulence velocities in the axial and vertical directions in both the (closely coupled) elbows-out-of-plane piping configuration and the "spaced" version of this arrangement,
2. the pressure loss measurements for both of the elbow-out-of plane configurations, and
3. the velocity distributions produced by the single elbow piping configuration.

INTRODUCTION

The increasing scarcity of fluid resources and the rising value of fluid products is placing new emphasis on improved fluid measurements. Improvement is sought from many starting points. Meters are being retrofitted into fluid systems that were not designed for them. This invariably means the flowmeters

are being installed in "non-ideal" conditions. Increased accuracy levels are desired for installed metering systems - either by upgrading the flow conditions that enter the meter or by replacing the device itself and/or its auxiliary components.

The industry-government consortium (members are listed in Appendix 1) research program currently underway at NBS is designed to help improve fluid metering performance in these situations. The design of the program is to produce a basic understanding of the flow phenomena that are produced in "non-ideal" pipe flows and to quantify these phenomena. When these phenomena and their quantified characteristics are correlated with the performance of specific types of meters, it becomes feasible to predict and achieve - satisfactory measurements in "non-ideal" meter installations.

Pipe flows from selected piping configurations are measured using laser Doppler velocimetry (LDV). Selections of piping configuration are done by consortium members; one or two such configurations can be done in one year.

The LDV techniques that have been and are being applied to determine pipe flows can also be used to measure the effects of other pipeline elements-valves, flow conditioning elements (for fluid velocity or pulsations, etc.), mixing devices, generic flowmeter geometries - or combinations of these. The resulting understanding provides the bases for improving the effectiveness of these devices and, in turn, for increasing the productivity of the continuous processes which depend upon them. [1-4]*

EXPERIMENTAL RESULTS:

In what follows, results are presented for a range of pipeline configurations that have been investigated in this NBS industry government consortium project: the elbows-out-of-plane configuration where the elbows are welded together [1,2], the elbows-out-of-plane with a short (2.42) length of straight pipe separating the elbows, and the single elbow.

1. Mean Velocity and Turbulence Measurements. The right hand coordinate system used in what follows has an origin at the pipe centerline in the exit flange plane of the elbows-out-of-plane configuration. The positive Z direction is downstream; the positive Y direction is upward; the X direction is therefore to the right looking upstream. The mean velocities in the X, Y, and Z directions are U, V, and W, respectively; the corresponding turbulence velocities, are u',v', and w'. All quantities are nondimensionalized using the bulk pipe flow velocity to normalize all velocities and using the pipe inside diameter to normalize lengths. For the elbows-out-of-plane configurations, the distributions of the mean components of the streamwise i.e., W (Z direction) and the vertical i.e., V (Y direction) components of the fluid velocities along the horizontal diameter are plotted in Figure 1 (a) and (b). These piping configurations are referred to as the "welded" and "spaced"

* Square bracketed integers refer to references given below.

elbows-out-of-plane configurations. The legend "L + X - Y" in the figure for the "welded" configuration: "L" refers to standard long-radius sweep elbows, "+ X - Y" means that the entrance directions of the first and the second elbows are in "+X" and "-Y" directions, respectively. In addition, weld-neck flanges are welded onto both ends of each elbow configuration, and the flow exiting from the elbow configuration is always in +Z direction. This means that the pipe flow which enters the configuration has a long length in the "+X" direction and the first elbow turns the pipe flow into the "-Y" direction. The second elbow then turns this pipe flow into the "+Z" direction. The "spaced" configuration is denoted by "2.42Y" as this is the length of the spacer separating the elbows. These graphs show the large deviations of the W profiles from the power law distributions that pertain to an "ideal" meter installation - i.e., very long lengths of straight, constant diameter piping preceeding the meter position. The significant features of our measured profiles are the "slow core" flows found near the centerline and the "high speed" regions nearer the pipe wall. Also significant is the asymmetry noted for the most upstream station for the "welded" elbows and the fact that the "spacer" alters the qualitative nature of the most upstream profile.

Figures 2 (a) and (b) show the distributions measured for the V component of the velocity that correspond to the results in figures 1 (a) and (b). Again it is noted that the "spacer" produces qualitatively different profiles at the most upstream station.

In figures 3 (a) and (b) are plotted the root-mean-square (r.m.s.) distributions of the axial, turbulence components. Comparisons of these results show that the spaced elbows values are reduced in level compared to those of the welded configuration. This reduction is also noted to apply to the r.m.s. profiles of the vertical, turbulent velocities shown in figures 4 (a) and (b).

The mean components of streamwise, W, and vertical, V velocity distributions are used to define the skew angle as the arctan (V/W). Figure 5 shows the skew angle distribution for the "welded" elbows configuration. Figure 6 shows corresponding values for the "spaced" elbows configuration. It is noted again that the levels for the "spaced" elbows configuration are reduced in comparison with the values for the "welded" configuration.

2. Swirl Decay. When a Swirl number is defined as

$$S1 = 4 \int_{-.5}^{+.5} WVX|X|dX$$

and the axial distributions are calculated for the respective piping configurations, the results can be shown as in figures 7 and 8. When exponential decay formulas are fitted to these results the decay rates obtained can be compared to the corresponding values determined by other investigators. Table 1 contains such a comparison. [3-7] It is noted from table 1 that the exponential decay rate is, according to these

values, a decreasing function of pipe diameter Reynolds number. Figure 9 presents these exponential decay rates versus diametral Reynolds number.

3. Pressure Measurements. Figure 10 presents a sketch of the piping configurations and the locations of the pressure taps used to measure the static pressure in these pipe flows. Dimensions are given in pipe diameters; the cross-sectional sketch shows the azimuthal locations of the four (4) taps positioned (looking upstream) at each streamwise station. Figures 11 and 12 present differential static pressure distributions (in numbers of velocity heads "Nvh") for the four (4) angular locations both upstream (A) and downstream (B) of the respective elbow-out-of-plane configuration. The reference pressure chosen for the differences is that of tap No. 4, see figure 10. These figures contain results for several diametral Reynolds numbers as noted in the legends.

Figure 13, shows the differential static pressure distributions both azimuthally and at four stream stations (lettered as A, B, C, and D shown in the legend) for both piping configurations. Pressure levels are shown relative to the minimum pressure measured - i.e., the lowest value measured at the station furthest downstream - in "Nvh". Results shown are those for $Re = 6 \times 10^4$. Comparison of pressure at the same stream stations indicates that the differentials, P - Pmin are larger for the welded elbows compared to the spaced elbows. A small, but noticeable (~0.15 Nvh) azimuthal pressure variations appear at each station. Due to the helical motion of the flow in the pipe, these pressure variations vary from station to station. Therefore, in some conditions, careful selection on the pressure tap positions should be taken.

4. Friction Factor Results. Figures 14-17 present the results for the pressure measurements plotted in the format of friction factor:

$$f = \Delta p/(1/2\rho W_b{}^2 L) = Nvh/L$$

In each of these figures, the letters A,B,C, and D denote streamwise stations along the pipe. As shown in the sketch, A precedes the double elbow configuration; B is the station at the configuration outlet; C and D are stations downstream. In figures 14 and 15 are shown, via the integers 1-4, the azimuthal pressure tap locations at each of the lettered stations, looking upstream.

Figure 14 shows results for the welded elbows configuration. Over the flow rate range

$$10^4 < Re < 10^5$$

it is noted that the friction factor is monotonically decreasing. Pressure differences measured for the No. 4 taps are the largest of the four between stations A and B which are separated by a distance of 7.13 along the pipe centerline. At station B, taps No. 1-3 indicate approximately the same pressure. It is concluded that this azimuthal distribution of pressure difference between stations A and B is due to the asymmetric swirl (helical motion) produced by this elbow

configuration. Figure 14 also shows that between the downstream stations C and D the differences between the No. 4 tap and the Nos. 1-3 taps appear to have diminished along the pipeline interval B-C.

Figure 15 shows results for the spaced elbows that are analogous to those of figure 14. With the possible exception of the lowest flow rate, similar trends are noted for the No. 4 tap and the Nos. 1-3 taps between stations A and B. Between station B and C - a distance of some 23.2 the largest differential pressure is measured between the No. 3 taps and Nos. 1,2, and 4 give closely similar results.

Figures 16 and 17 present cross-sectionally averaged pressure differences between the lettered stations versus flow rate in Reynolds number for the welded and spaced configurations, respectively. The conclusions drawn here are:

(1) that the swirled flows produced within the elbow configurations produce the largest friction factors, and

(2) that the friction factor decreases with distance downstream of the pipe length along which it is determined.

Figure 18 presents the pressure losses produced through the elbow configurations - i.e., from stations A to B in terms of equivalent lengths of straight pipe, in diameters. These results quantify the pressure losses and show that for the spaced elbow configuration exceeds that of the welded configuration. However, it is noted that the pressure loss ratio closely approximates the length ratio for these configurations. Thus, it does not appear that firm conclusions can be drawn here regarding differences between the pressure losses per unit length that might exist due to differences in the swirl characteristics.

5. Single Elbow Velocity Surveys. Figures 19 and 20 present, respectively, the horizontal and vertical profiles of the mean vertical velocity component at the 1.5 station downstream of the single elbow. The legend and the sketch identify the data and the traversed diameter. As in the previously investigated elbow configuration, this elbow is a standard, long-radius sweep elbow with weld-neck flanges. It is noted from figure 19 that the secondary flow in this pipe flow consists of two counter-rotating vortices symmetrically oriented with respect to the vertical diameter. Figure 20 shows that the maximum negative (i.e., downward) velocity component occurs about the 10% of the diameter point above the centerline of the pipe.

It is concluded here that these flow characteristics are likely to be present in the previous double elbow configurations where the pipe flows exit the first of the two elbows. For the welded elbow configuration, these distributions may not be developed completely before entering the second elbow. For the spaced elbows these motions flow through the straight pipe length that separates the two elbows before entering the second elbow.

Figures 21 and 22 present, respectively, the horizontal and vertical profiles, at Z = 1.5, of the mean component of the streamwise velocity. Included also in these figures is the power law velocity distribution (shown dashed) for the respective Reynolds number. Figure 21 shows the symmetry of this profile about the vertical diameter through the pipe centerline. It shows velocity over-shoots on either side of the pipe flow with a slow center "core-flow". Figure 22 shows a high velocity region near the bottom of the pipe and a slow "core-flow" over a large central section of the pipe.

Figures 23 (a) and (b) and 24 (a) and (b) are analogous to figures 19 and 20, respectively, in that they show similar results for the three streamwise stations devoted by Z = 1.5, 5.0, and 10.0; the respective diametral Reynolds number of 10^4 or 10^5 are given in the legend of each figure. It is noted from these results that there is rapid decay of these secondary motions over these pipe lengths. This is surprising when it is recalled that the swirl from the welded elbow configuration was determined to persist at significant levels (i.e., swirl angle > 2°) 100 downstream! It is noted that the (dimensionless) velocity ordinates are generally larger for the higher diametral Reynolds number flow than they are for the lower. Of course, dimensionally the differences would be much greater.

Figures 25 (a) and (b) and 26 (a) and (b) are analogous to figures 21 and 22, respectively, for the same stations. These confirm the unexpected swirl decay effects noted above over the same pipeline distances. These non-dimensional distributions show that some of the ordinates for the lower Reynolds number cases exceed those for the higher Reynolds number case. Of course, dimensionally the higher Reynolds values will exceed those for the lower.

Figures 27 (a) and (b) and 28 (a) and (b) show respectively, the power spectral distributions measured for the vertical and horizontal velocity components on the pipe centerline for Re = 10^4 and 10^5. These are log-log plots and they confirm that no ordered structures appear to be present in these pipe flows.

Figures 29 (a) and (b) present measurement results for the root-mean-square (r.m.s.) of the vertical component of the turbulent velocity along horizontal diameters at the streamwise stations, Z = 1.5, 5.0, and 10.0 for the two Reynolds numbers, as noted. Figure 30 presents Laufer's data for Reynolds number = 5 x 10^5.[7] This Laufer data, which is normalized in the same manner as the current results, is found to have significantly reduced levels. It is also noted that the distributions measured near the exit of the single elbow deviate qualitatively from the Laufer results, but these differences also diminish rapidly with downstream distance.

The vertical profile of the r.m.s. turbulent component in the vertical direction is shown in figures 31 (a) and (b) for our two Reynolds numbers, as noted. Again, it is apparent that a rapid decay of the broad peak observed just below the pipe centerline at the Z = 1.5 station

occurs within the first ten diameters from this elbow. The Laufer data corresponding closely to that shown in figure 31 (b) is shown in figure 32. This distribution indicates that the radial component of the turbulence is less than 4% of the bulk averaged flow velocity at Laufer's Reynolds number of 5×10^5. As noted from figure 31 (b) at the streamwise station denoted by Z = 10 the distribution shows our radial turbulence component to be greater than 5% of the bulk velocity at all locations along the vertical diameter.

The axial component of the turbulence velocity for our two Reynolds numbers, for the same three stations near the exit plane of the single elbow is shown in figures 33 (a) and (b). At the most upstream of these, the double-peaked distribution has maxima near 14% of the bulk average velocity in the pipe for both Reynolds numbers. The qualitative nature of this distribution changes differently with downstream distance for the two Reynolds numbers. For $Re = 10^4$ the double-peaked profile has essentially disappeared at Z = 5. For $Re = 10^5$ the double peaked profile is preserved as shown in the profile at the Z = 5 station. However, by the succeeding profile at Z = 10, the cross stream profile for the $Re = 10^5$ flow has changed to resemble, qualitatively, the distribution measured by Laufer. This is shown in figure 34, for a Reynolds number of 5×10^5. That Laufer's pipe flow results show this component of the turbulence to be less that 8% of the bulk velocity everywhere along this horizontal diameter corresponds to the comparisons made above.

Figures 35 (a) and (b) show the vertical profile of the axial r.m.s. component of the turbulent velocity for the Reynolds numbers as noted. The peaked distribution for $Re = 10^4$ indicate a maximum of almost 16% at the upstream station while that for $Re = 10^5$ indicates a maximum level of almost 14% of the bulk averaged velocity. These levels occur at differing radial locations along the pipe diameter below the pipe centerline. These peaked profiles are observed to decay rapidly with downstream distance so that by the station Z = 10 turbulence levels are essentially less than 10% of the bulk velocity everywhere along the vertical diameter.

6. Skew Flux Distributions. The mean components of streamwise and vertical velocity distributions can be combined to produce momentum flux distributions. If the skew flux is defined as the product of axial and vertical mean velocities WV, it can be considered as the axial flux of the vertical momentum per unit density. The distribution of this quantity across the horizontal diameter for Reynolds number 10^5 is shown in figure 36 for the three stations Z = 1.5, 5, and 10. These distributions essentially mirror those shown in figure 23 but reduce the minima on the centerline because of the "slow core" flow noted in the axial distributions shown in figure 25. Maxima are shown in the skew flux near the pipewall because of the axial velocity maxima occurring there as shown in figure 25.

The vertical profile of the skew flux, WV is shown in figure 37 for Reynolds number of 10^5. These profiles closely duplicate those of the vertical profiles of vertical velocity shown in figure 24.

7. Skew Angle. Defining the skew angle as the arctan (V/W), the horizontal profiles for the skew angle are shown in figure 38 (a) and (b) for the three stations near the elbow exit for two Reynolds numbers. These indicate that skew angle levels for Reynolds number 10^5 reach -14° along the pipe centerline. Subsequent profiles show that these extreme levels of skew angle at the pipe centerline rapidly diminish to 3° or less by the Z = 10 station.

   Figures 39 (a) and (b) show skew angle distributions along the vertical diameter for the three stations for two Reynolds numbers, as noted. The most upstream distribution shows that, for a skew angle of -16° at about 10% of the pipe diameter above the pipe centerline. Again, rapid decay of these skew angle distributions is noted with the Z = 10 station showing that the skew angle is everywhere less than 2°.

8. Swirl Intensity. If the swirl intensity is defined as the axial flux (per unit density) of the moment of momentum about the pipe centerline, the product is WVx. The cross-stream distribution for this product for the single elbow for two Reynolds numbers for our same three stations is shown in figure 40 (a) and (b). The zero crossings at the centerline and at two locations at approximately 20-25% diameter points on either side of the centerline along a horizontal diameter show the presence of two symmetric, counter-rotating vortices. It is not clear if the centers of these vortices lie on this horizontal diameter, or above it - as perhaps shown by figure 24 or 37. The decay of these two vortices is more rapid than that observed earlier in the results for the elbow-out-of-plane configurations.

   When the swirl intensity data is plotted relative to these vortex centers, the distribution is shown in figures 41 (a) and (b). These distributions incorporate the sign-change pertinent to the counter-rotation of these two vortices.

9. Vortex Modelling. Several classic vortex models are briefly described and fitted to our measured distributions. The one put forth by G.I. Taylor seems to achieve the best agreement with our results to date.

   The three models considered are Euler, Hamel-Oseen, and the G.I. Taylor descriptions.[9,10] The Euler model produces a two-dimensional tangential velocity (about the axis of rotation) that varies inversely with distance from this axis. This is written as $V = G/2\pi r$. This model has the unrealistic feature of having infinitely large velocities in the limit as $r \rightarrow o$.

The Hamel-Ossen distribution is a modification of the Euler version that can be written

$$V = \frac{G}{2\pi r} (1 - e^{-cr^2})$$

This distribution has the realistic features of zero tangential velocity on the axis of rotation and a core of fluid rotating about the axis with a motion resembling "solid-body" rotation.

The G.I. Taylor distribution is written:

$$V = (Cr)\, e^{-(r/r_o)^2/2}$$

This distribution does not directly exhibit the velocity variation that is inverse with radius. Instead, it gives more emphasis to the solid body rotation near the axis of rotation and the exponential decay further from this axis. In our pipe flow, it appears that these features more closely model the characteristics of our vortices.

When Taylor vortices are hypothesized to exist at $\pm$ 0.25 on either side of the pipe centerline on the horizontal diameter, and the core radius is selected so that, $r_o = 0.2$, the distribution obtained is shown in figure 42. These show the tangential velocity produced in the pipe cross-section due to each vortex. The composite flow field is obtained by algebraic summation.

When these distributions are fitted to our data for the Z = 1.5 station at Reynolds number 10^5 the V1 and V2 distributions shown on figure 43 are obtained. The composite distribution which is the summation is shown and labelled Va. It is noted that this approximates that given in figure 23.

Similarly, when the Taylor model is fitted to the swirl intensity distribution shown in figure 41, the results are given in figure 44. Again, the close resemblance gives the conclusion that our vortices appear to be modelled by the Taylor version.

Conclusions

It is concluded from the results reported here that significant deviations are found between the ideal, equilibriated pipe flow distributions for these Reynolds numbers and relative roughness conditions and our measurement results for both the "welded" and the "spaced" elbows-out-of-plane configurations. These deviations were found in both the mean and the turbulent velocity distributions. That these configurations can produce significant fluid metering errors becomes clear - especially with the slow decay of these deviations in the downstream piping.

The pressure experiments conducted in these flows indicate that increased loss occurs due to the secondary flows produced by these piping configurations. These losses are attributed to the fluid shearing stresses produced at the

inner pipe wall by these flows and the turbulent phenomena present over the flow cross-section.

The pipe flow measurements for the single elbow indicate that a dual-eddy secondary flow field is produced by this configuration. Although our measurement program for this configuration is not yet complete, it is apparent that this secondary flow pattern decays with downstream distance more rapidly than for the elbow-out-of-plane configurations. These measurements will be completed in the next phase of this work.

REFERENCES

1. Mattingly, G.E., Yeh, T.T., and Robertson, B., Flowmeter Installation-Effects: A New Approach to an Old but Prevalent Problem. Procs. Int'l Symp. on Flow Measm't in the 1980's, NEL UK East Kilbride, Scotland U.K., June 1986.

2. Mattingly, G.E., Yeh, T.T., Robertson, B. and Kothari, K., NBS Research on In-Situ Flowmeter Installations, Procs. AGA Distribution and Transmission Confr. Las Vegas NV, May 1987.

3. Fejer, A., Lavan, Z., and Wolf, L. Jr., Study of Swirling Fluid Flow, ARL 68-0713, Aerospace Research Laboratories, USAF, Wright-Patterson Air Force Base, Ohio, Oct. 1968.

4. Musolf, A.O., An Experimental Investigation of the Decay of Turbulent Swirl Flow in a Pipe, M.S. Thesis, Univ. of Colorado, Dept. of Civil Engineering (1963).

5. Kreith, F. and Sonju, O., The Decay of Turbulent Swirl in a Pipe, Journal of Fluid Mechanics, Vol. 22, part 2, pp. 257-271 (1965).

6. Mottram, R.C. and Rawat, M.S., Attenuation Effects of Pipe Roughness on Swirl and The Implications for Flowmeter Installation. International Symposium on Fluid Flow Measurement, American Gas Association (1986).

7. McManus, S.E., Bateman, B.R., Brennan, J.A., Pantoja, I.V. and Mann, D.B. The Decay of Swirling Gas Flow in Long Pipes, Procs., AGA Distribution and Transmission Conf. Boston, MA. May, 1985.

8. Hinze, J.O., Turbulence, McGraw-Hill, New York (1959) (Laufer's data in chapter 7).

9. Schlichting, H. Boundary Layer Theory, McGraw-Hill Book Co., New York.

10. Dryden, H., Murnaighan, F.D, and Bateman, H. Hydrodynamics, Dover Publ. Co., New York, NY 1956.

APPENDIX 1

NBS Industry-Government Consortium Membership

As of the 1988 research period, the NBS Industry-Government Consortium Research Program on Flowmeter Installation Effects included the following members, in alphabetical order:

1. Ametek-McCrometer
2. Chevron Oil
3. Daniel Industries
4. Department of Energy
5. Dow Chemical Co.
6. E.I. DuPont de Nemours
7. Fischer & Porter
8. Ford Motor Co.
9. Gas Research Institute
10. Gas Unie
11. Instrument Testing Service
12. ITT Barton
13. NBS-Boulder
14. Rockwell International
15. Rosemount

SWIRL DECAY

$$S = S_o * \exp(-Cz)$$

GROUP	C	
Fejer et al (air)	0.018<C<0.052 80K<Re<360K	$140Re^{-0.7}$
Musolf (water)	0.031<C<0.041 20K<Re<120K	$0.2Re^{-0.16}$
Kreith & Sonju (water)	0.014<C<0.019 10K<Re<100K	$0.051Re^{-0.11}$
Mottram & Rawat (Smooth)	0.25<C<0.034 40K<Re<200K	$0.24Re^{-0.19}$
NBS-G L+X-Y	0.020<C<0.031 10K<Re<100K	$0.18Re^{-0.19}$
NBS-G L+X-Y2.4	0.031<C<0.042 10K<Re<100K	$0.14Re^{-0.13}$
NBS-B	.8M<Re<1.4M	0.014

Table 1 **Exponential Swirl decay constants**

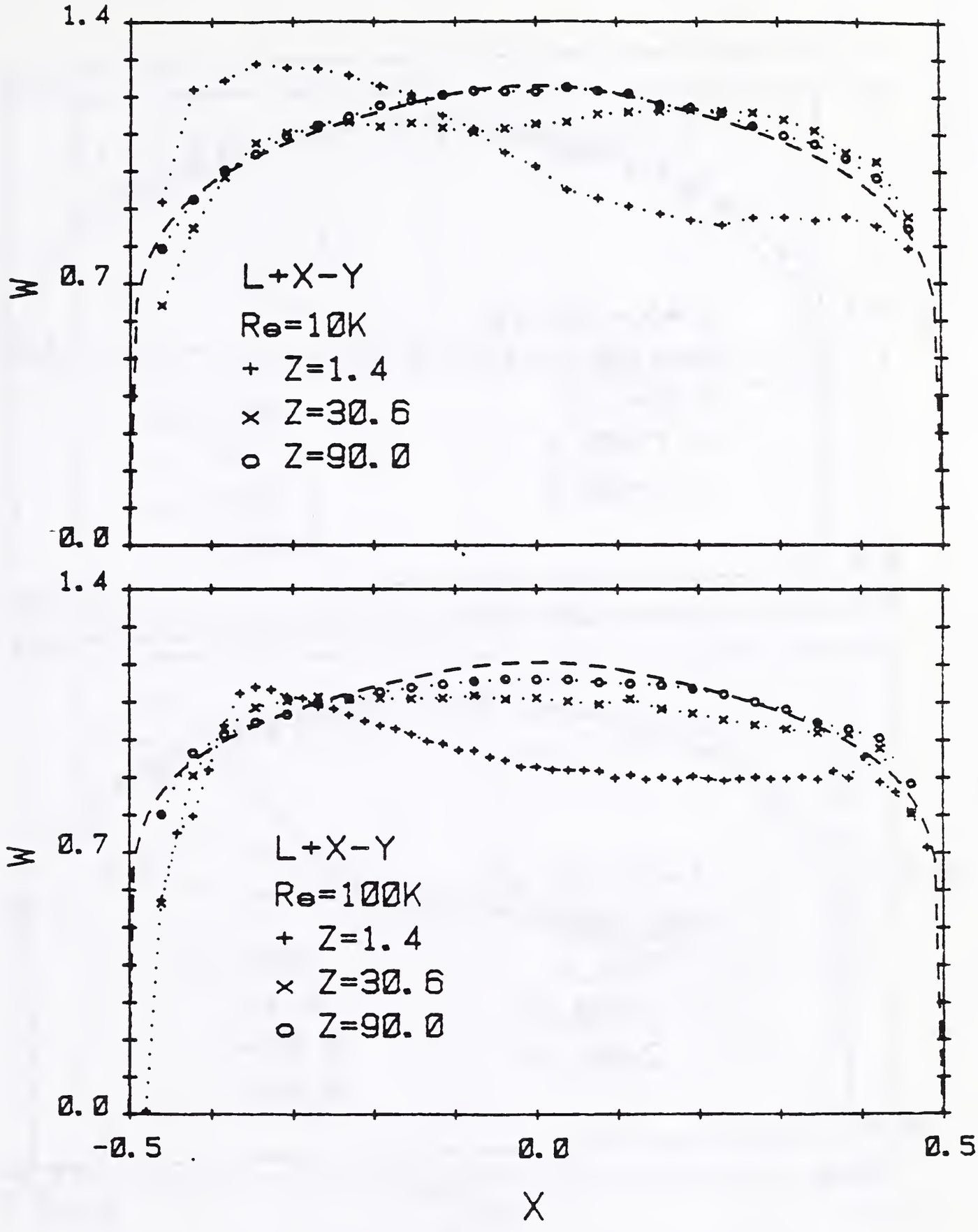


Fig. 1 (a) Mean axial velocity distribution for welded elbows-out-of-plane configuration

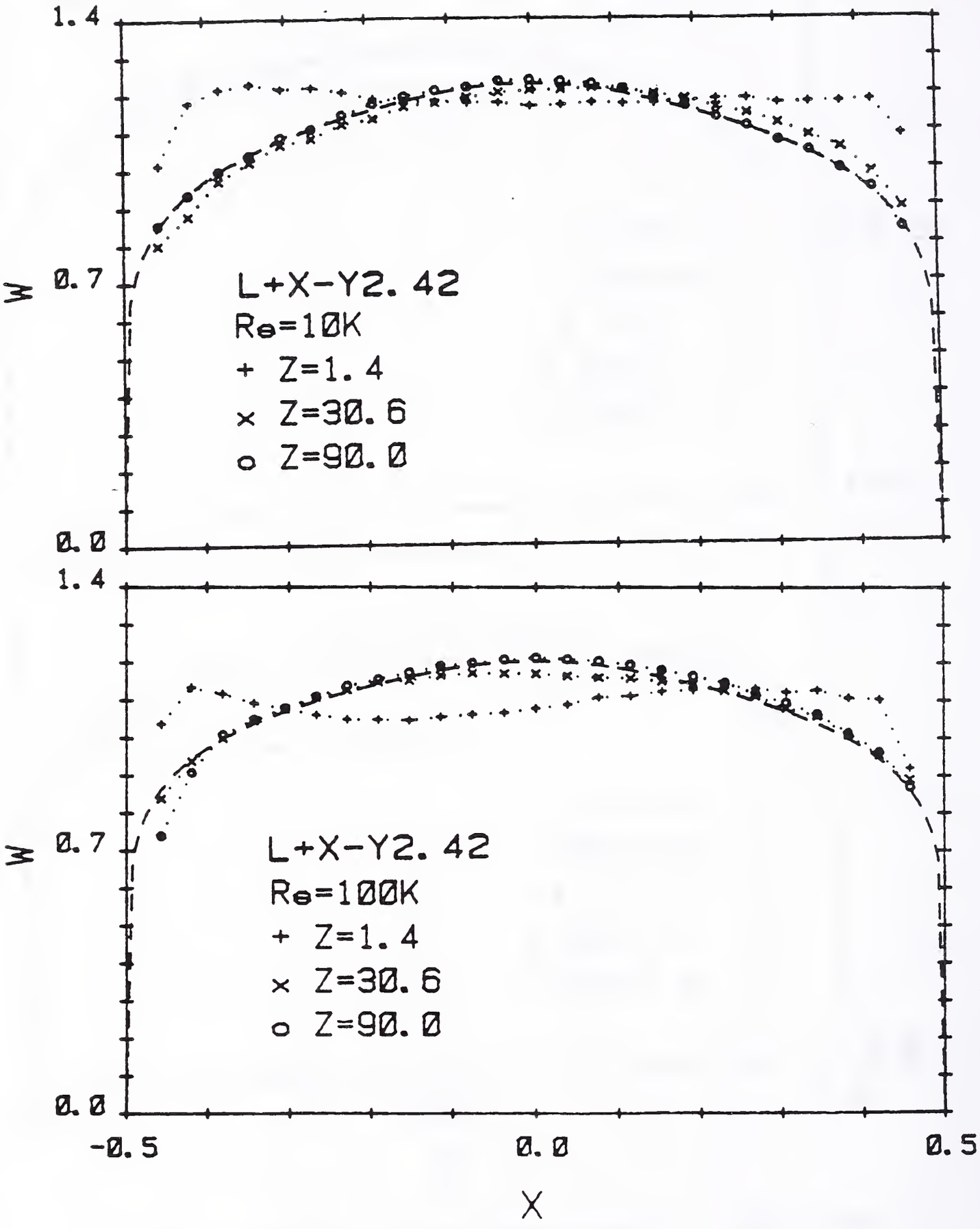


Fig. 1 (b) Mean axial velocity distribution for spaced elbows-out-of-plane configuration

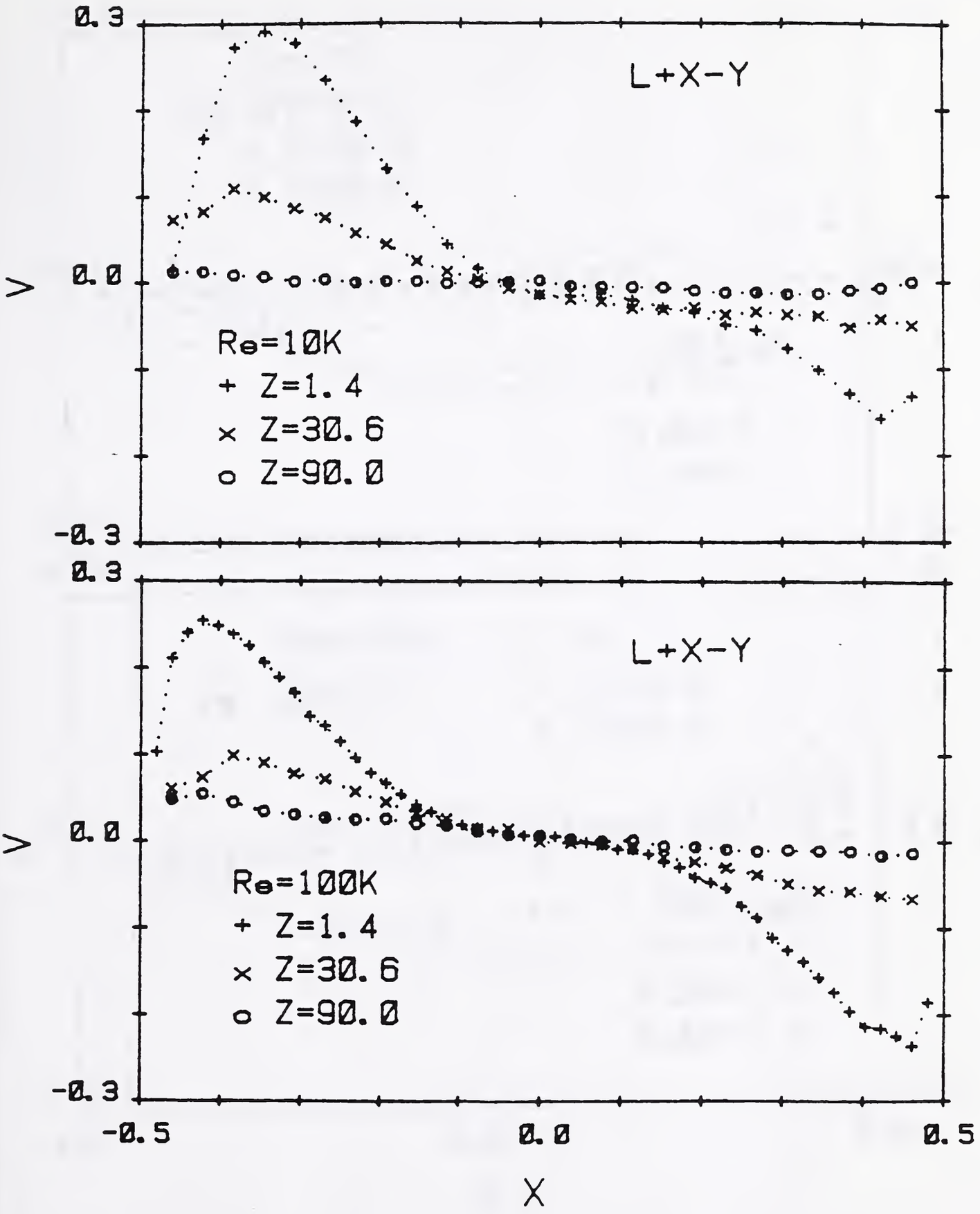


Fig. 2 (a) Mean vertical velocity distribution for welded elbows-out-of-plane configuration

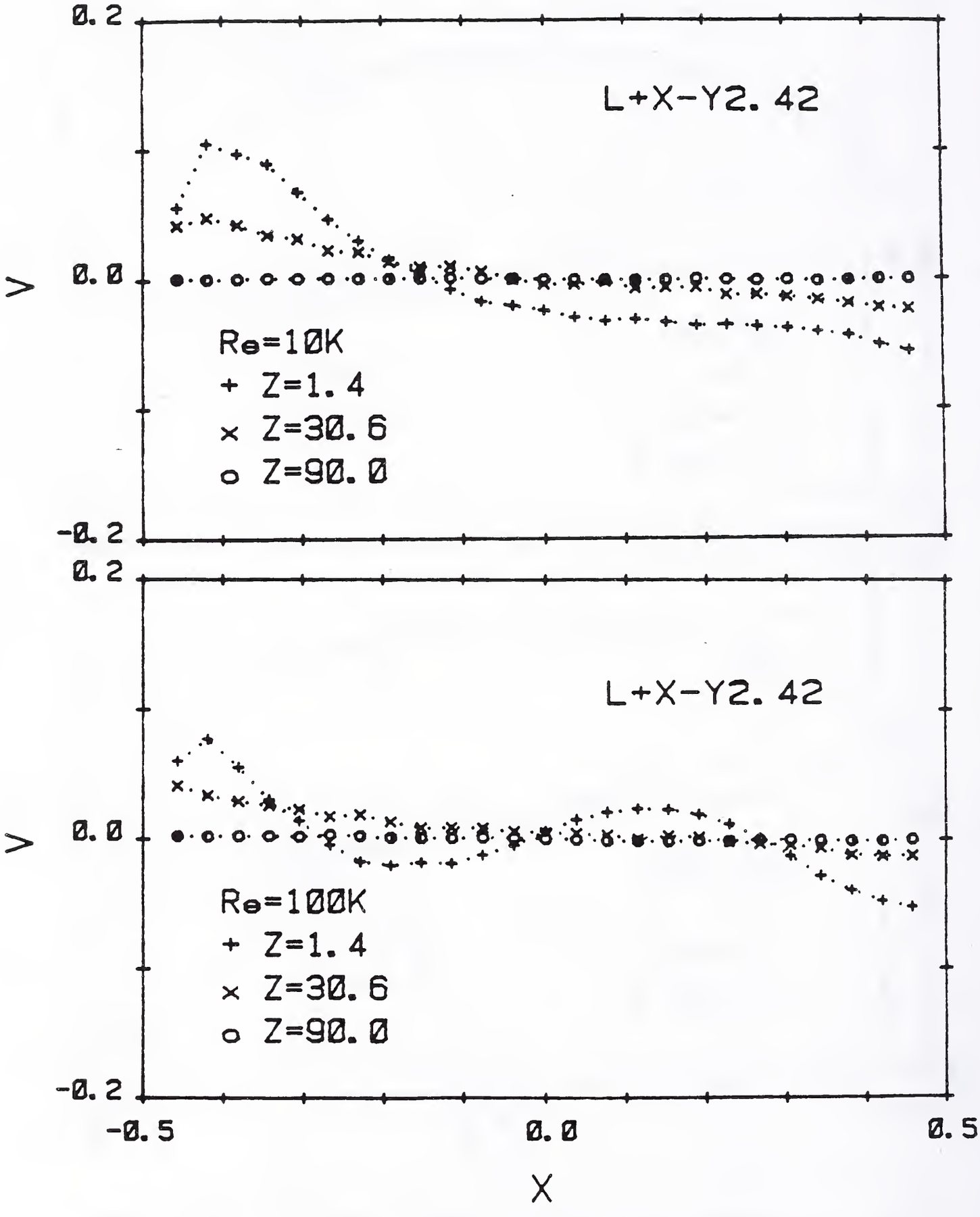


Fig. 2 (b) Mean vertical velocity distribution for spaced elbows-out-of-plane configuration

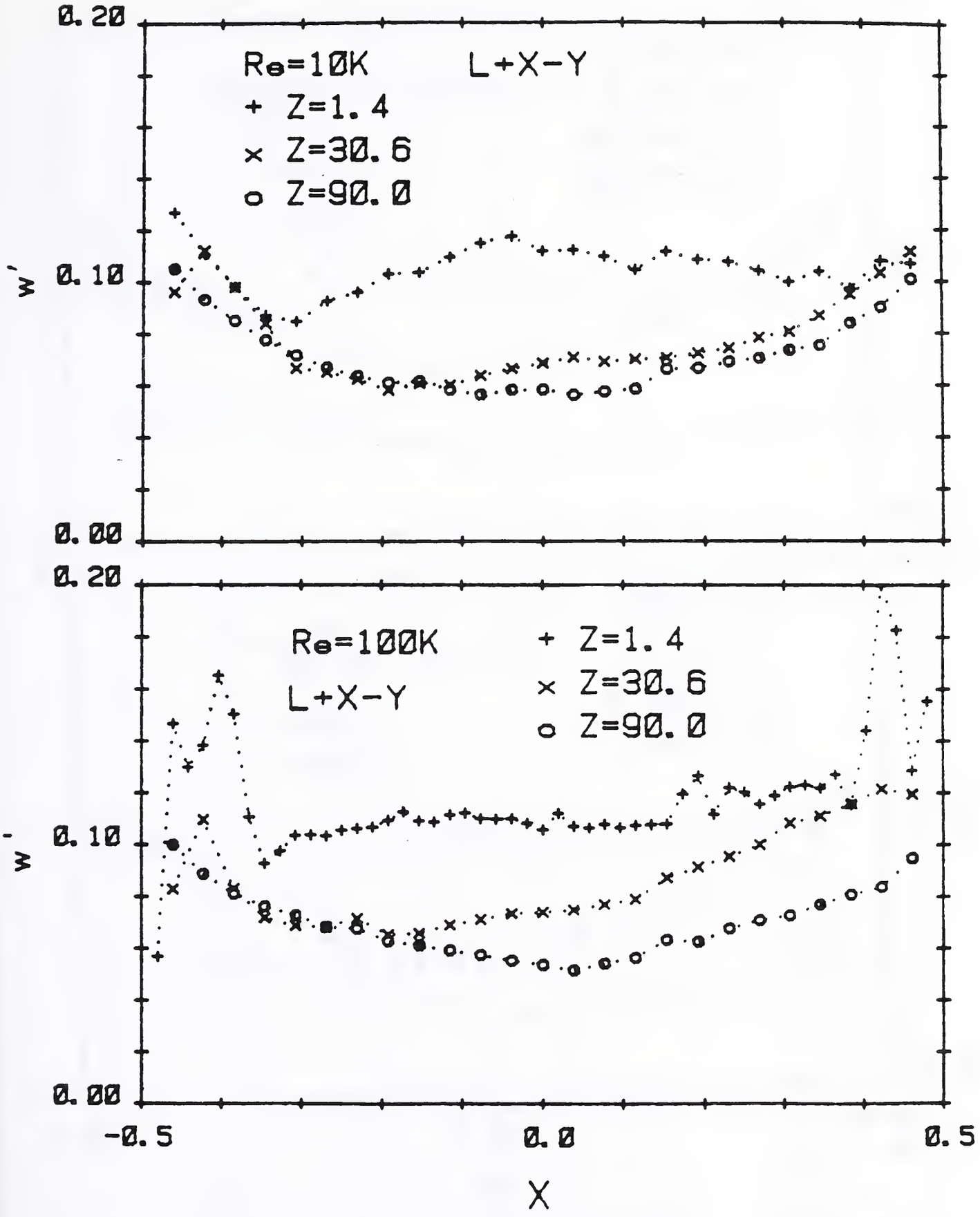


Fig. 3 (a) Turbulence axial velocity distribution for welded elbows-out-of-plane configuration

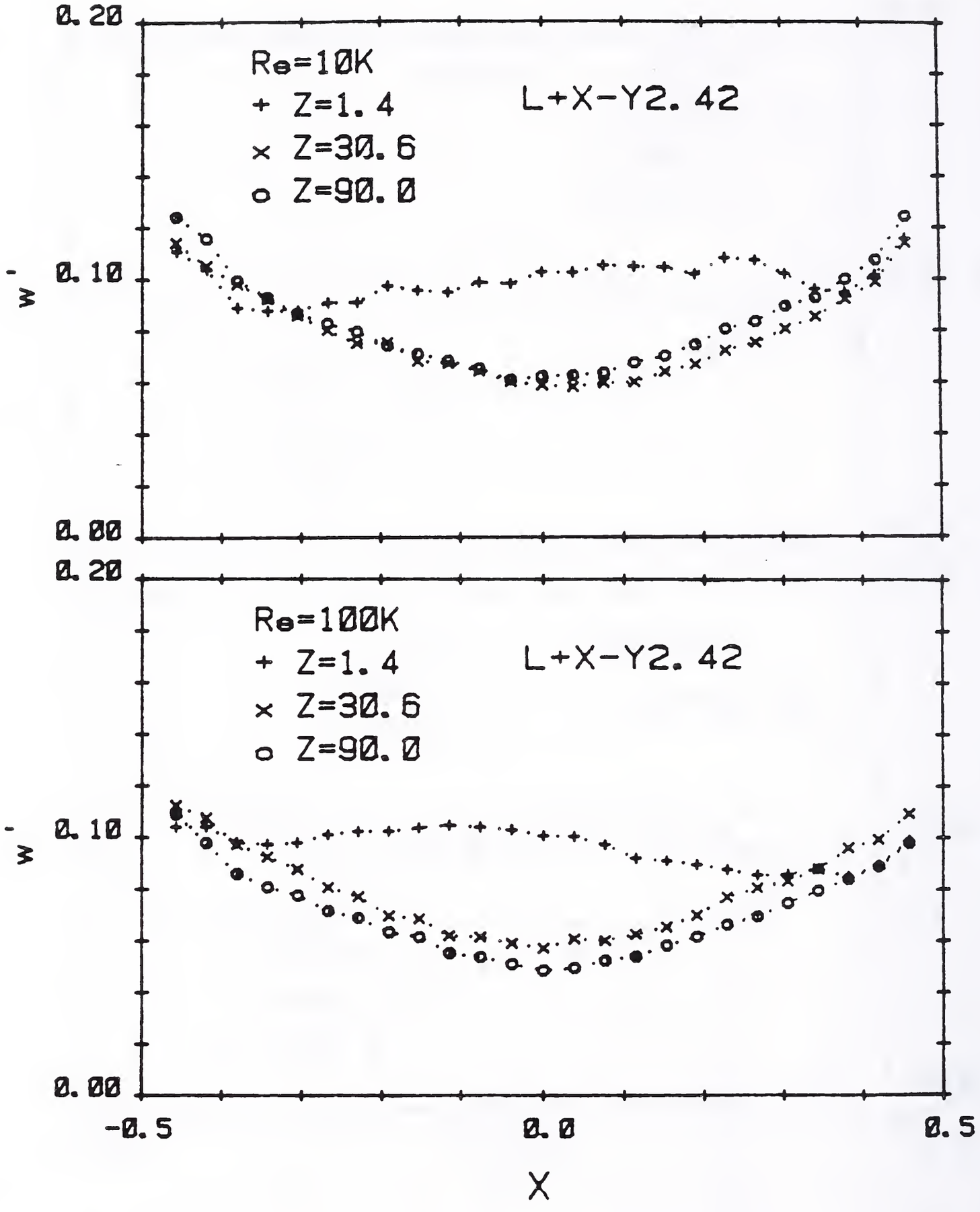


Fig. 3 (b) Turbulence axial velocity distribution for spaced elbows-out-of-plane configuration

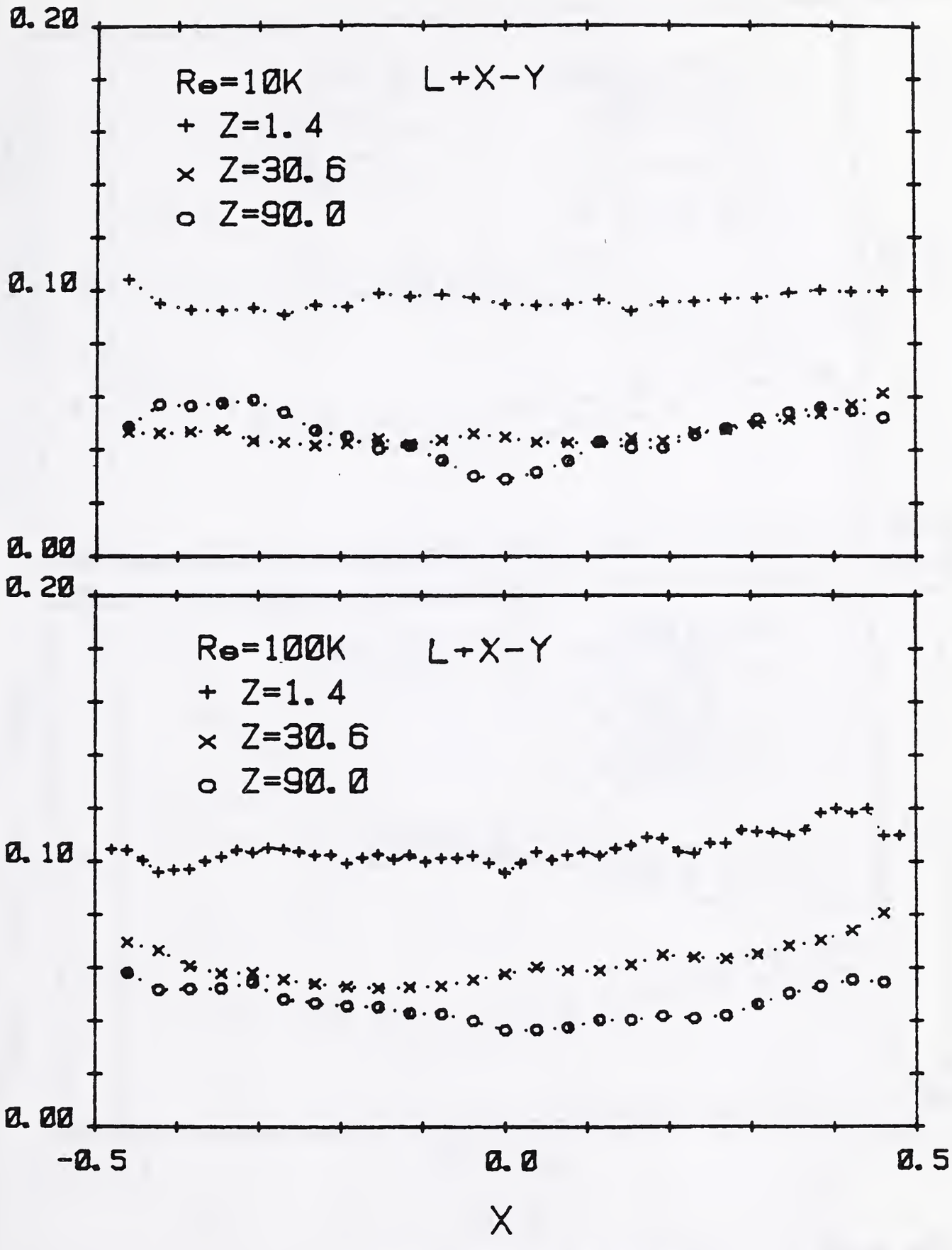


Fig. 4 (a) Turbulence vertical velocity distribution for welded elbows-out-of-plane configuration

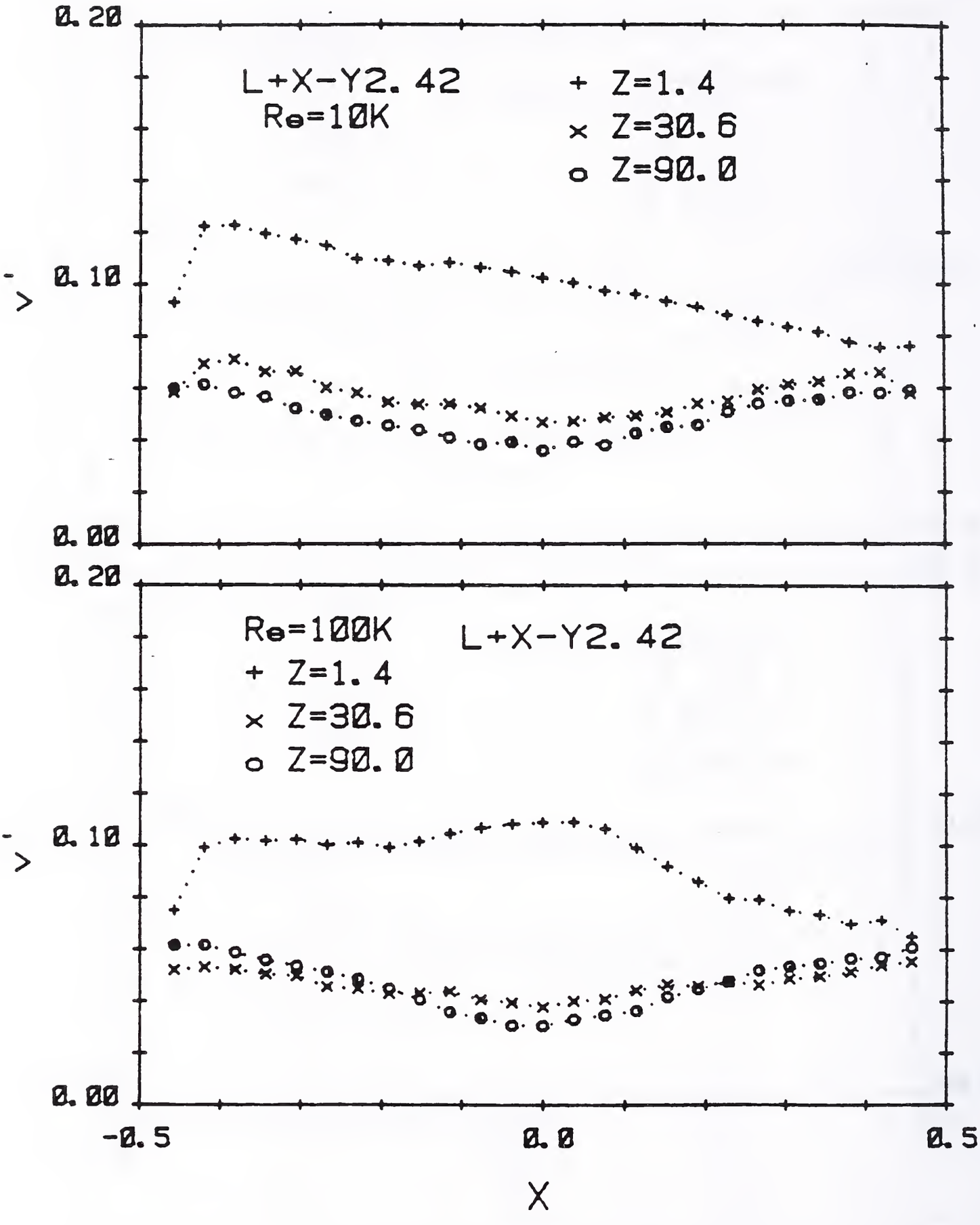


Fig. 4 (b) **Turbulence vertical velocity distribution for spaced elbows-out-of-plane configuration**

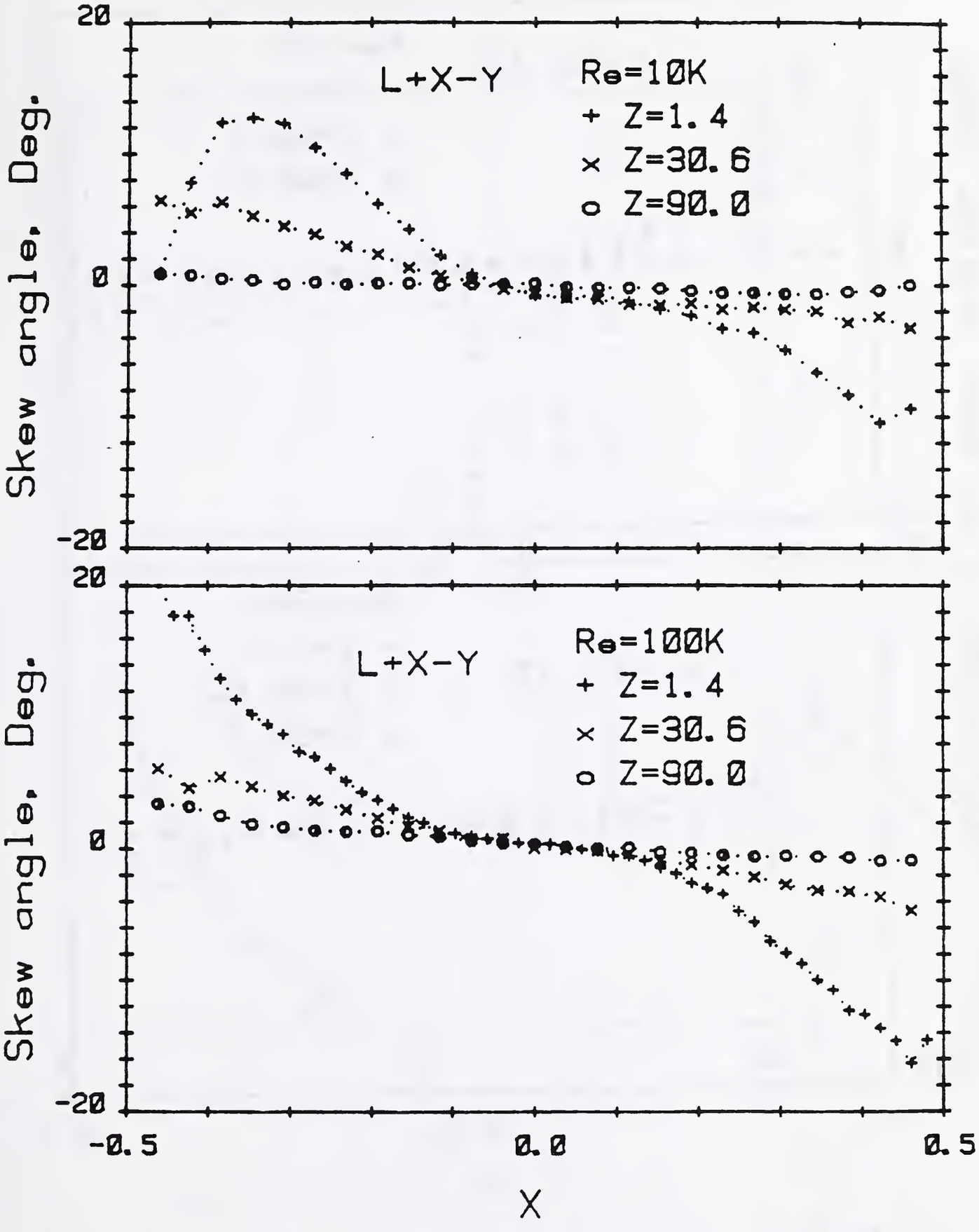


Fig. 5 Skew angle distribution for welded elbows-out-of-plane configuration

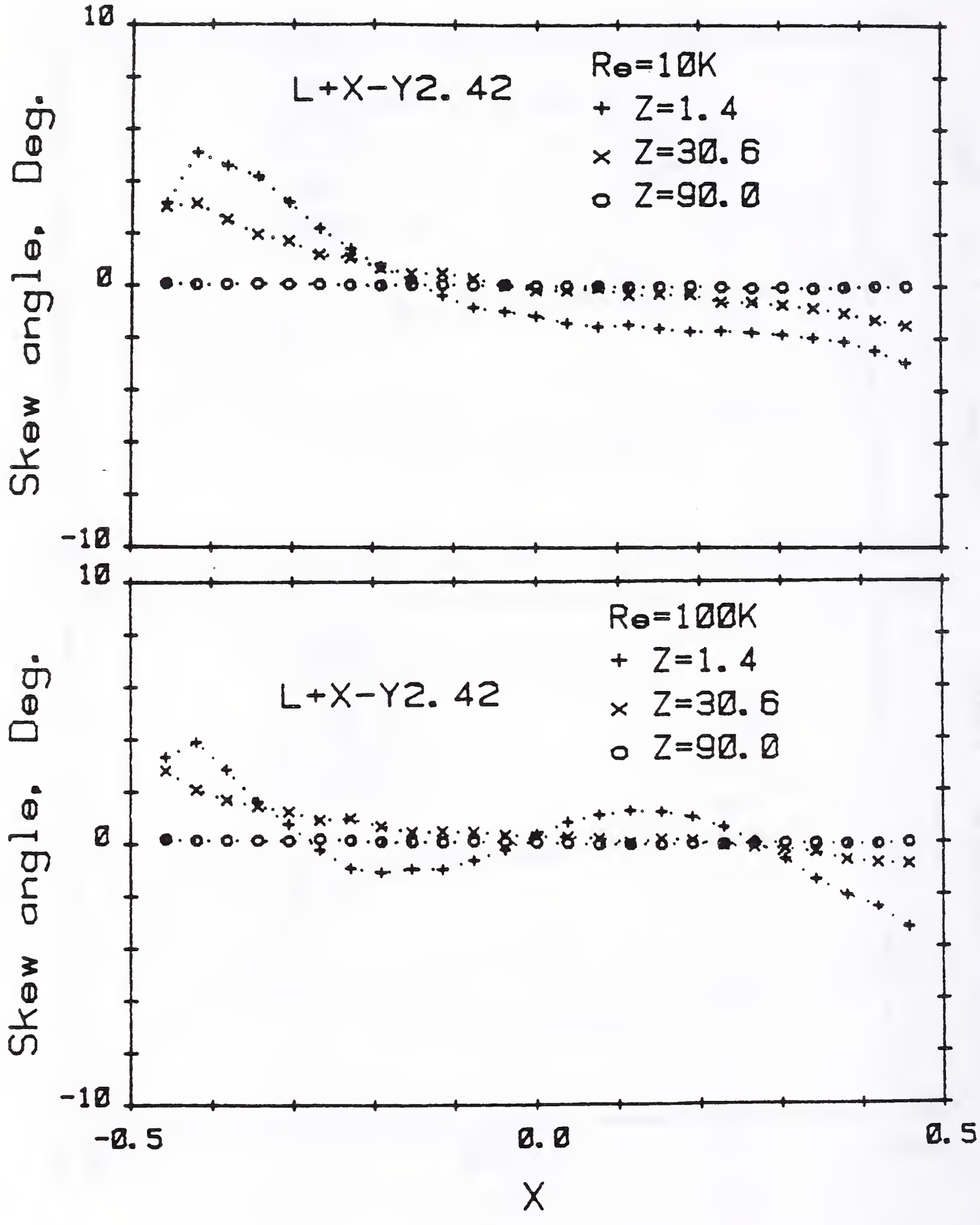


Fig. 6 Skew angle distribution for spaced elbows-out-of-plane configuration

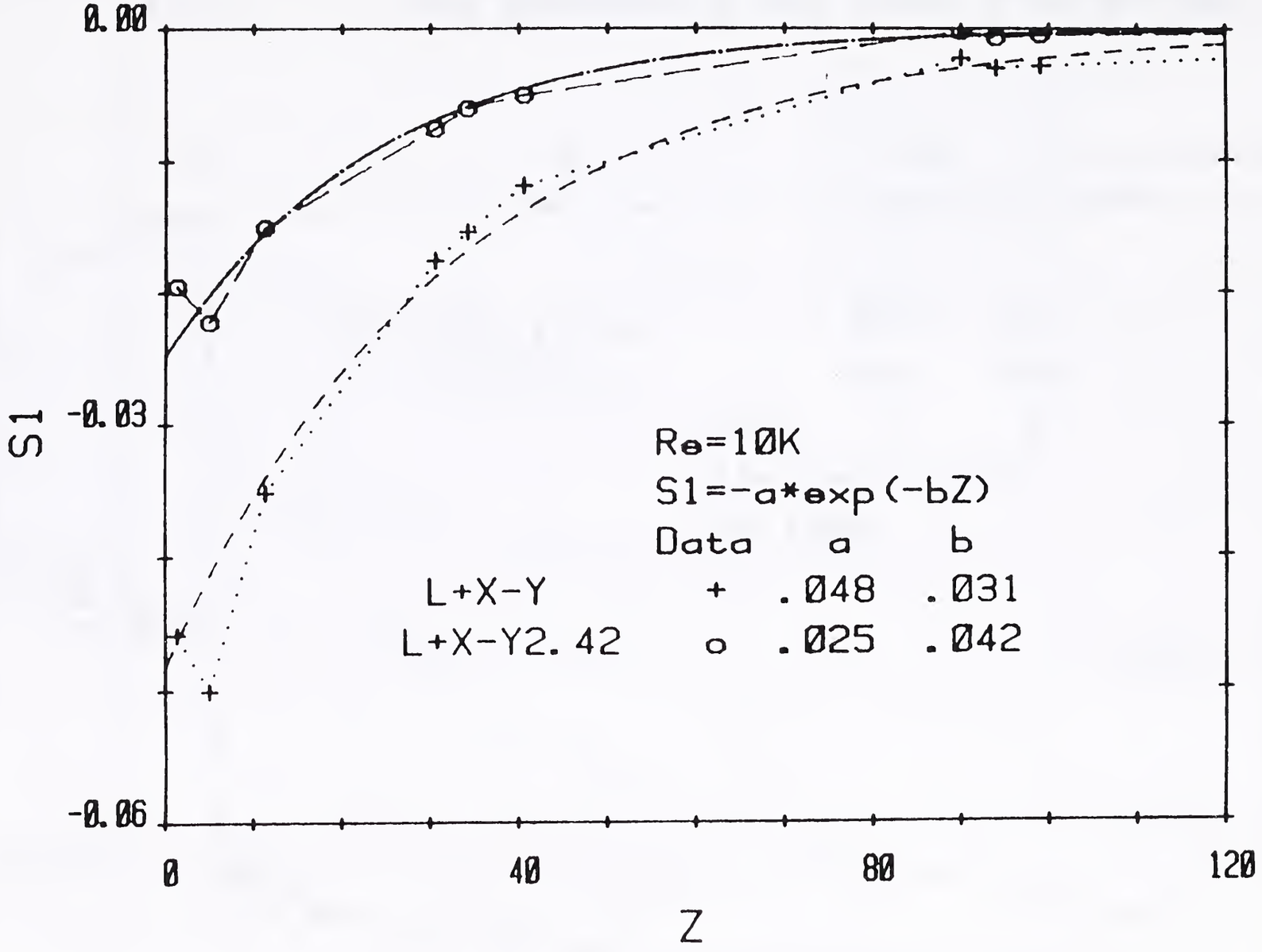


Fig. 7 Axial distribution of swirl number S_1 for $Re = 10^4$

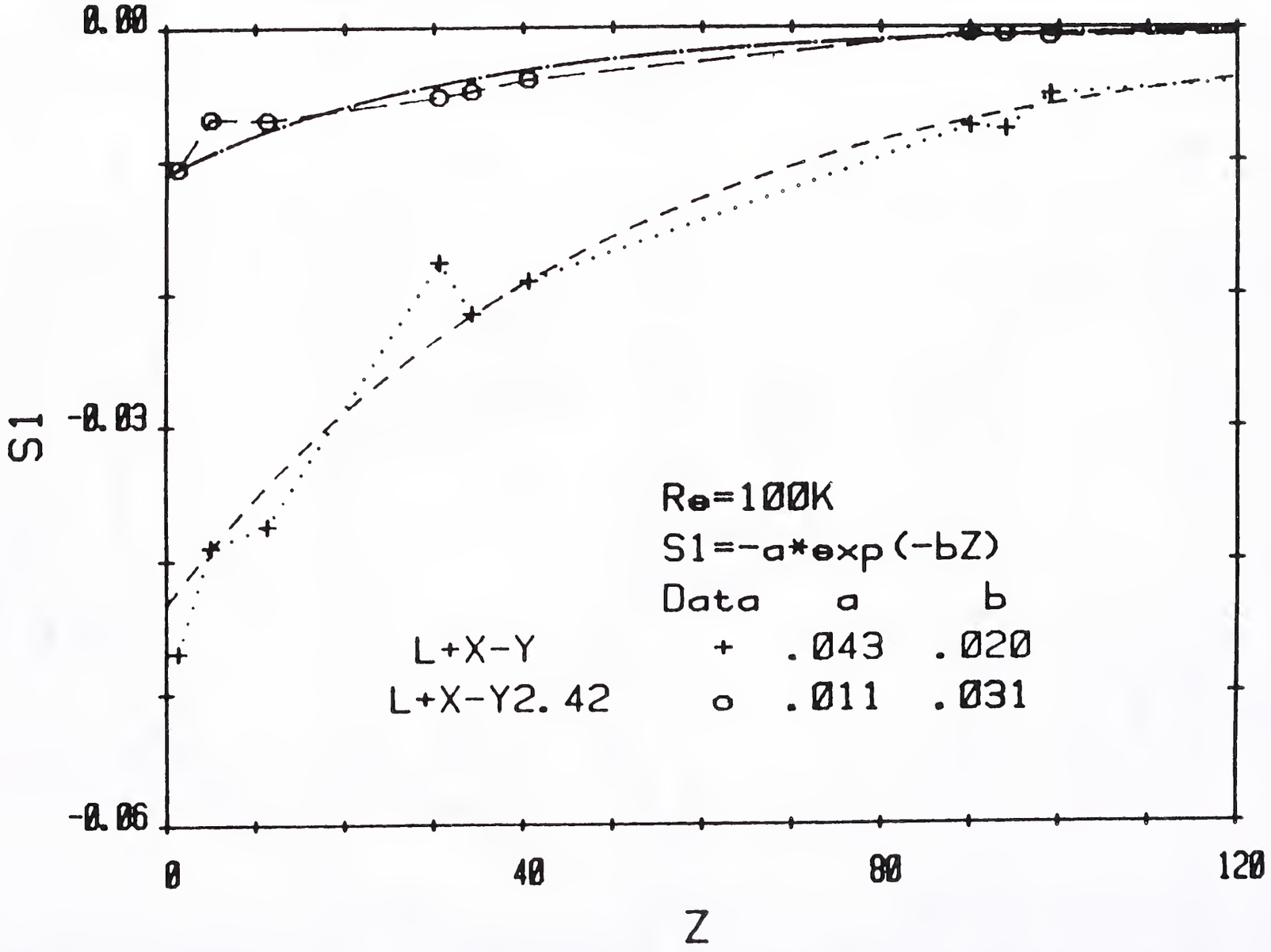


Fig. 8 **Axial distribution of swirl number S_1 for $Re = 10^5$**

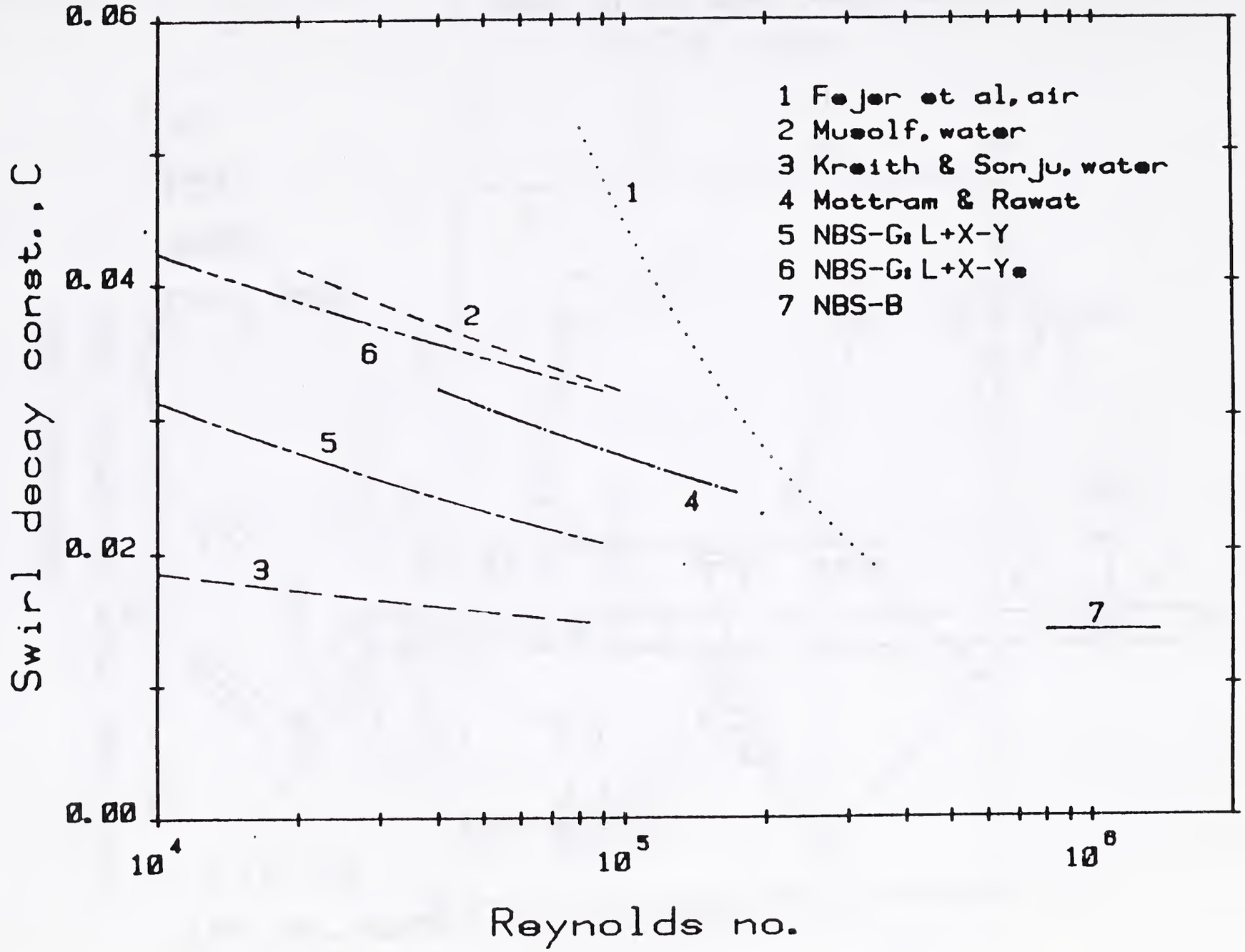
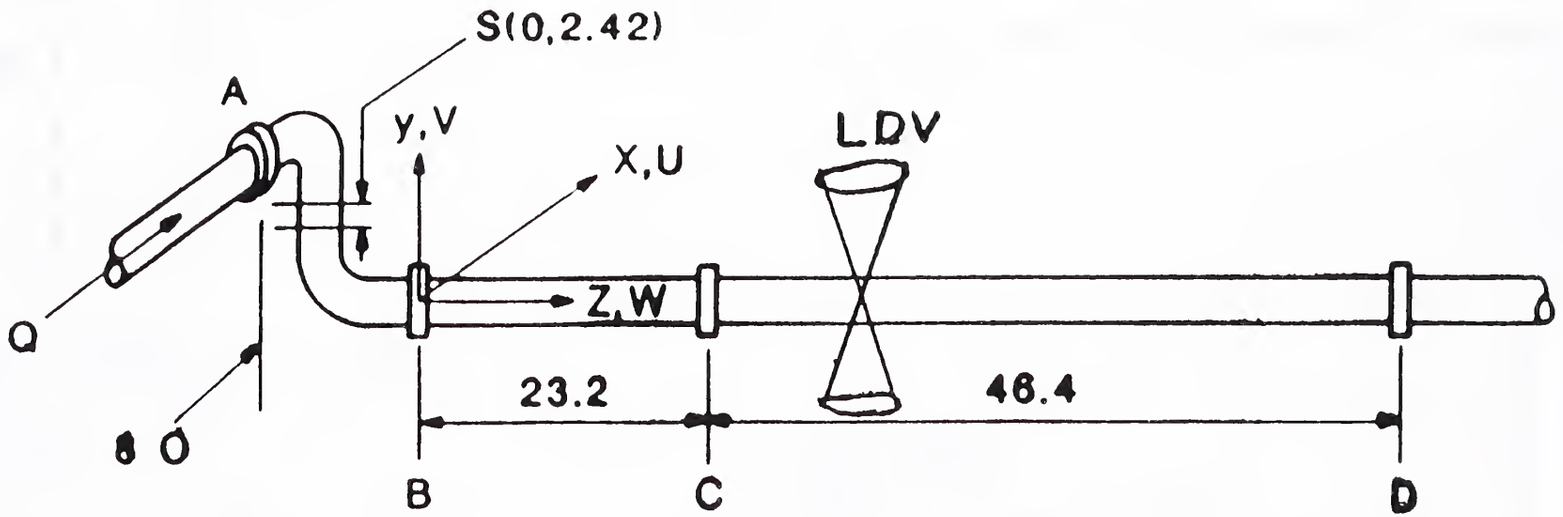
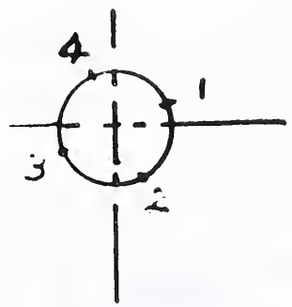


Fig. 9 Exponential swirl decay constant versus Reynolds number

- Two 90° elbows out-of-plane

  L+X-YS





- D= 2" pipe

  Water

  LDV

  Δp

Fig. 10 A sketch of the piping configurations and the pressure tap locations

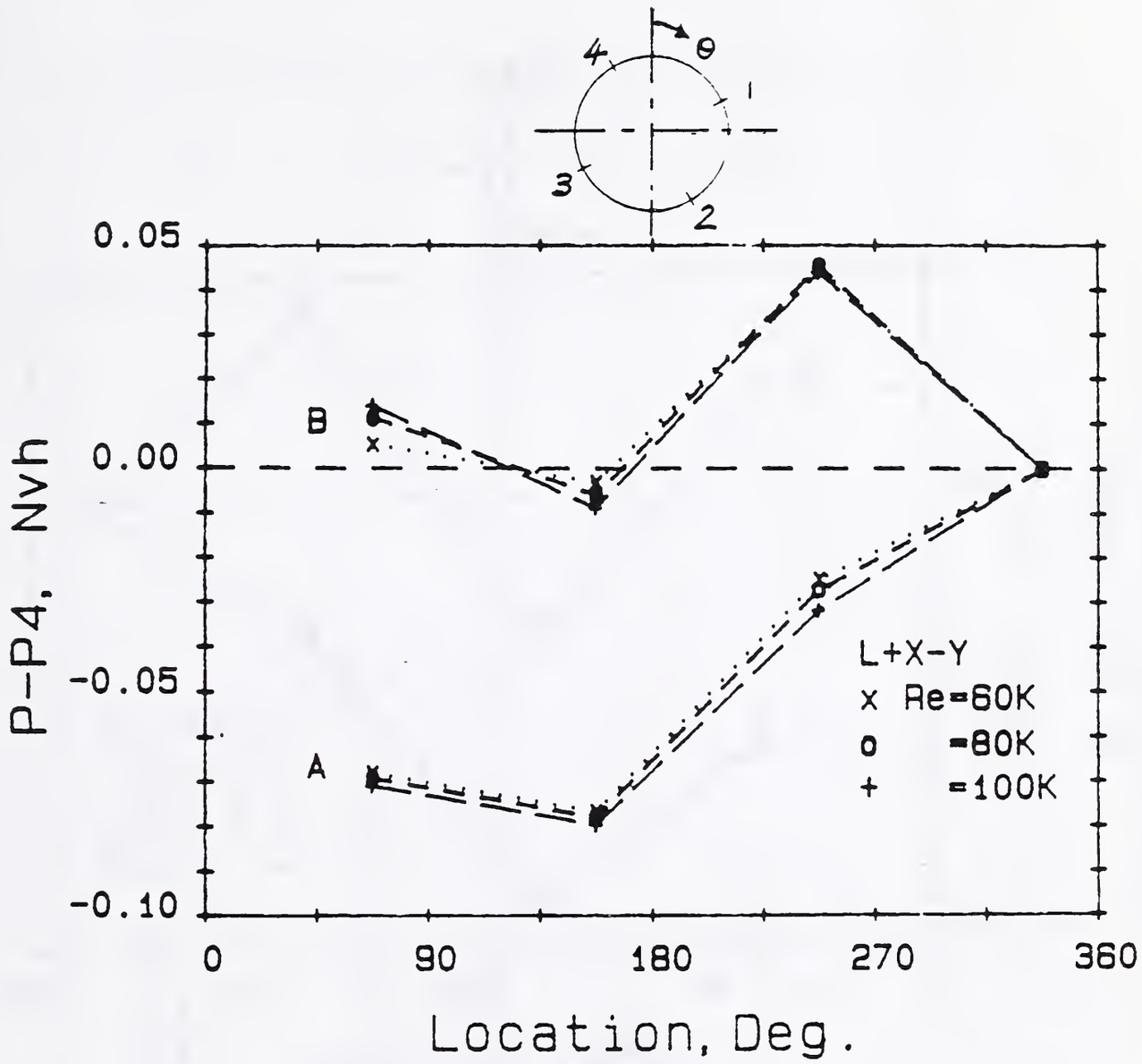


Fig. 11 **Angular distributions of differential static pressure for welded elbow-out-of-plane configuration**

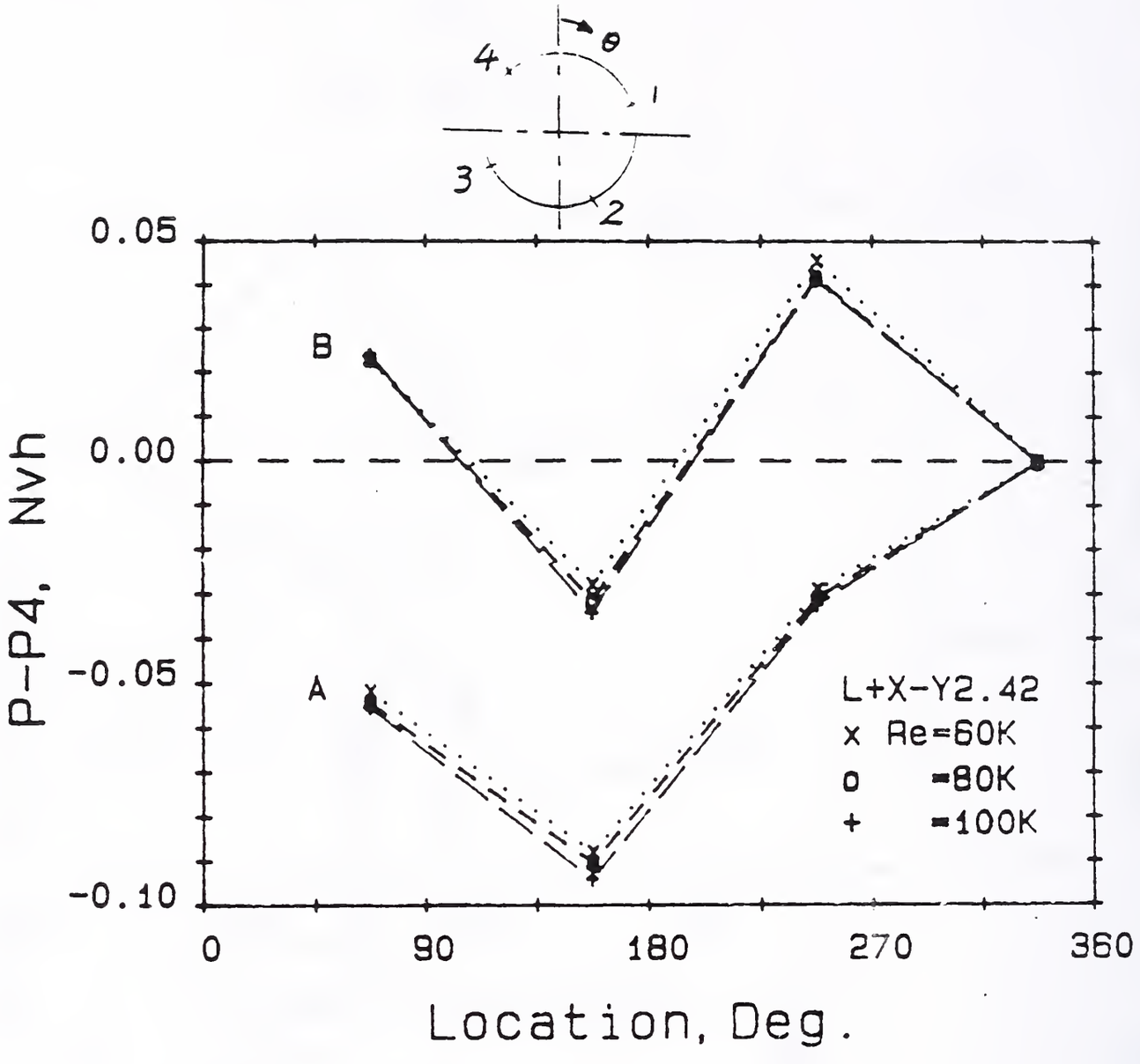


Fig. 12 **Angular distributions of differential static pressure for spaced elbow-out-of-plane configuration**

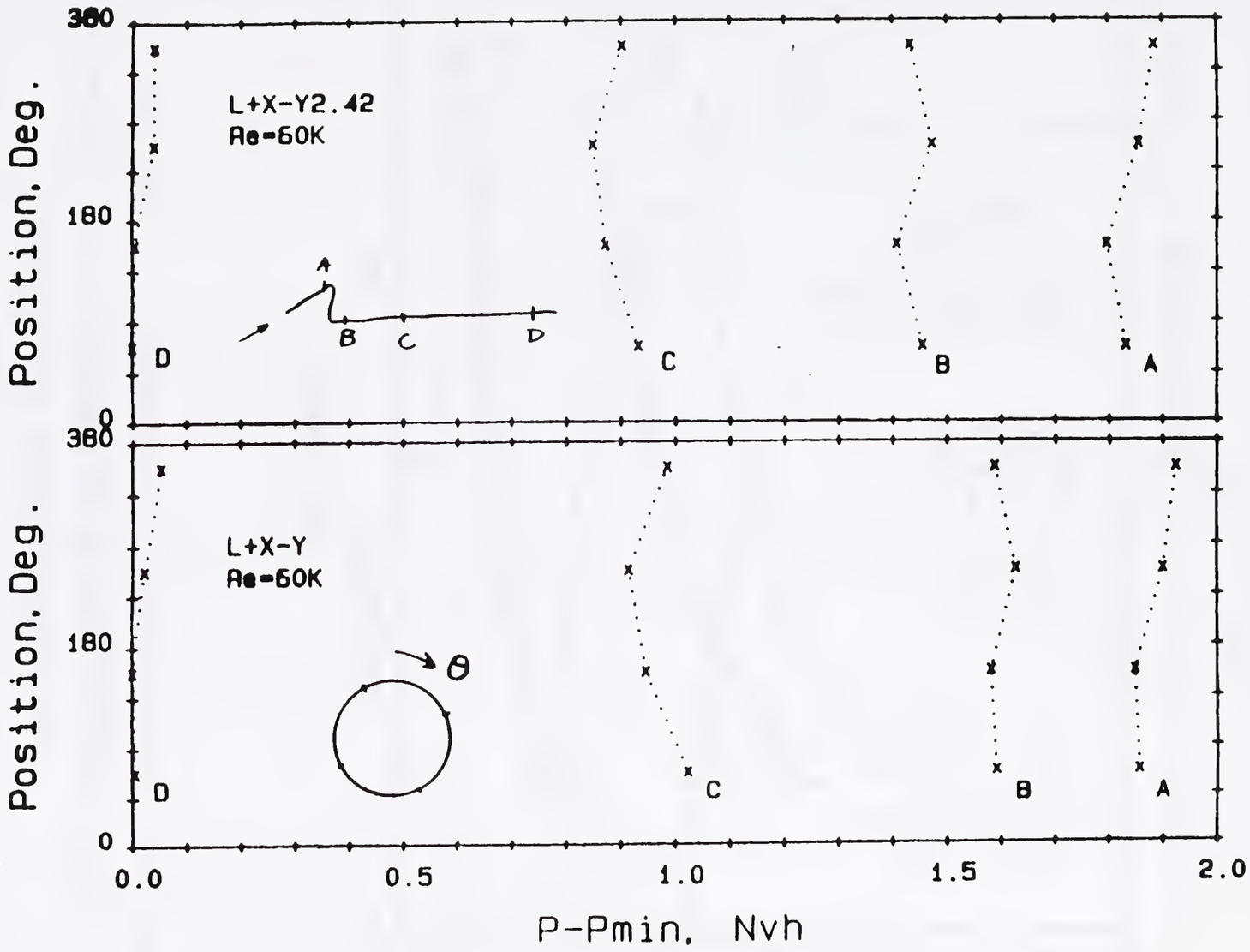


Fig. 13 **Differential static pressure distributions for both piping configurations**

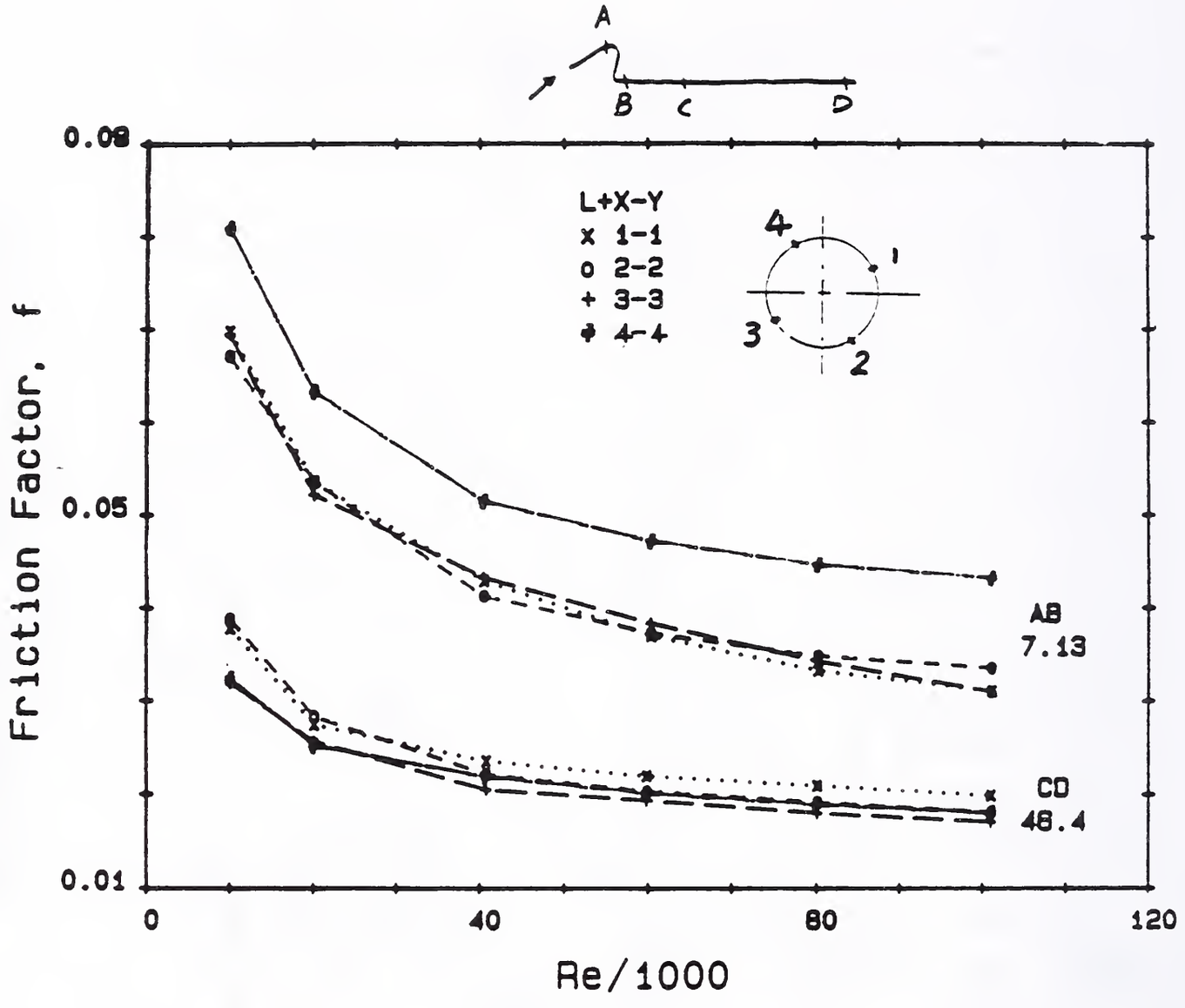


Fig. 14 Variations of friction factor for welded elbow-out-of-plane configuration

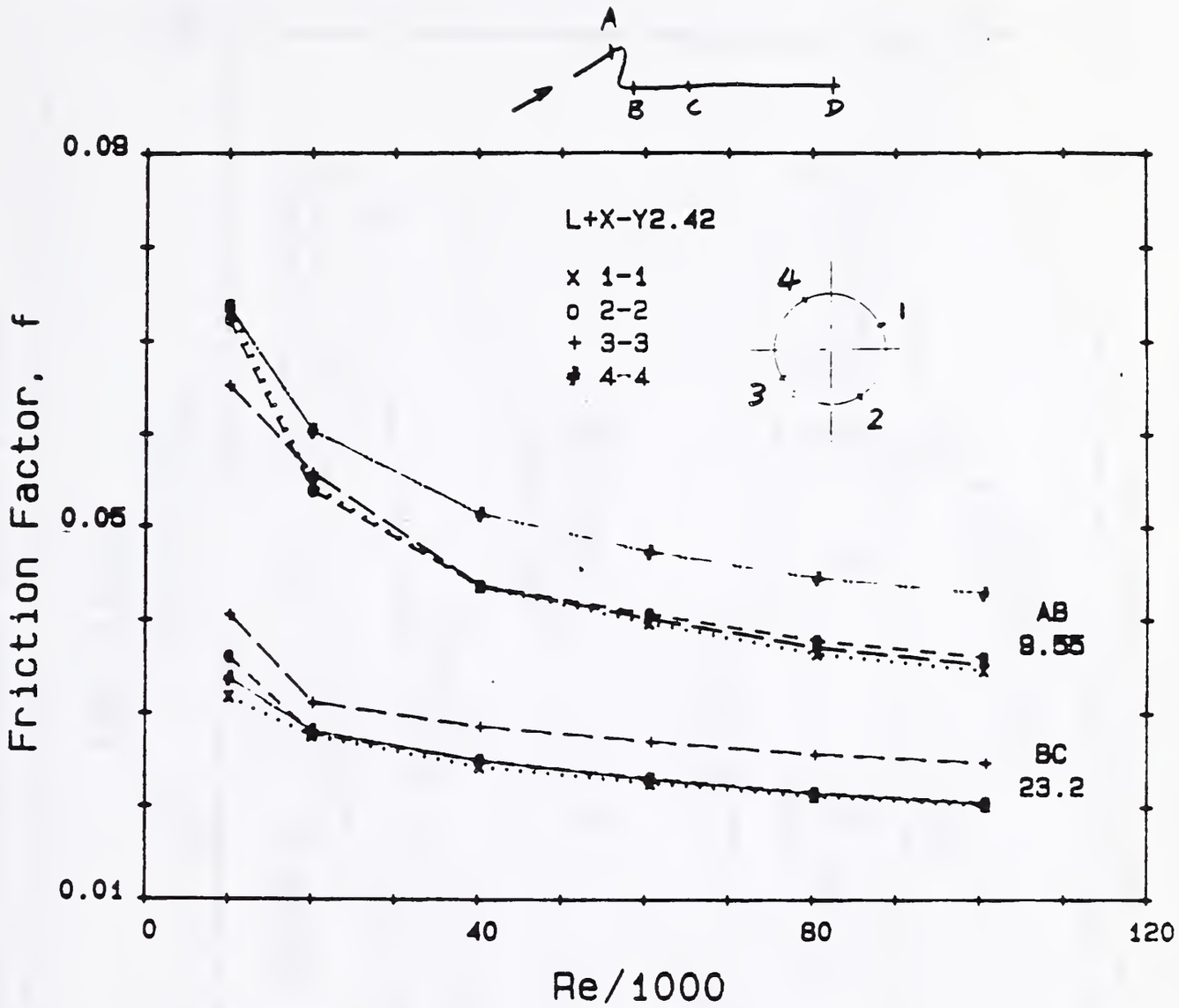


Fig. 15 Variation of friction factor for spaced elbow-out-of-plane configuration

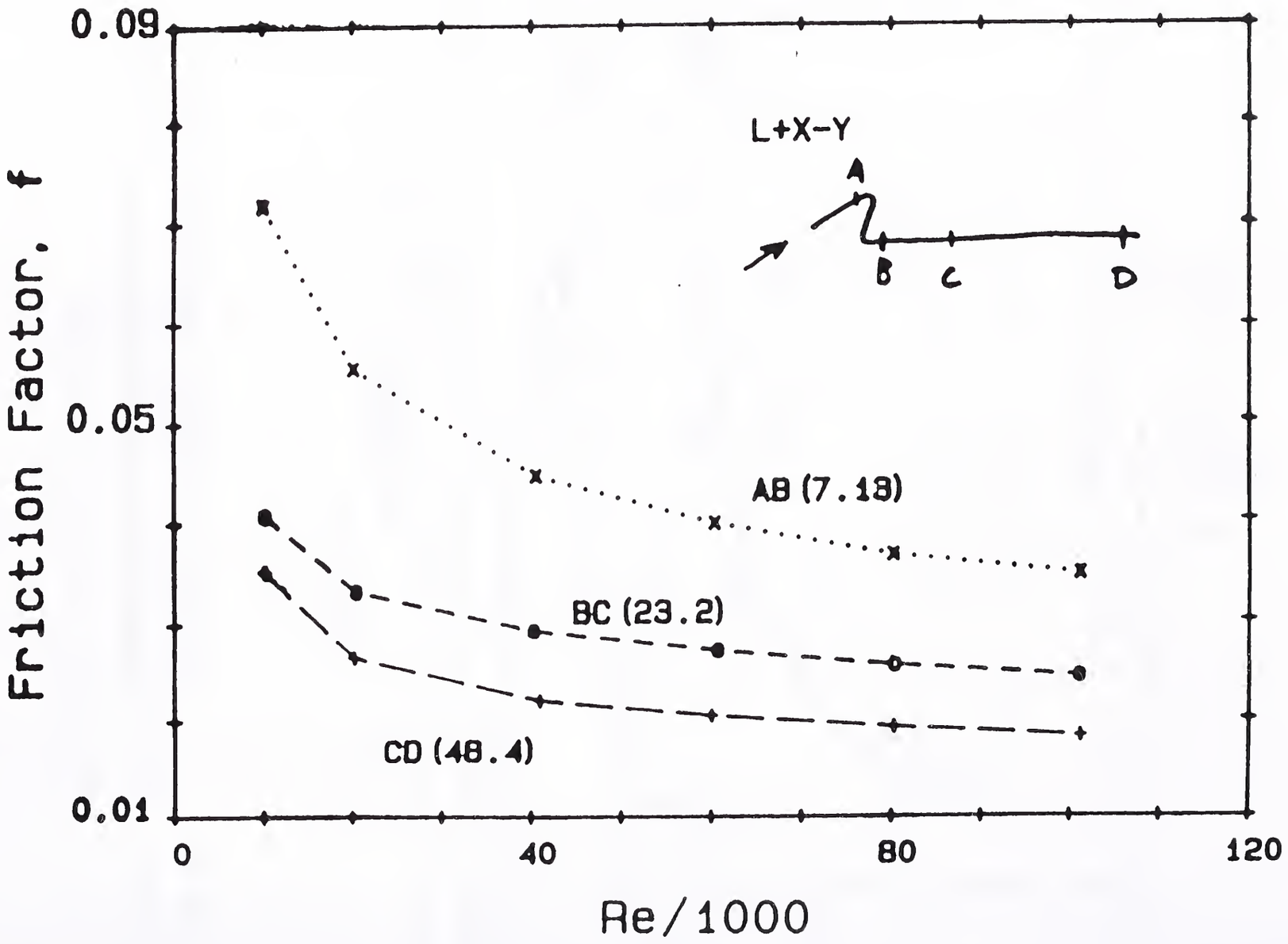


Fig. 16 Angular averaged friction factors between the lettered stations for welded configurations

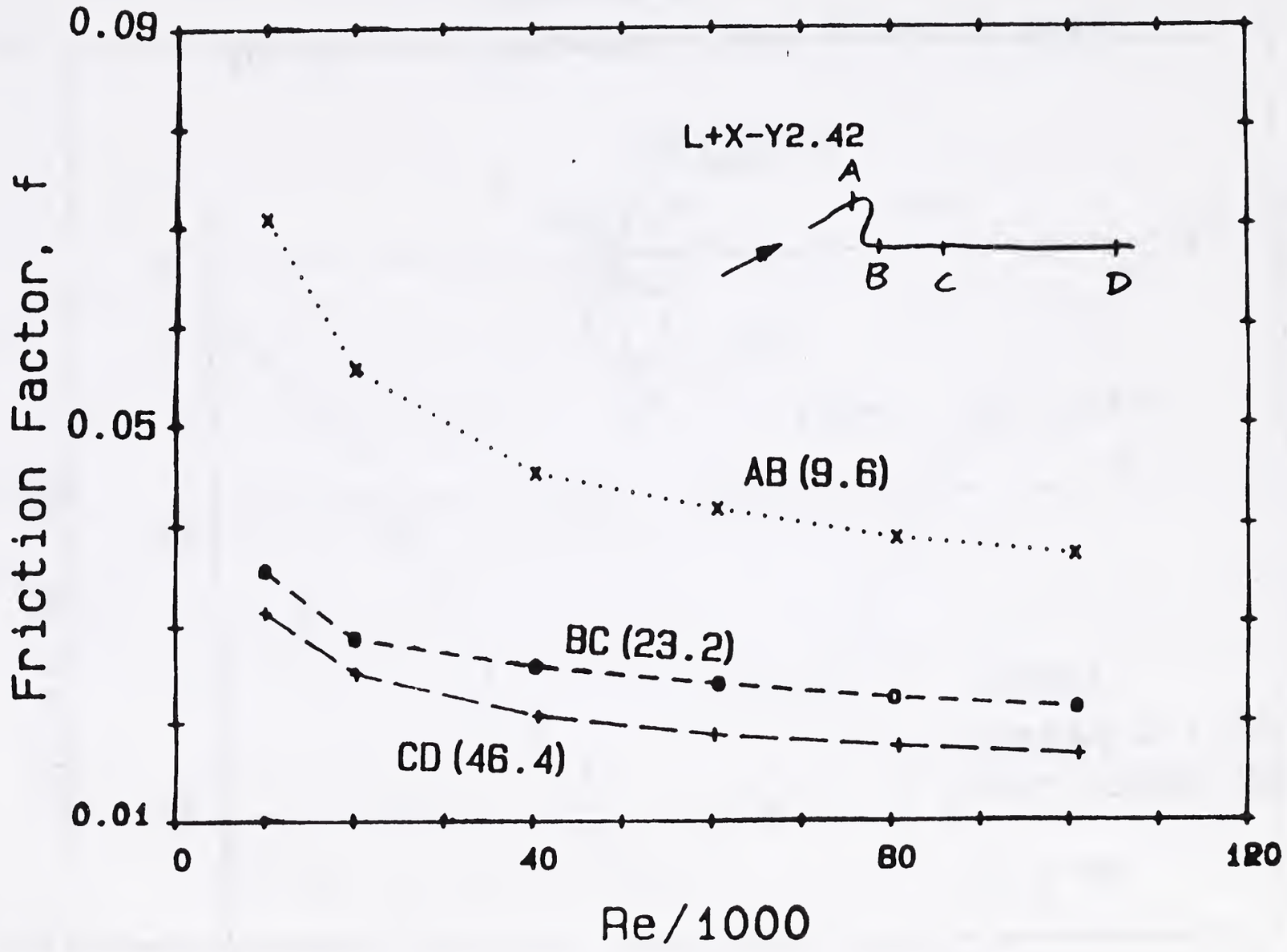


Fig. 17 Angular averaged friction factors between the lettered stations for spaced configuration

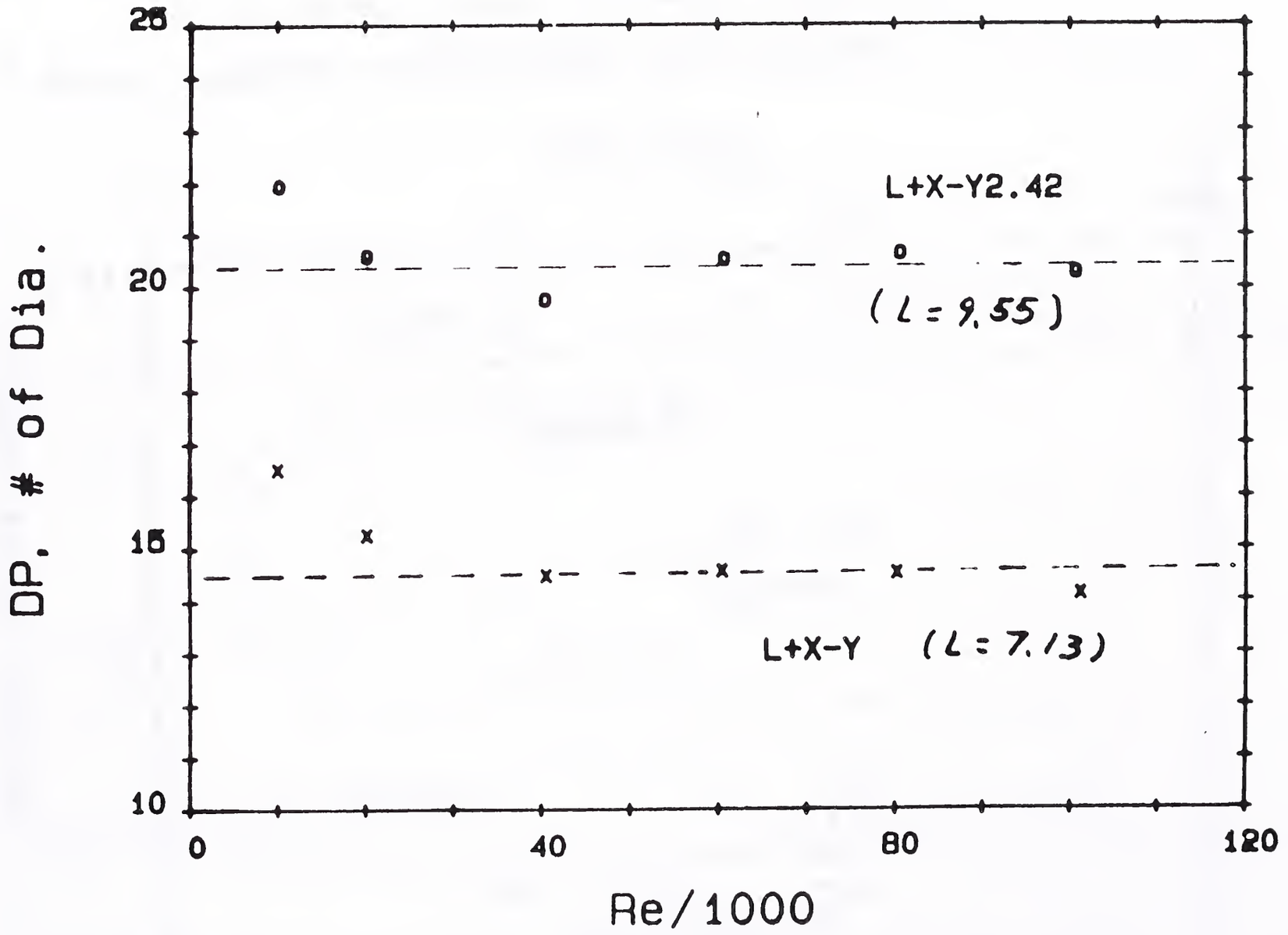


Fig. 18 The pressure losses across the elbow configurations

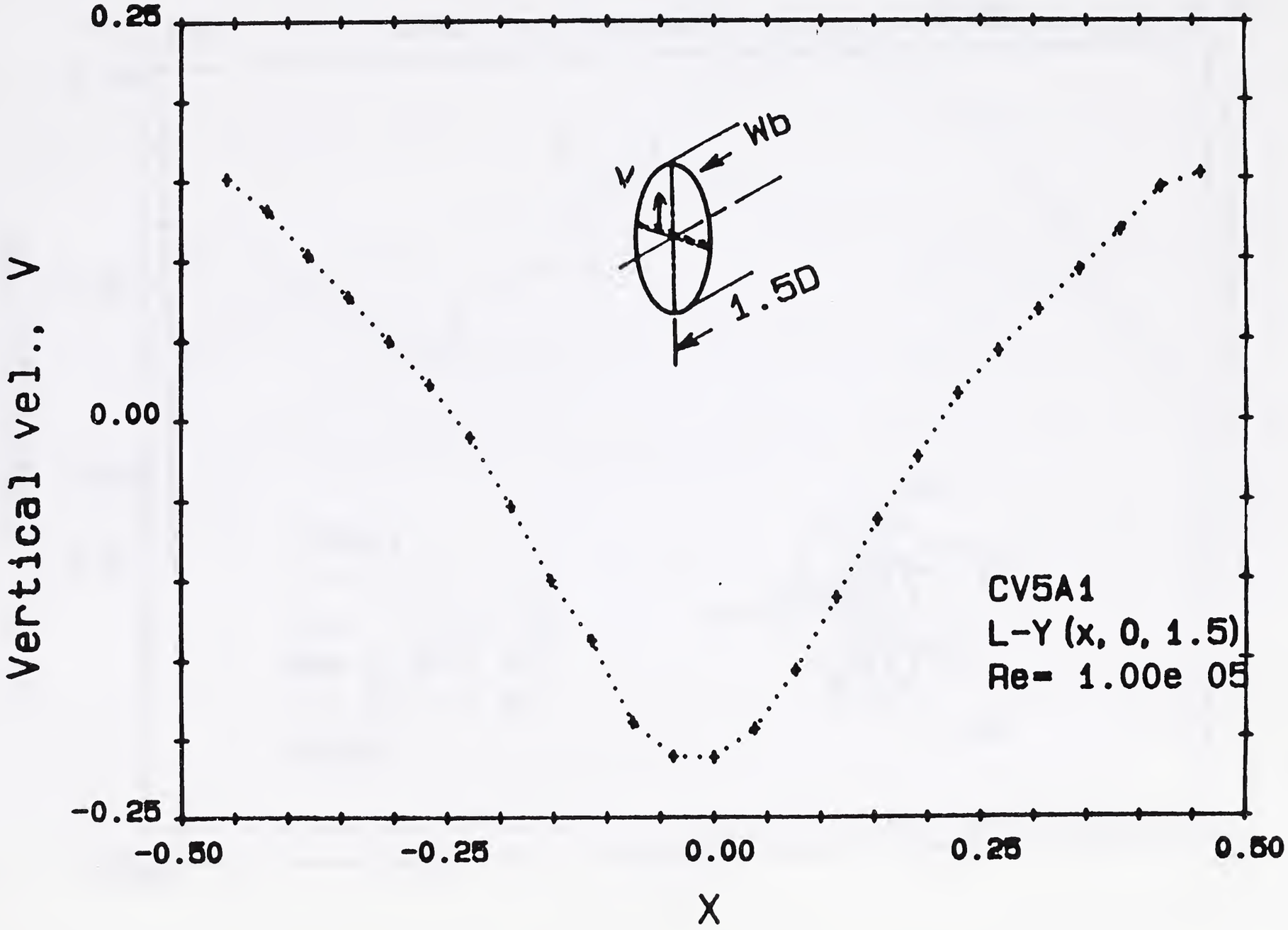


Fig. 19 The horizontal profiles of the mean vertical velocity for $Re = 10^5$

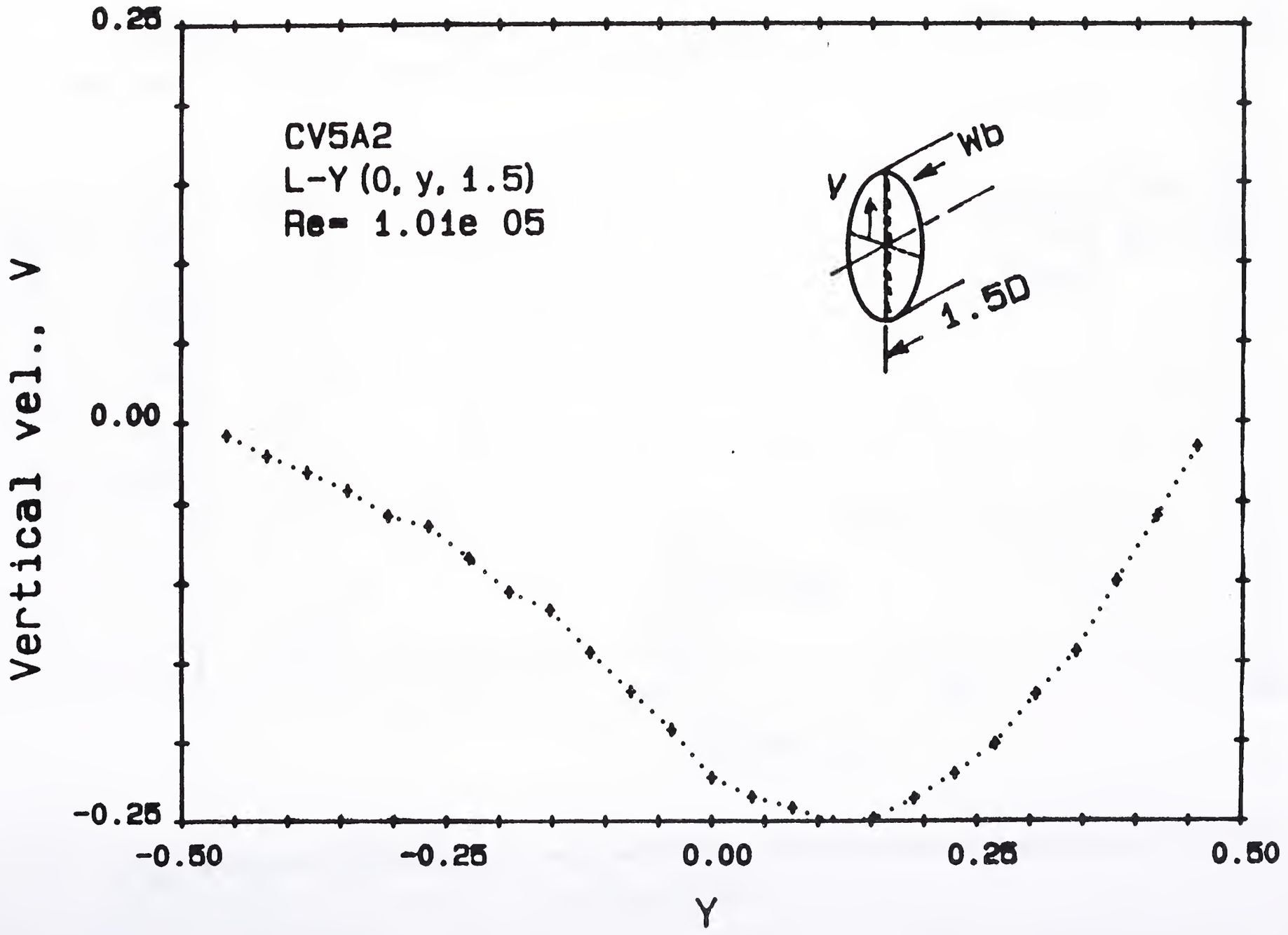


Fig. 20 The vertical profile of the mean vertical velocity for $Re = 10^6$

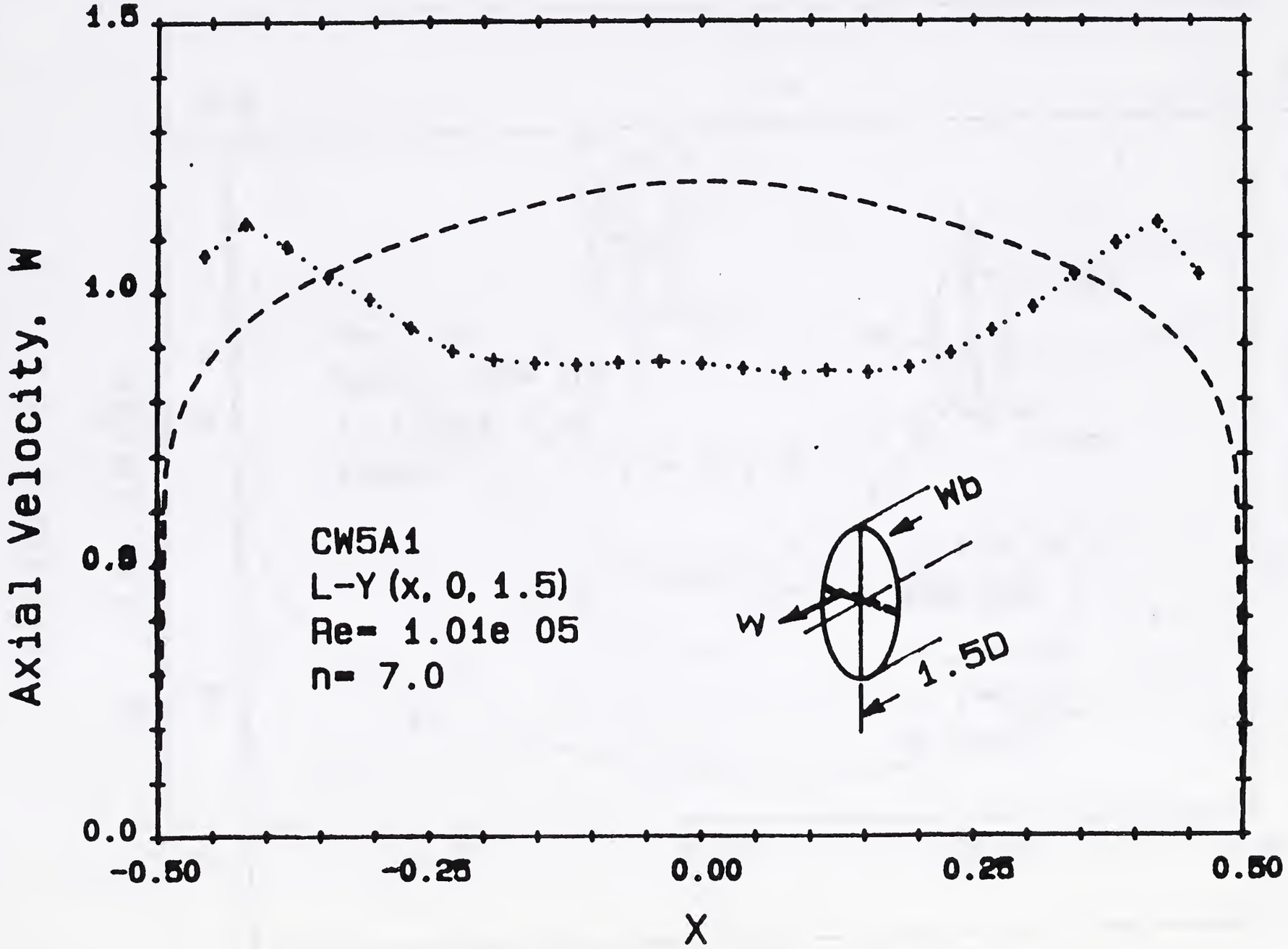


Fig. 21 The horizontal profile of the mean axial velocity for $Re = 10^5$

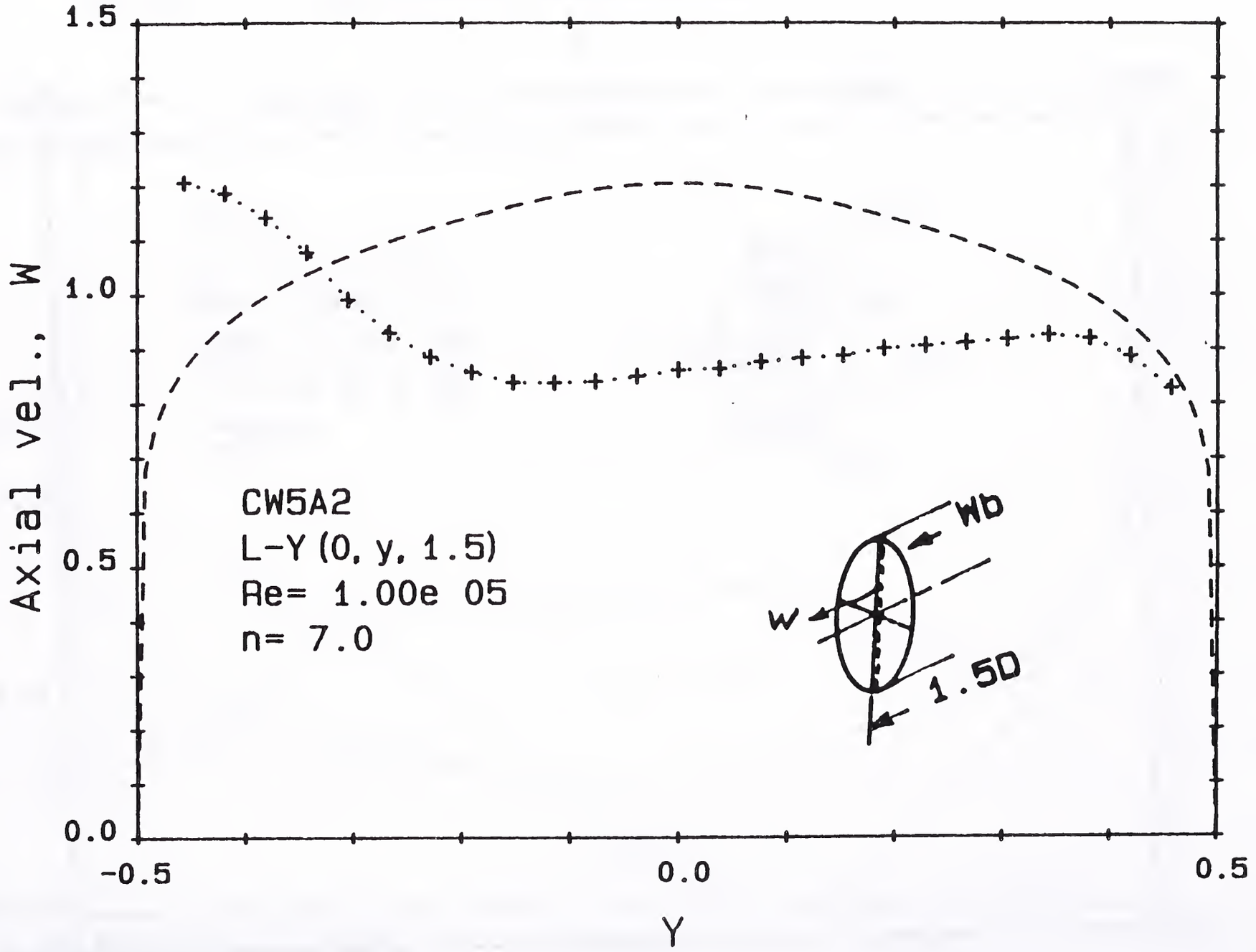


Fig. 22 The vertical profile of the mean axial velocity for $Re = 10^5$

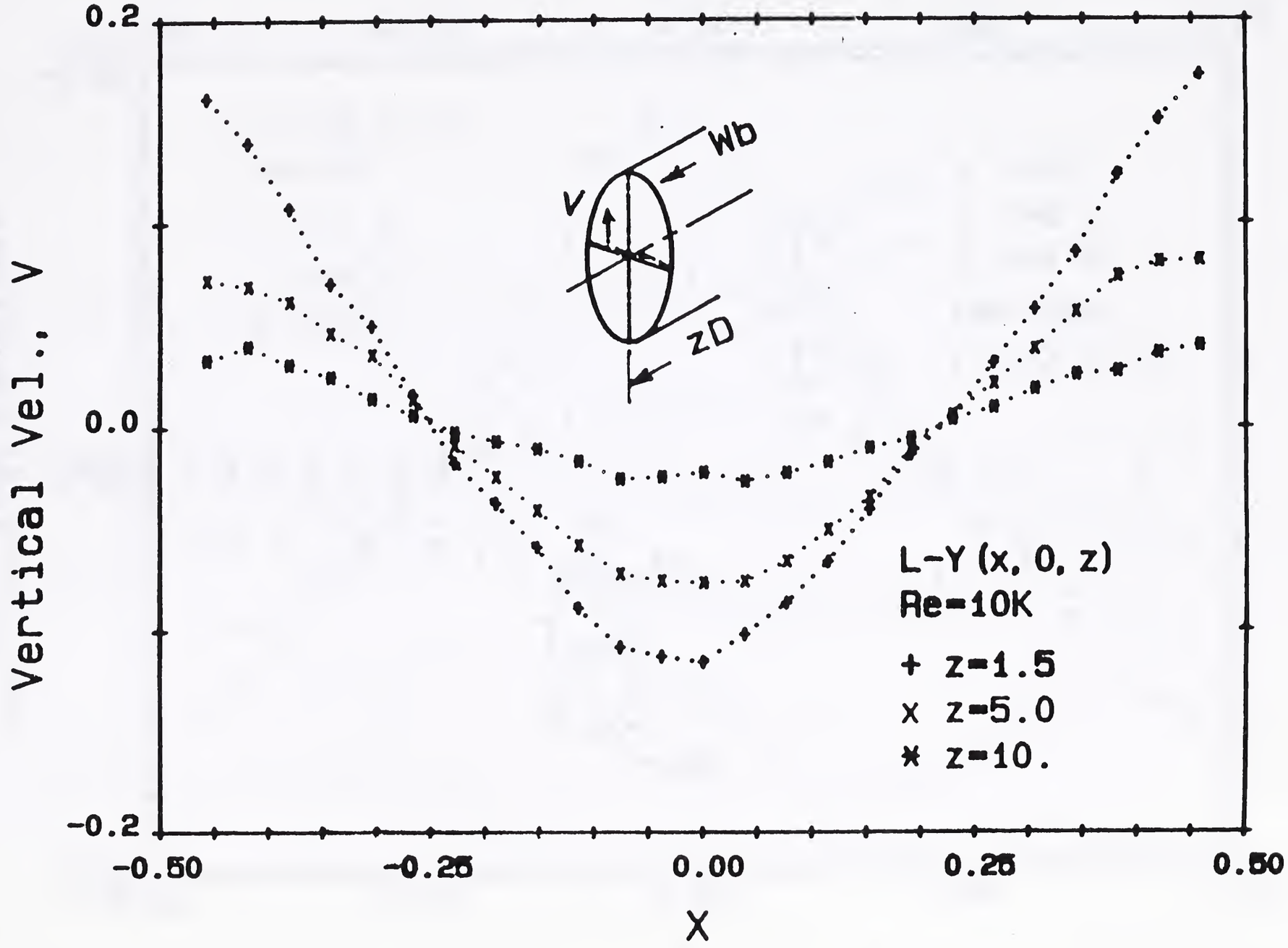


Fig. 23 (a) The horizontal profiles of the mean vertical velocities for $Re = 10^4$

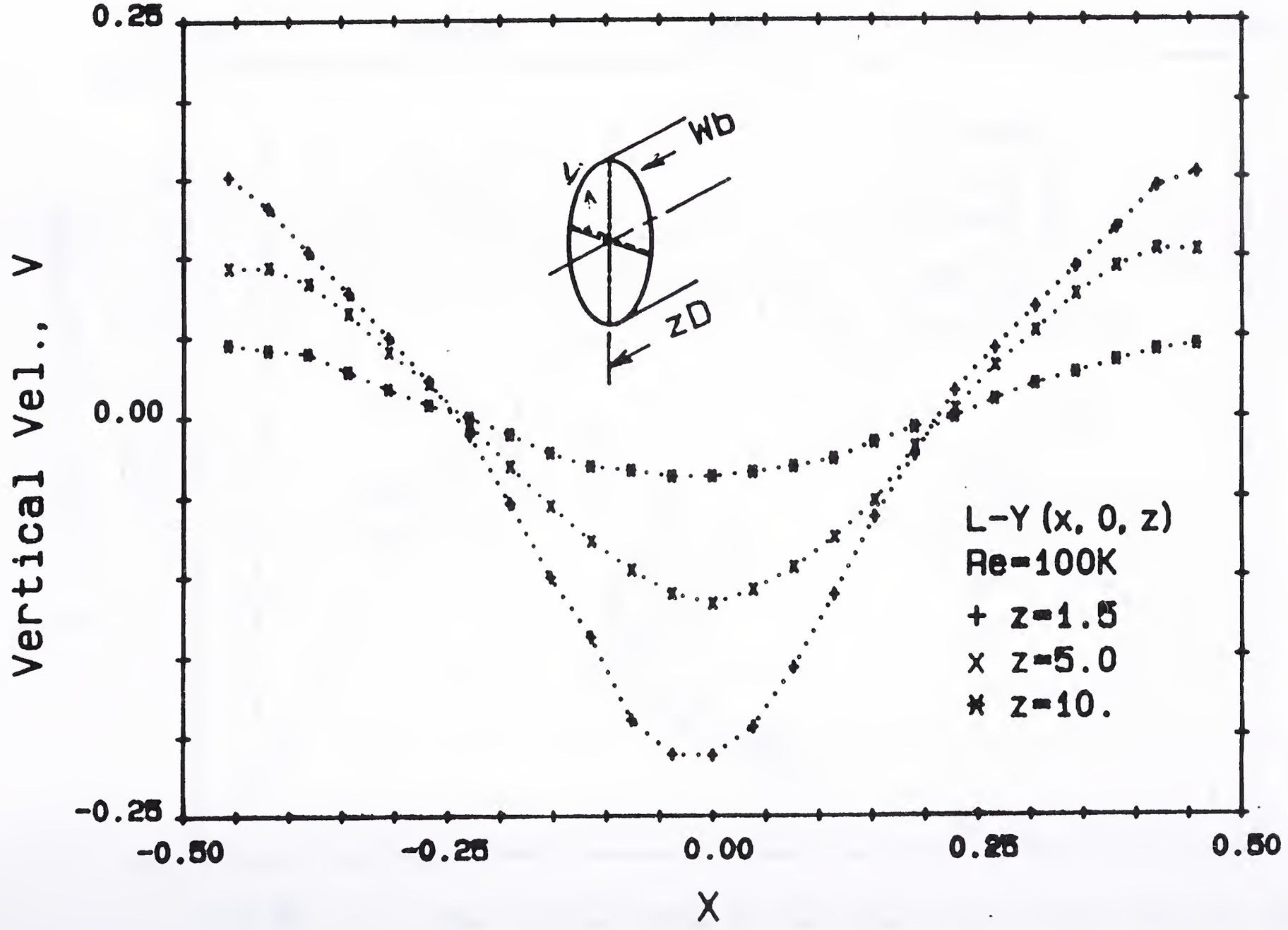


Fig. 23 (b) The horizontal profiles of the mean vertical velocities for $Re = 10^6$

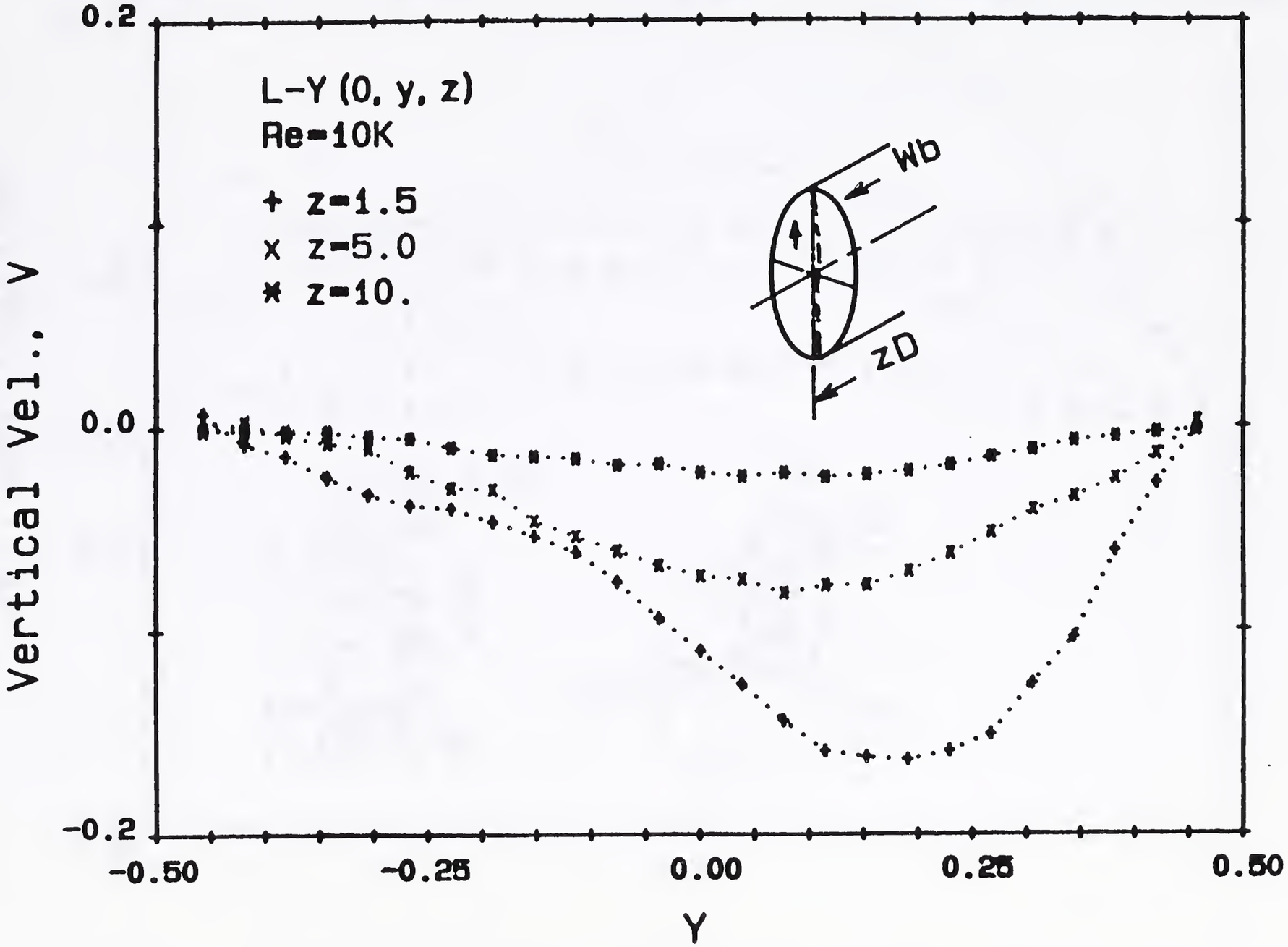


Fig. 24 (a) The vertical profiles of the mean vertical velocities for $Re = 10^4$

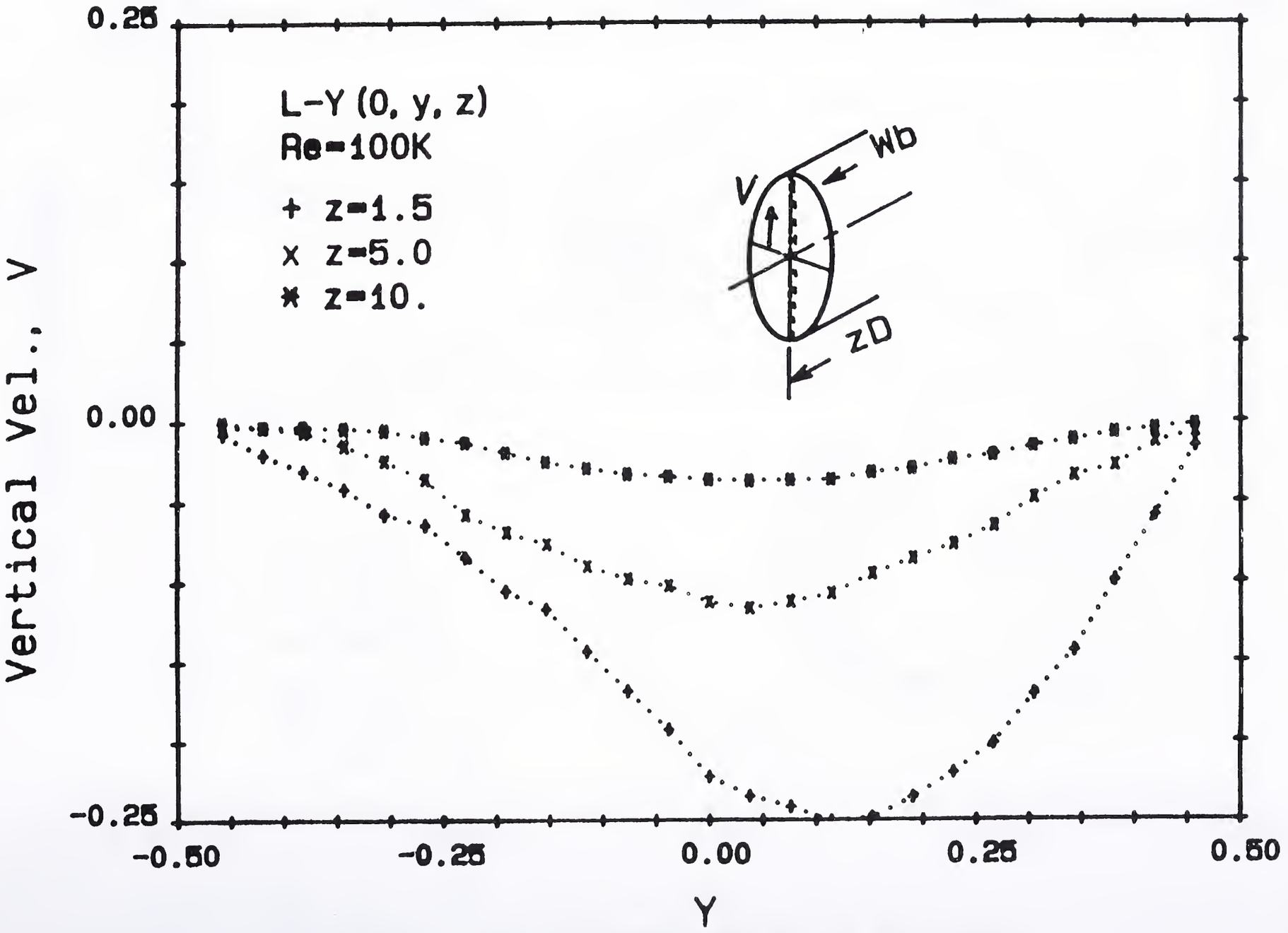


Fig. 24 (b) The vertical profiles of the mean vertical velocities for $Re = 10^5$

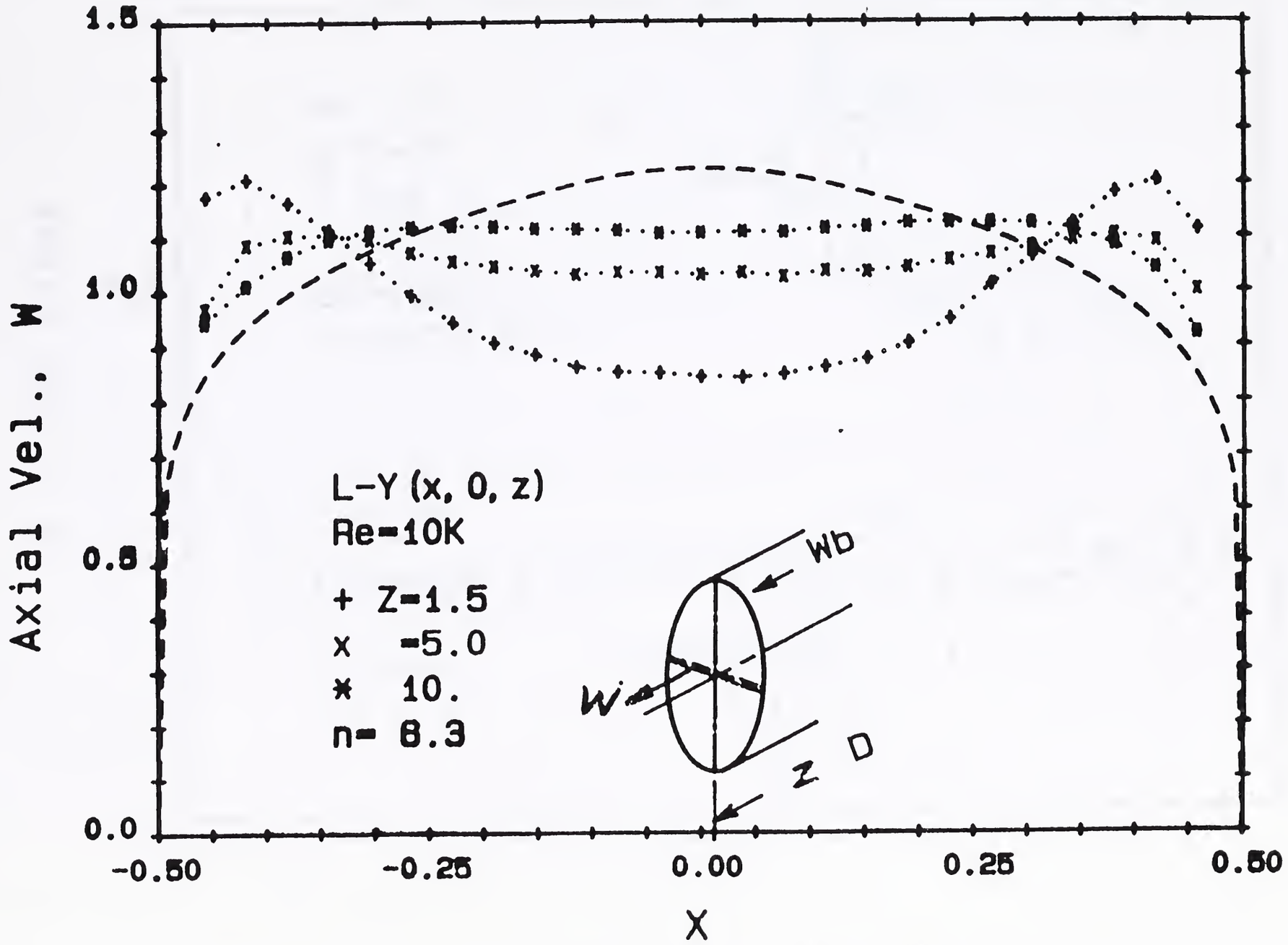


Fig. 25 (a) The horizontal profiles of the mean axial velocities for $Re = 10^4$

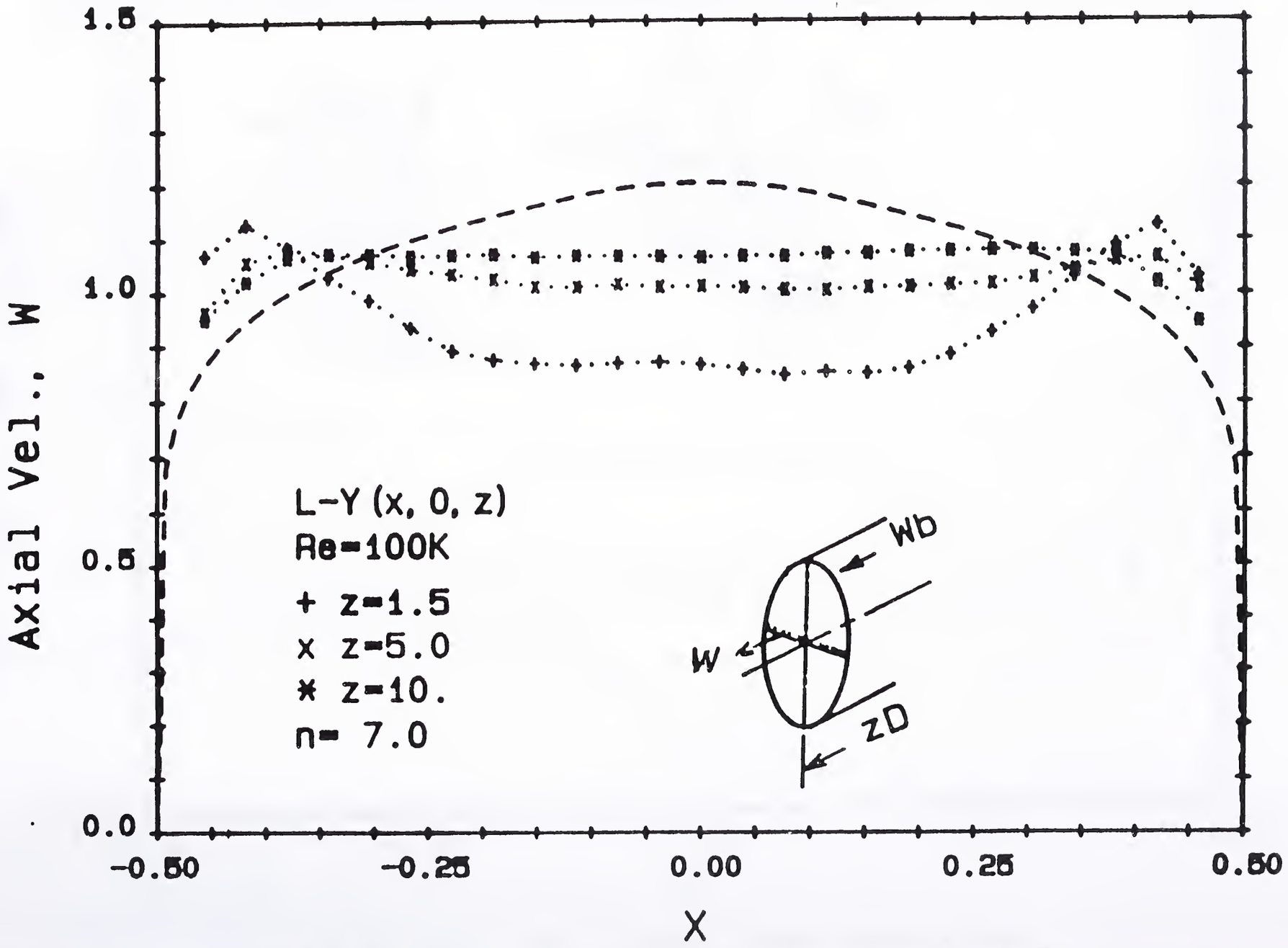


Fig. 25 (b) The horizontal profiles of the mean

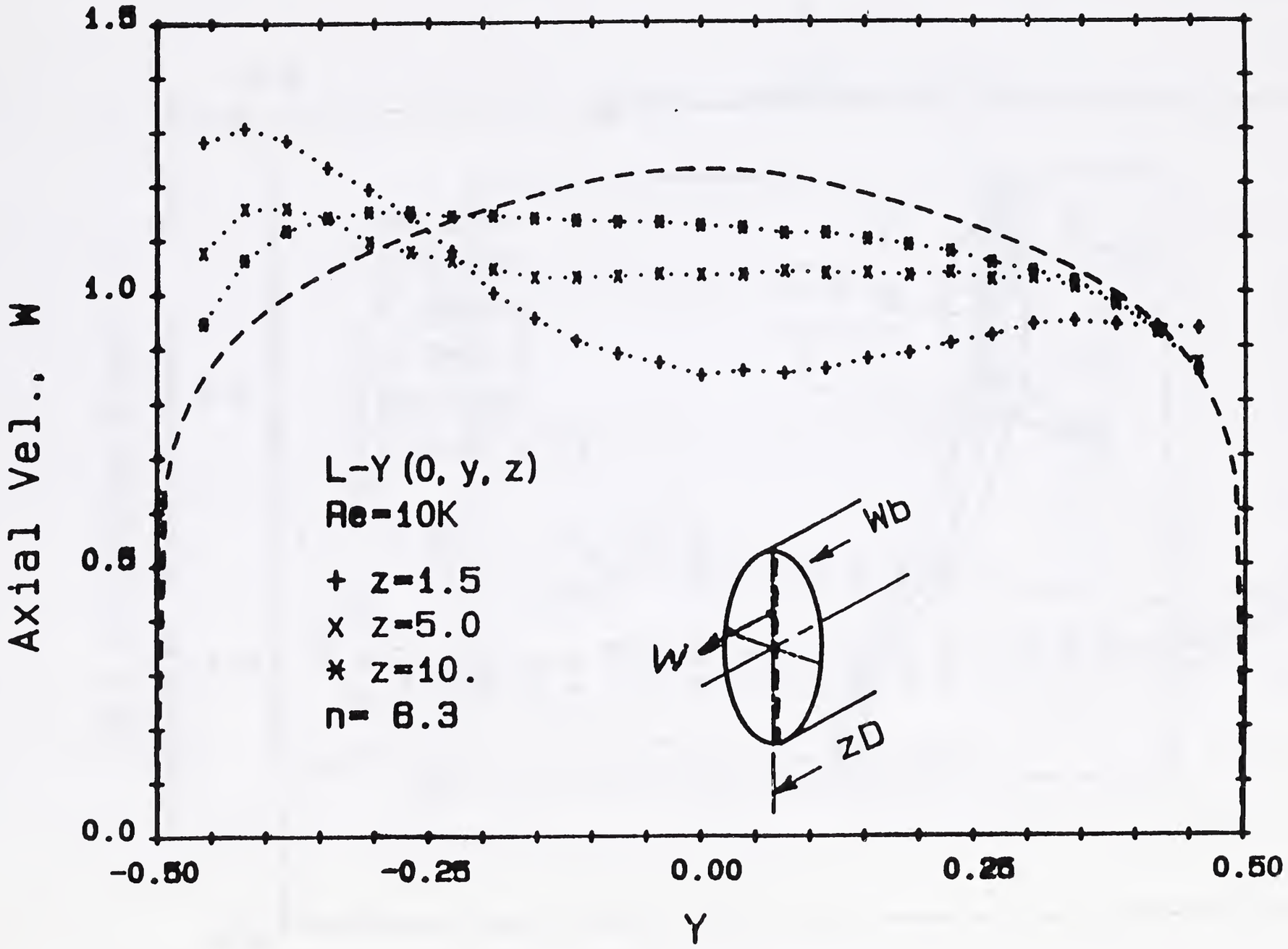


Fig. 26 (a) The vertical profiles of the mean axial velocities for $Re = 10^4$

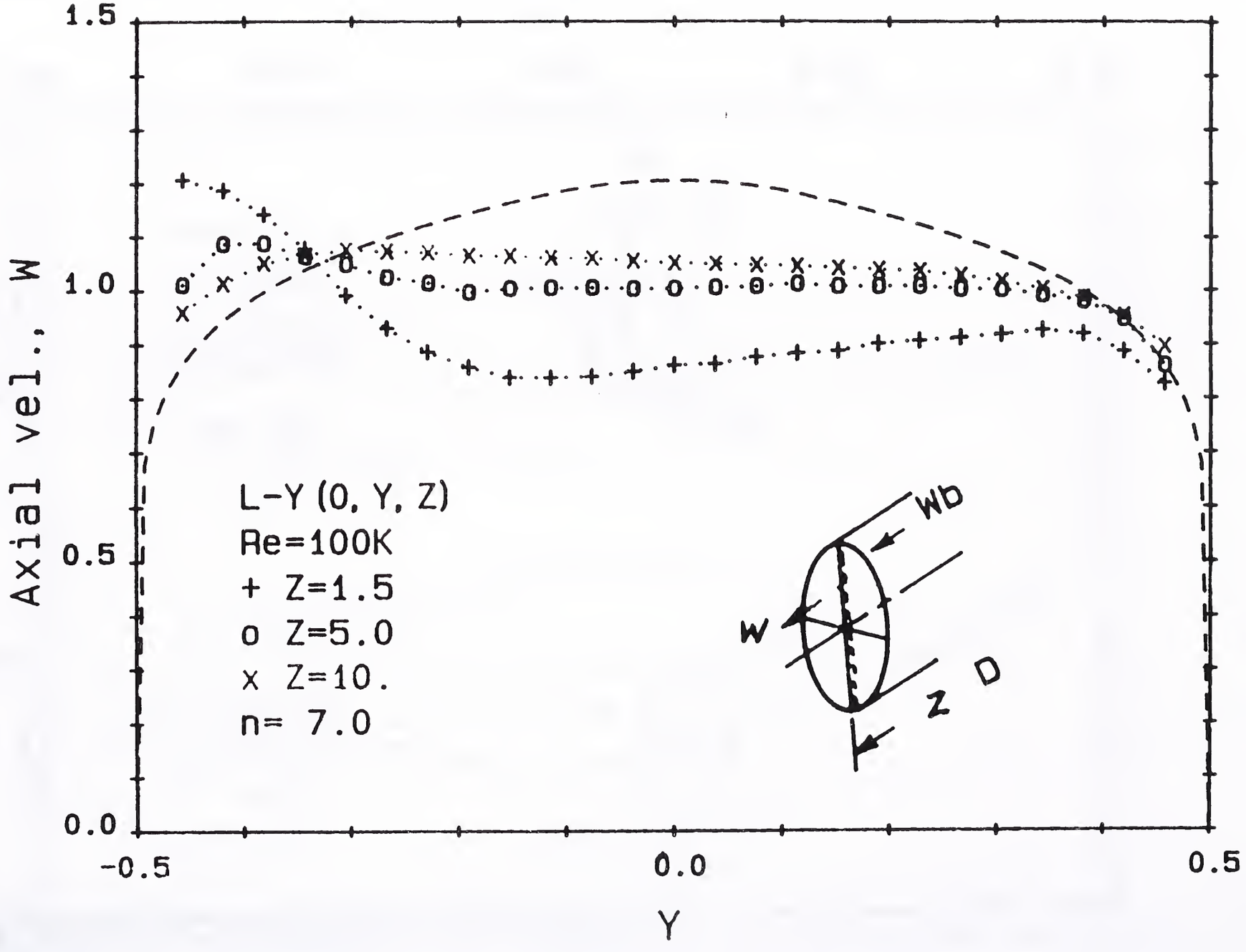


Fig. 26 (b) The vertical profiles of the mean axial velocities for $Re = 10^6$

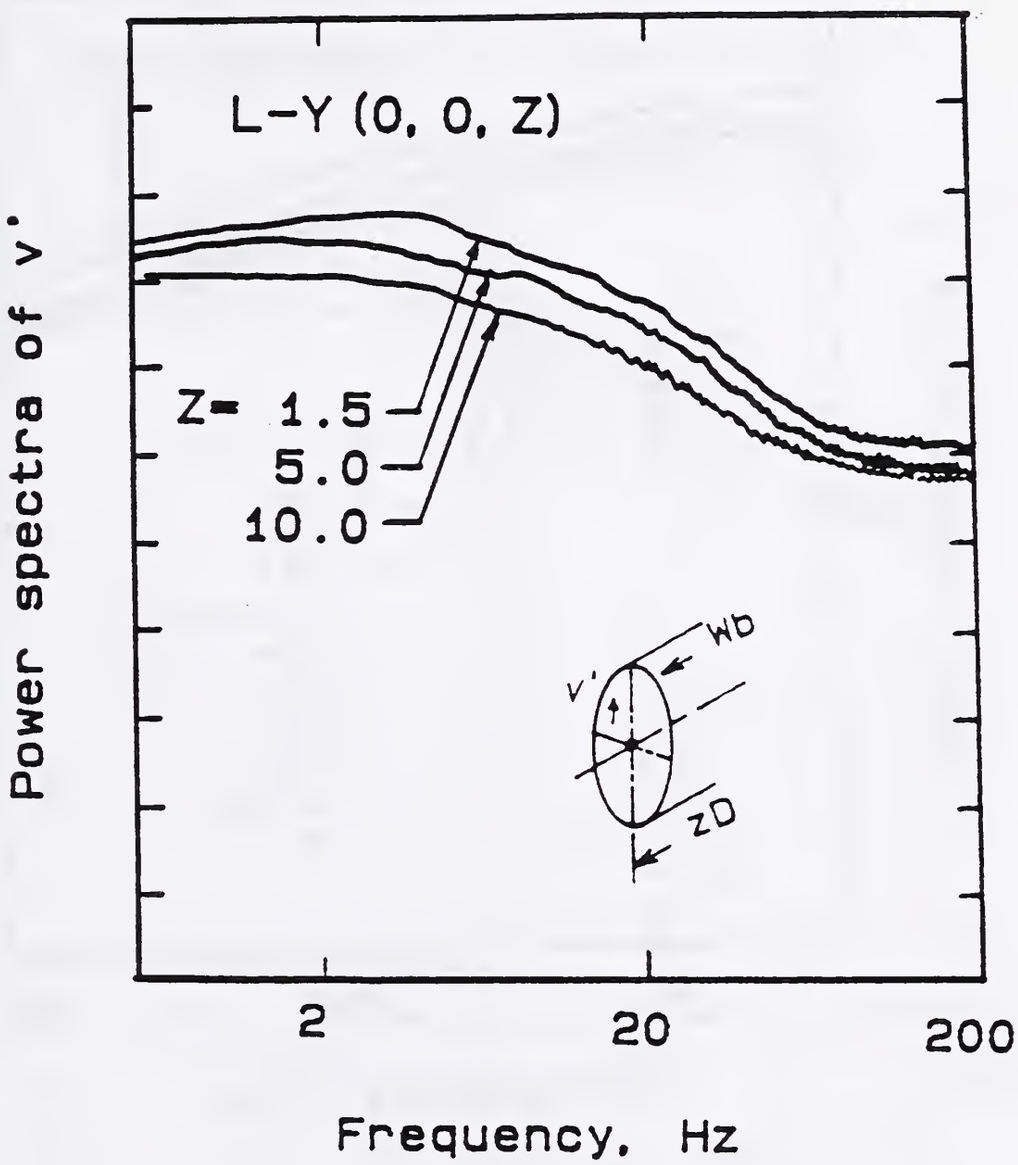


Fig. 27 (a) **Power spectra for the turbulence vertical velocities for Re = 10^4**

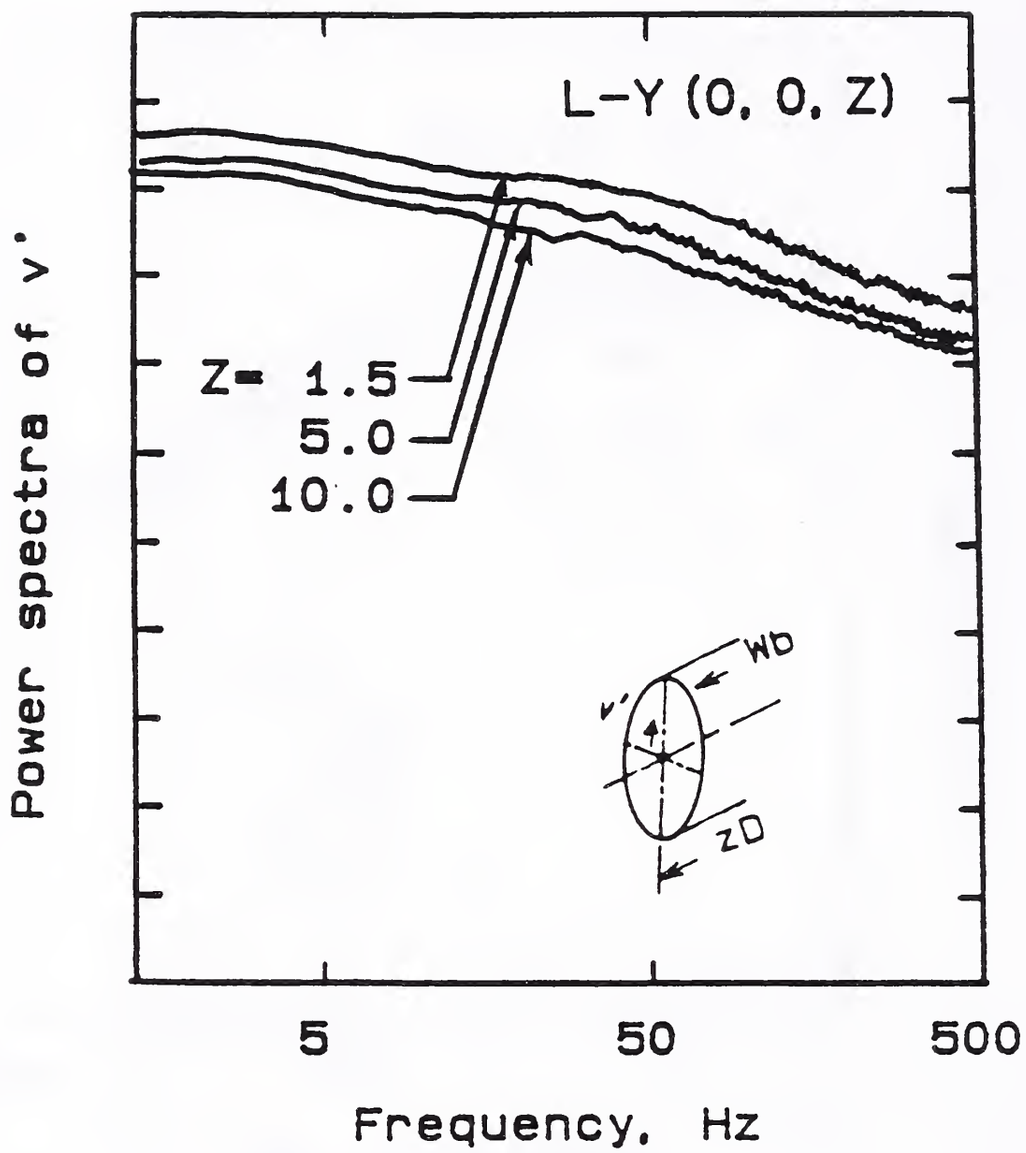


Fig. 27 (b) **Power spectra for the turbulence vertical velocities for Re = 10^5**

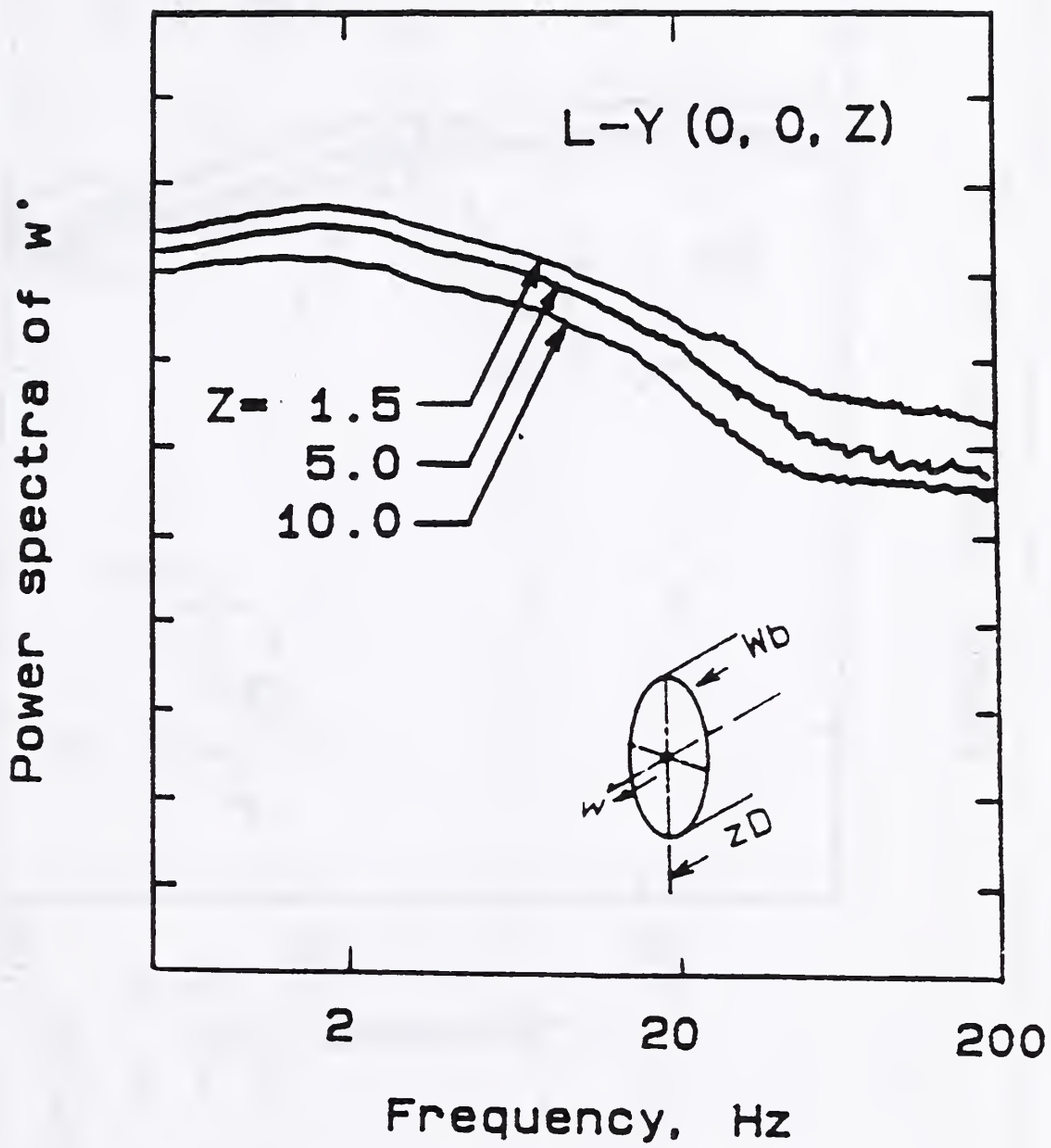


Fig. 28 (a) **Power spectra for the turbulence axial velocities for Re = 10^4**

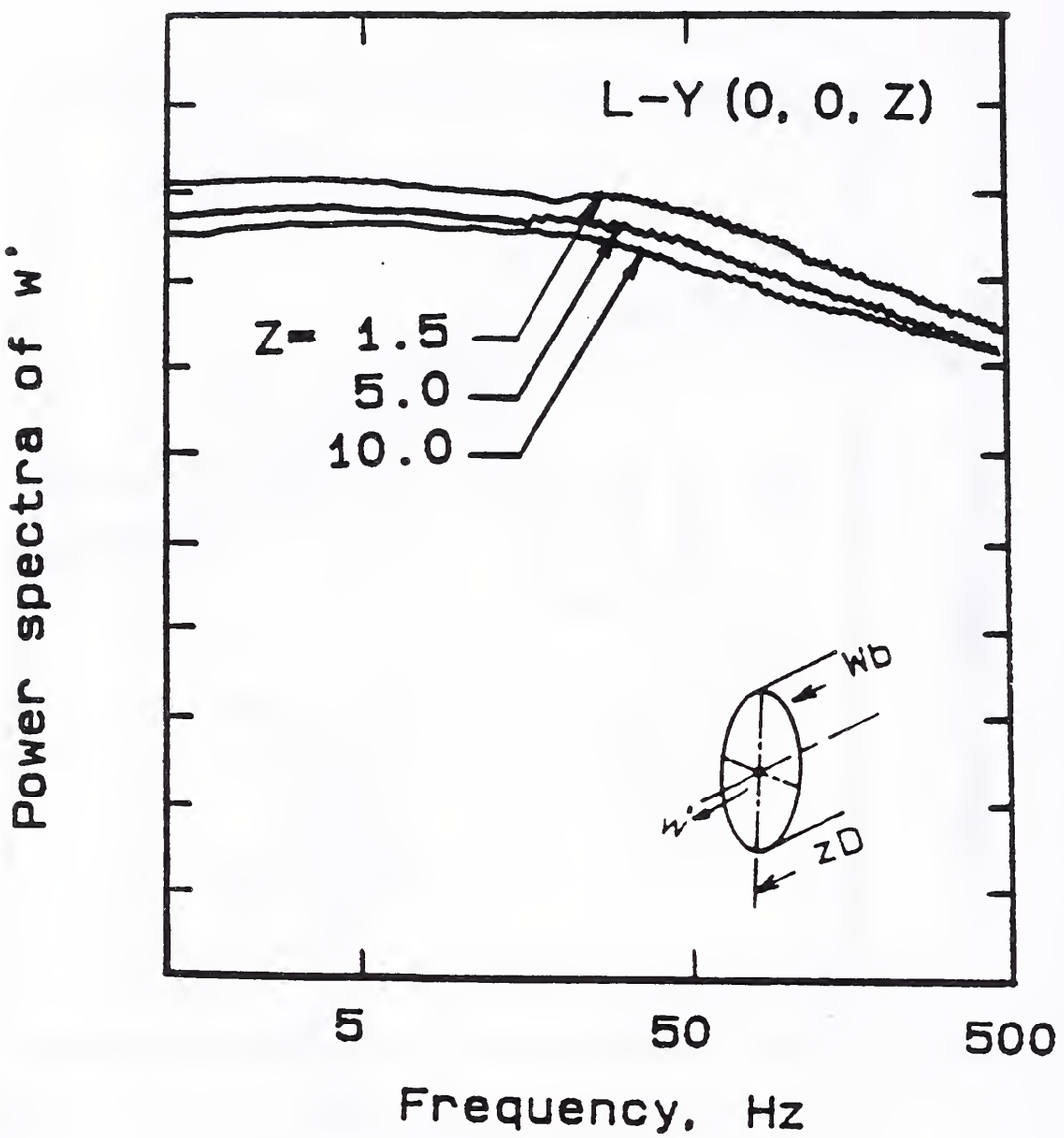


Fig. 28 (b) Power spectra for the turbulence axial velocities for $Re = 10^5$

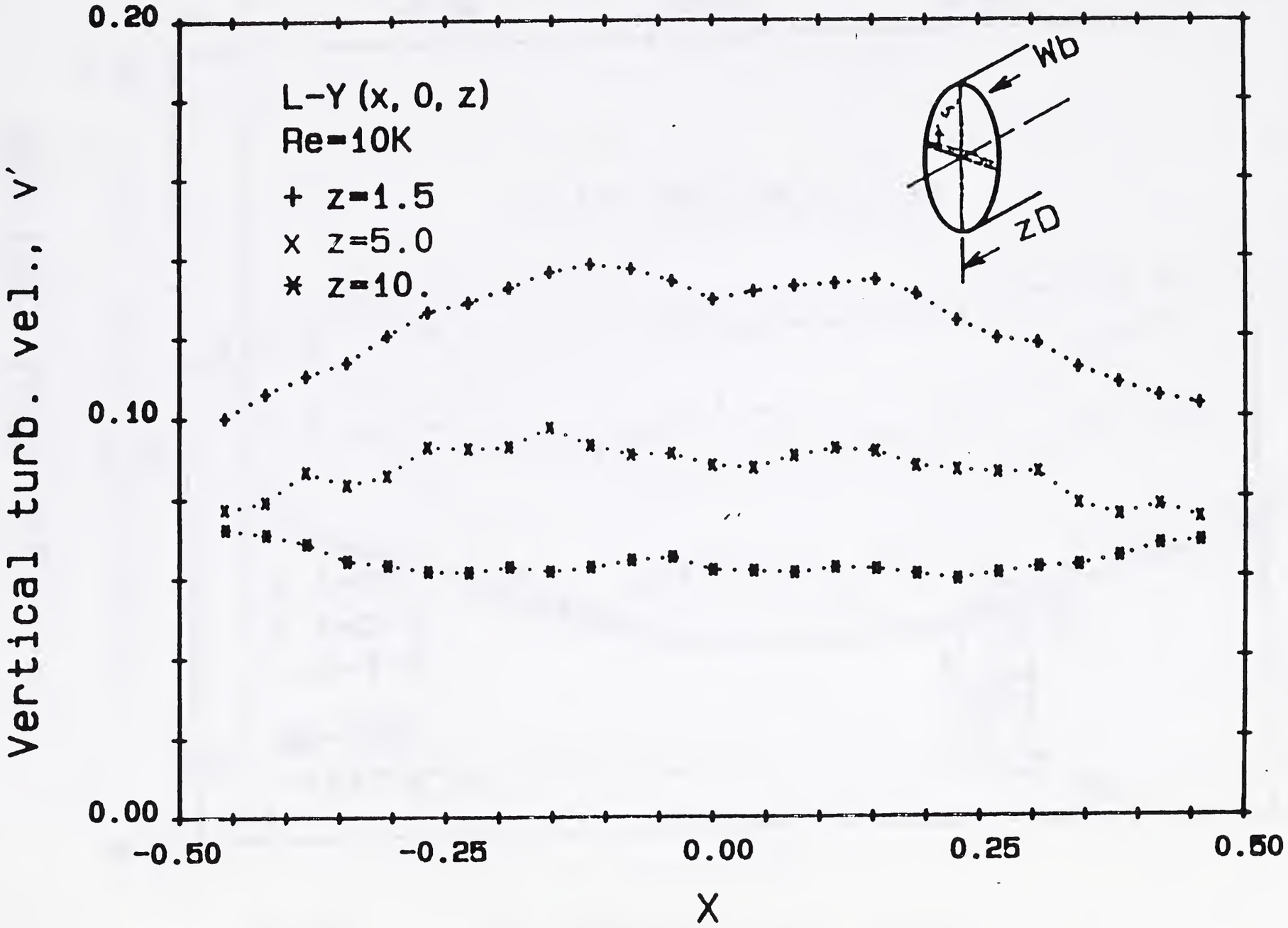


Fig. 29 (a) The horizontal profiles of the turbulence vertical velocities for Re = 10^4

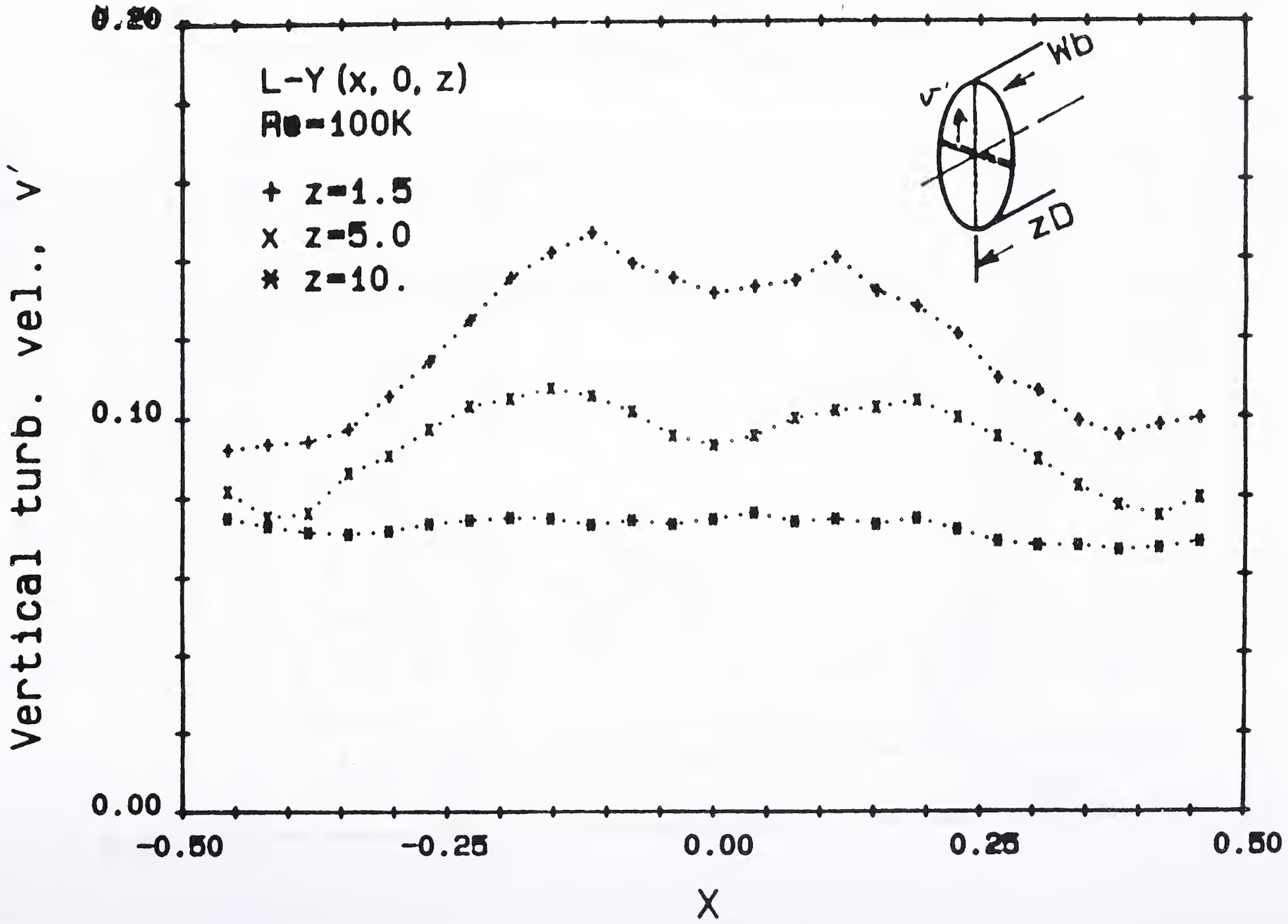


Fig. 29 (b) The horizontal profiles of the

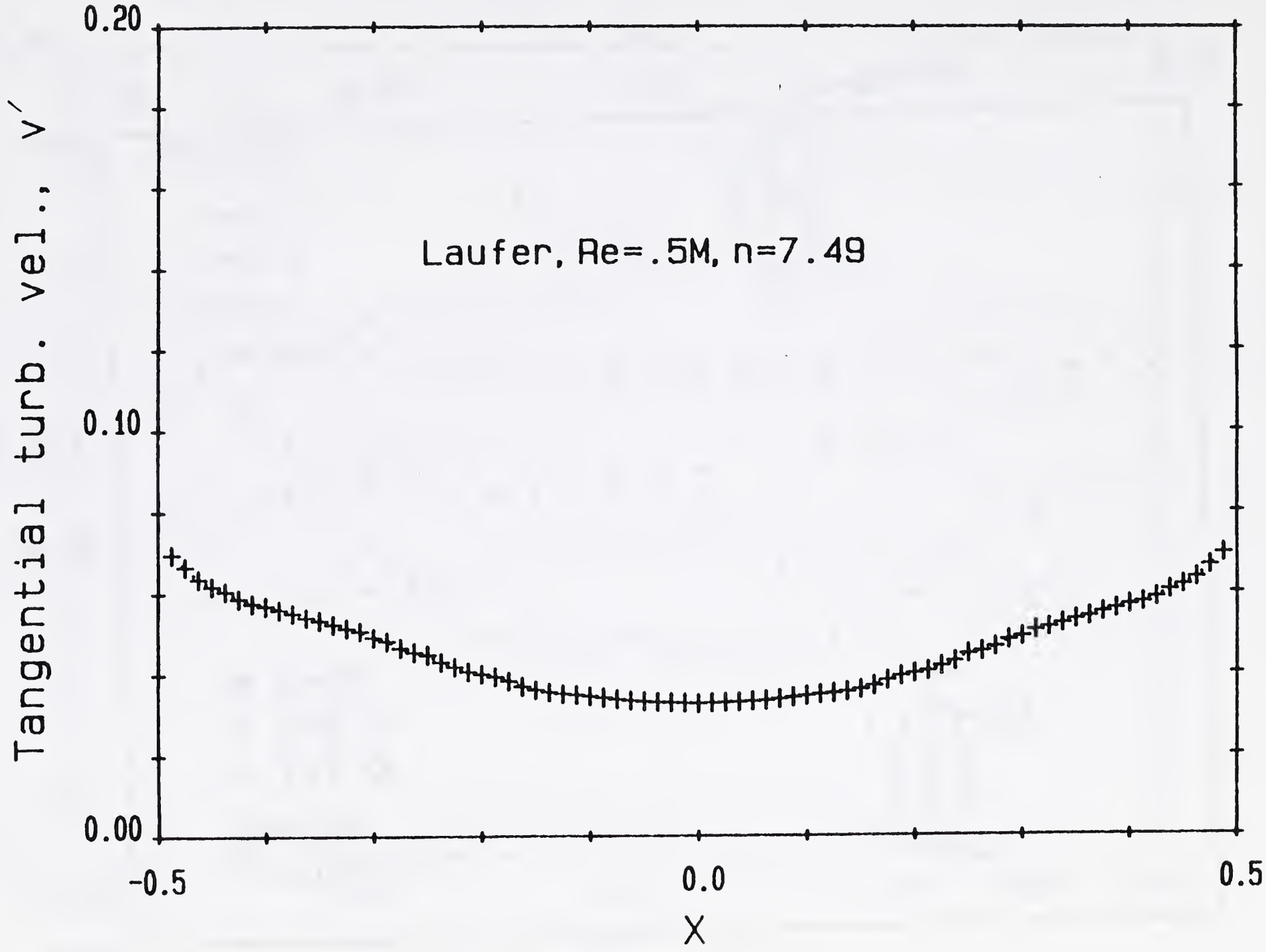


Fig. 30 The tangential turbulence velocity profile from Laufer's data, $Re = 5 \times 10^5$

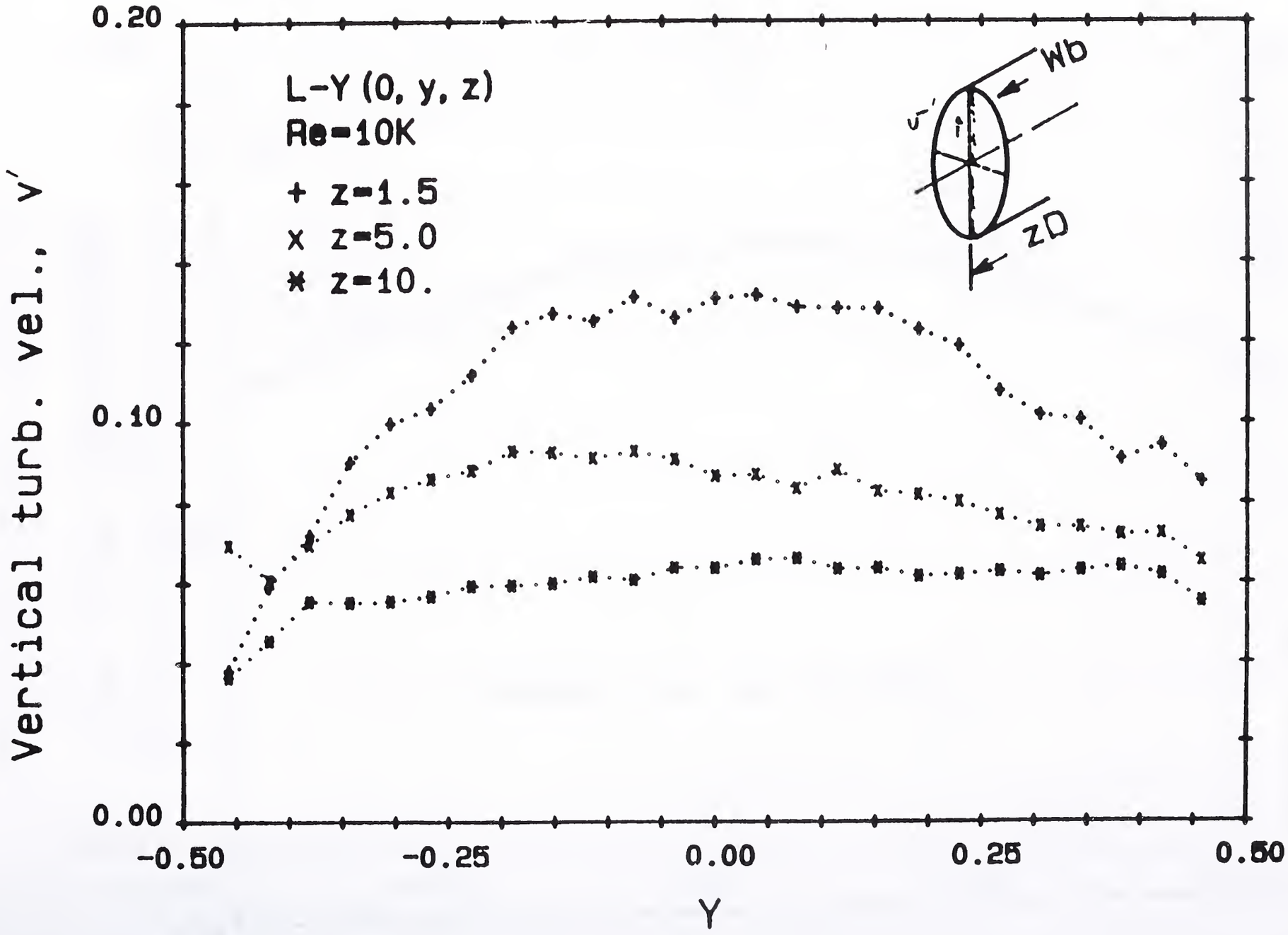


Fig. 31 (a) The vertical profiles of the turbulence vertical velocities for $Re = 10^4$

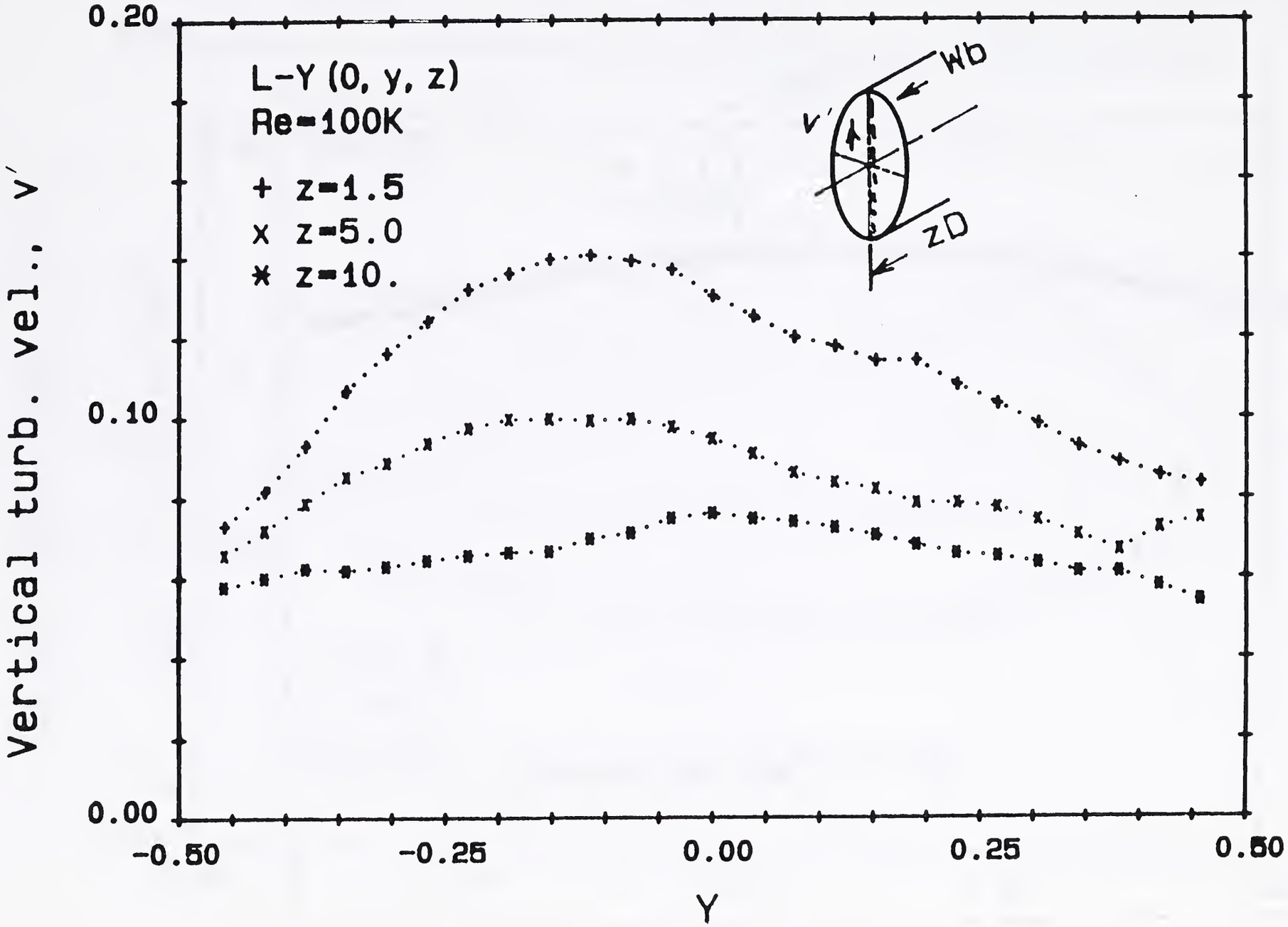


Fig. 31 (b) The vertical profiles of the turbulence vertical velocities for $Re = 10^6$

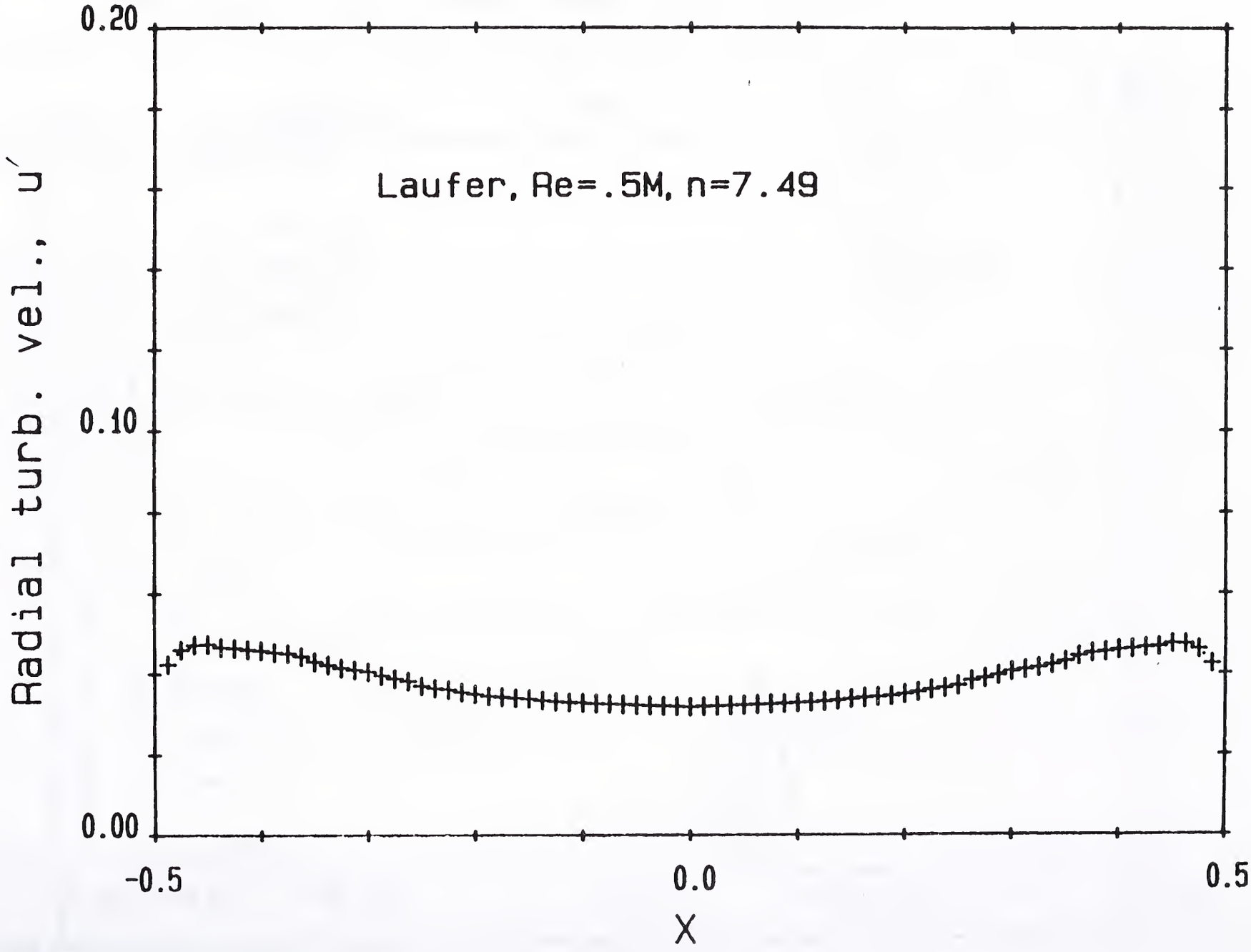


Fig. 32 The radial turbulence velocity profile from Laufer's data, $Re = 5 \times 10^5$

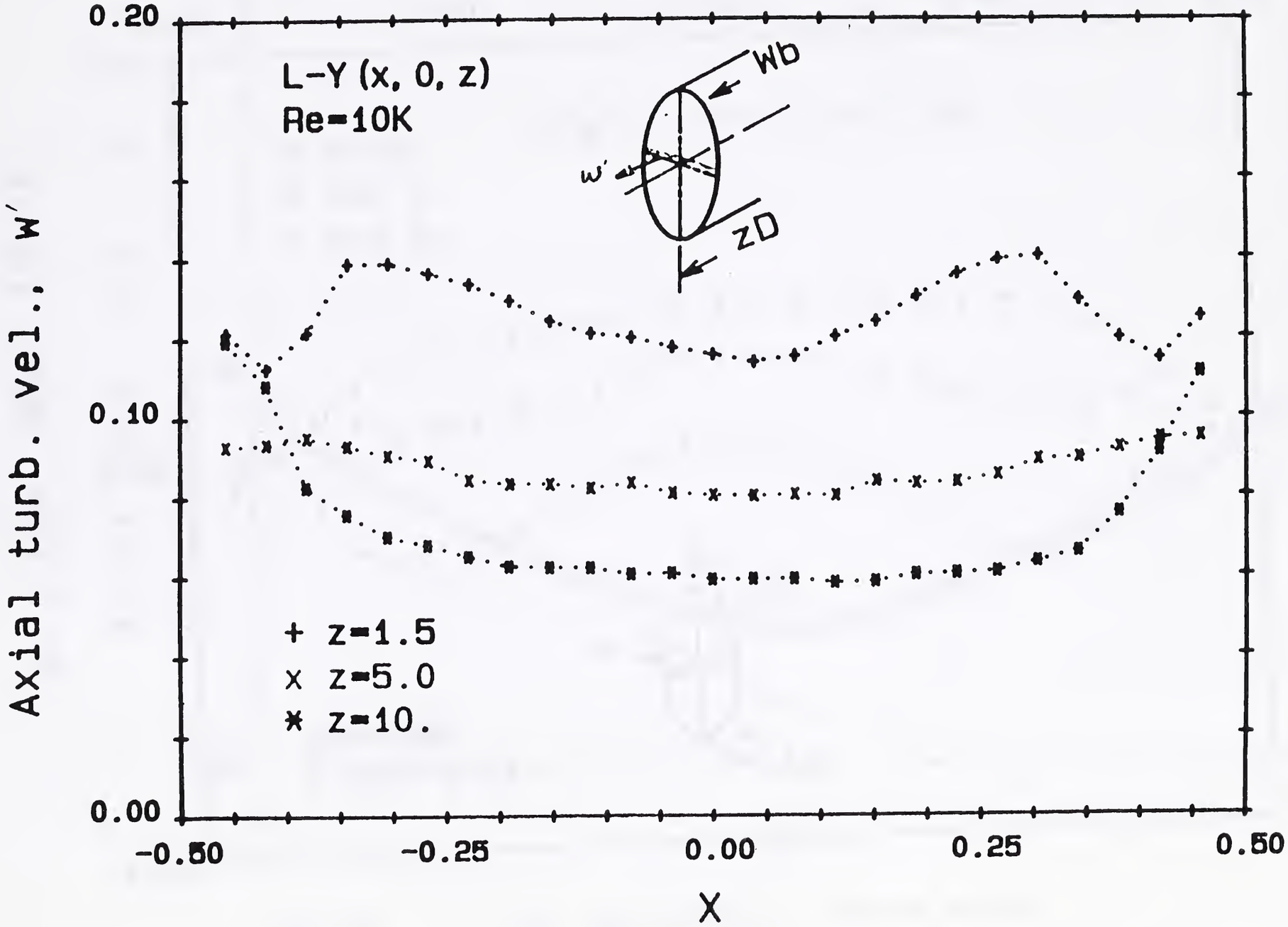


Fig. 33 (a) The horizontal profiles of the turbulence axial velocities for $Re = 10^4$

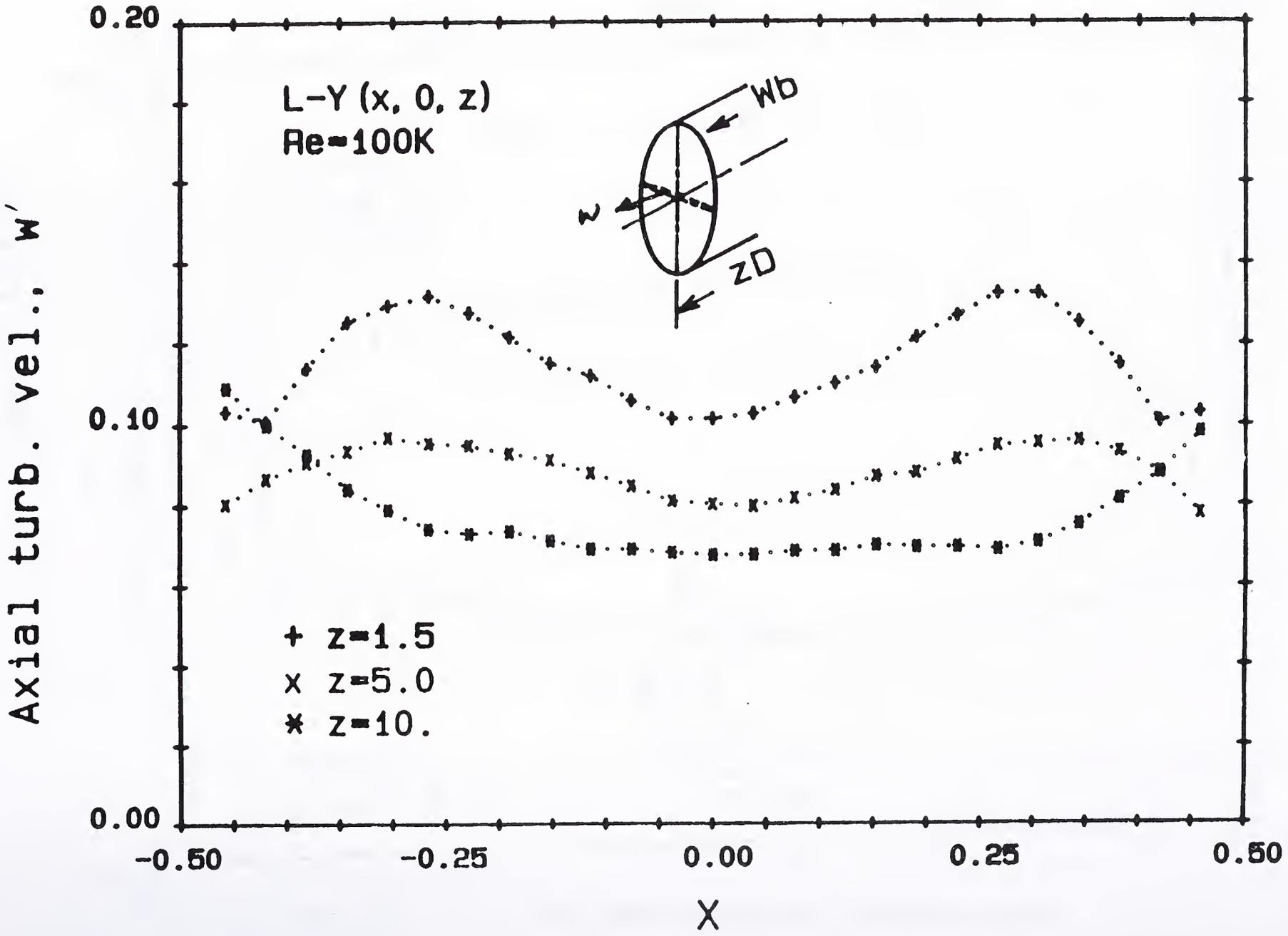


Fig. 33 (b) The horizontal profiles of the

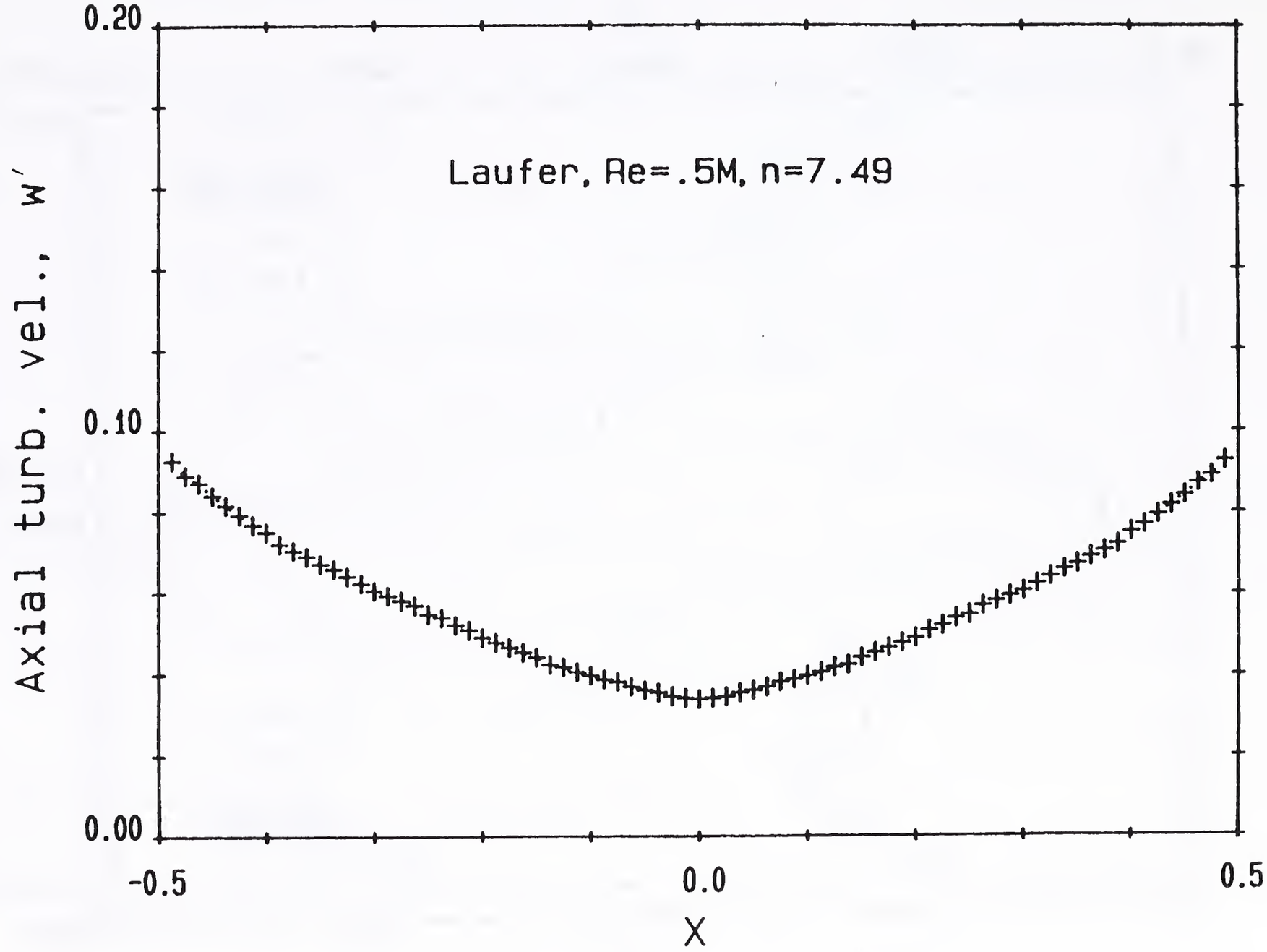


Fig. 34 The axial turbulence velocity profile from Laufer's data, Re = 5×10^6

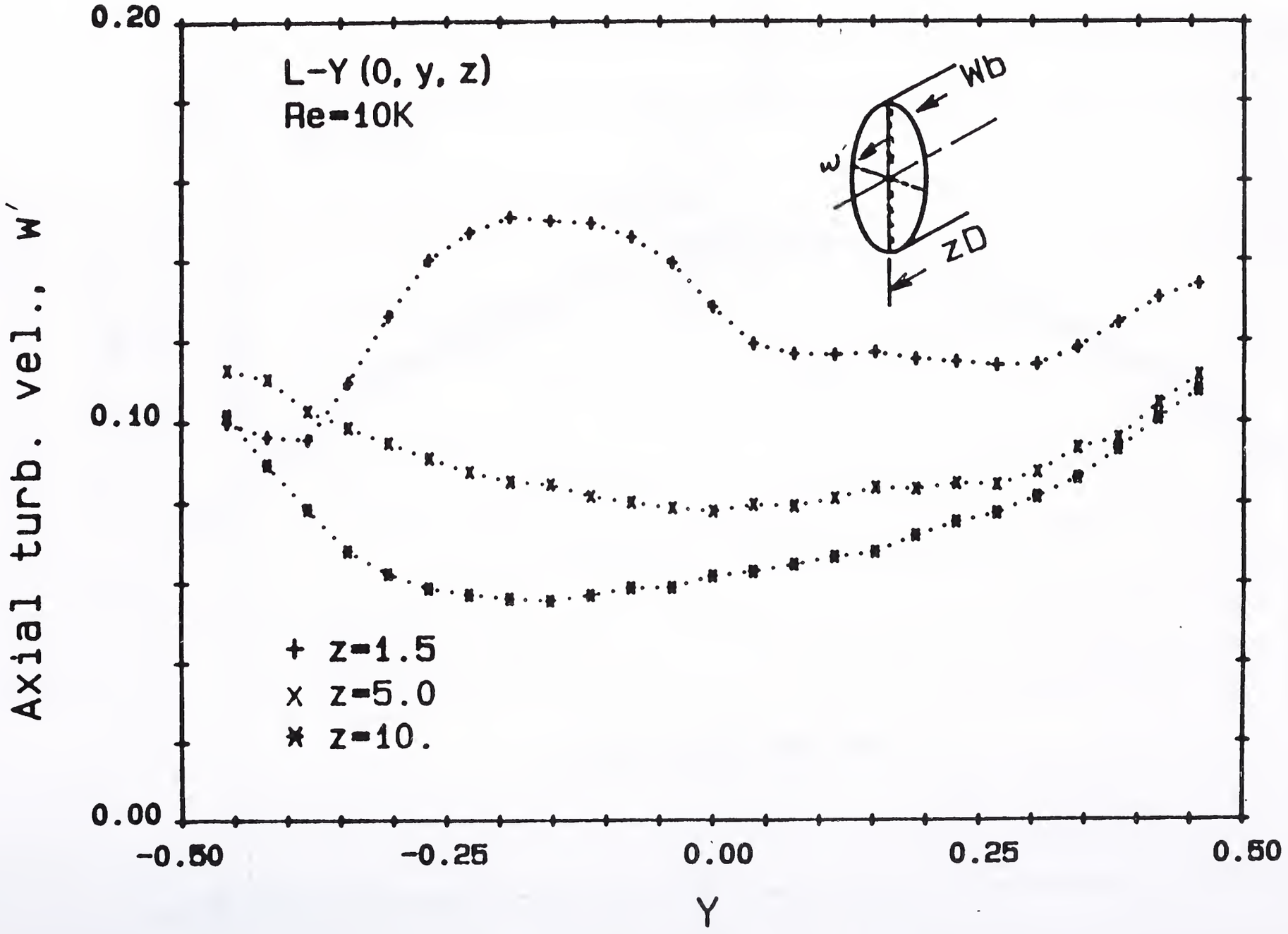


Fig. 35 (a) The vertical profiles of the turbulence

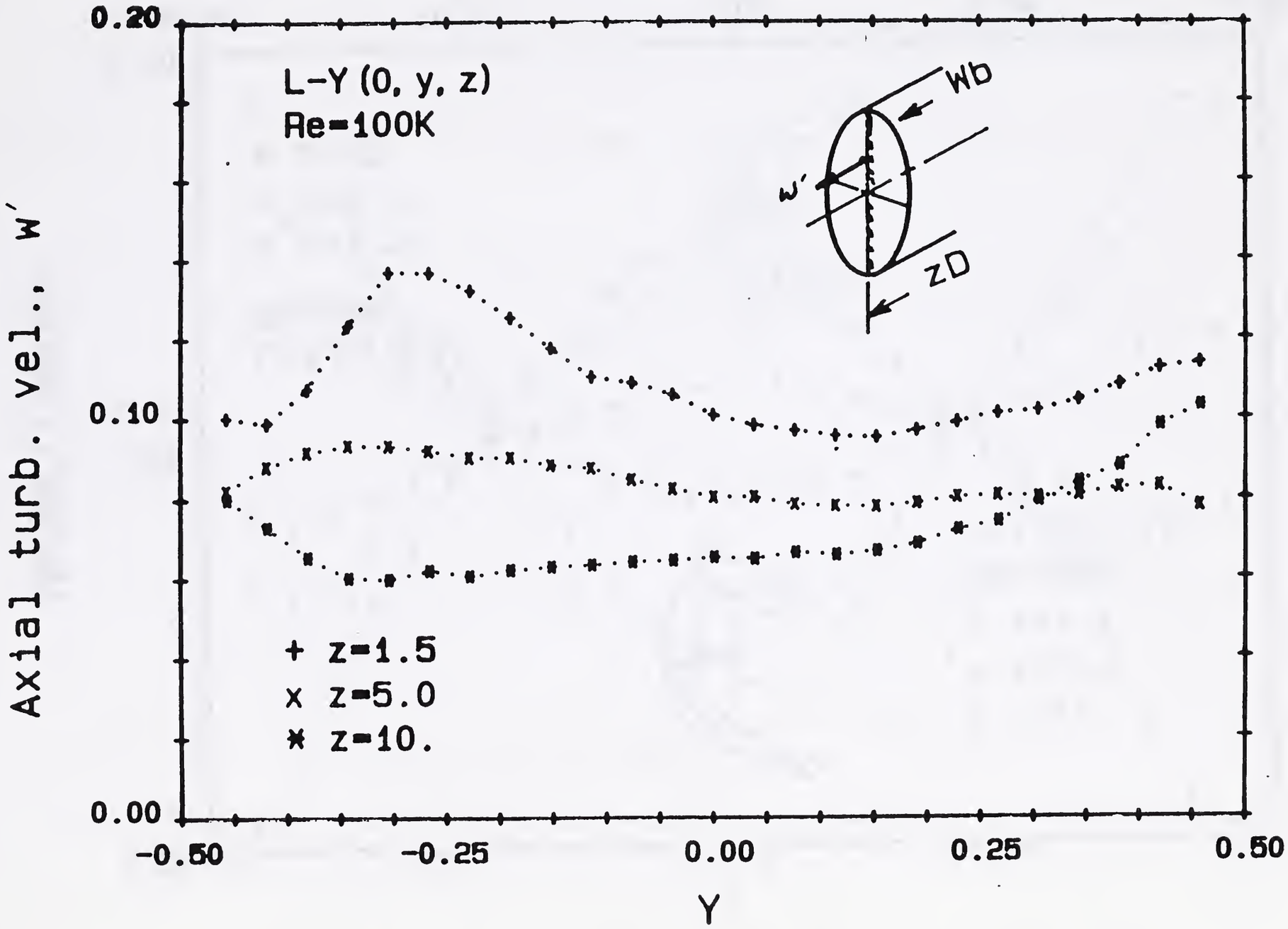


Fig. 35 (b) The vertical profiles of the turbulence axial velocities for $Re = 10^5$

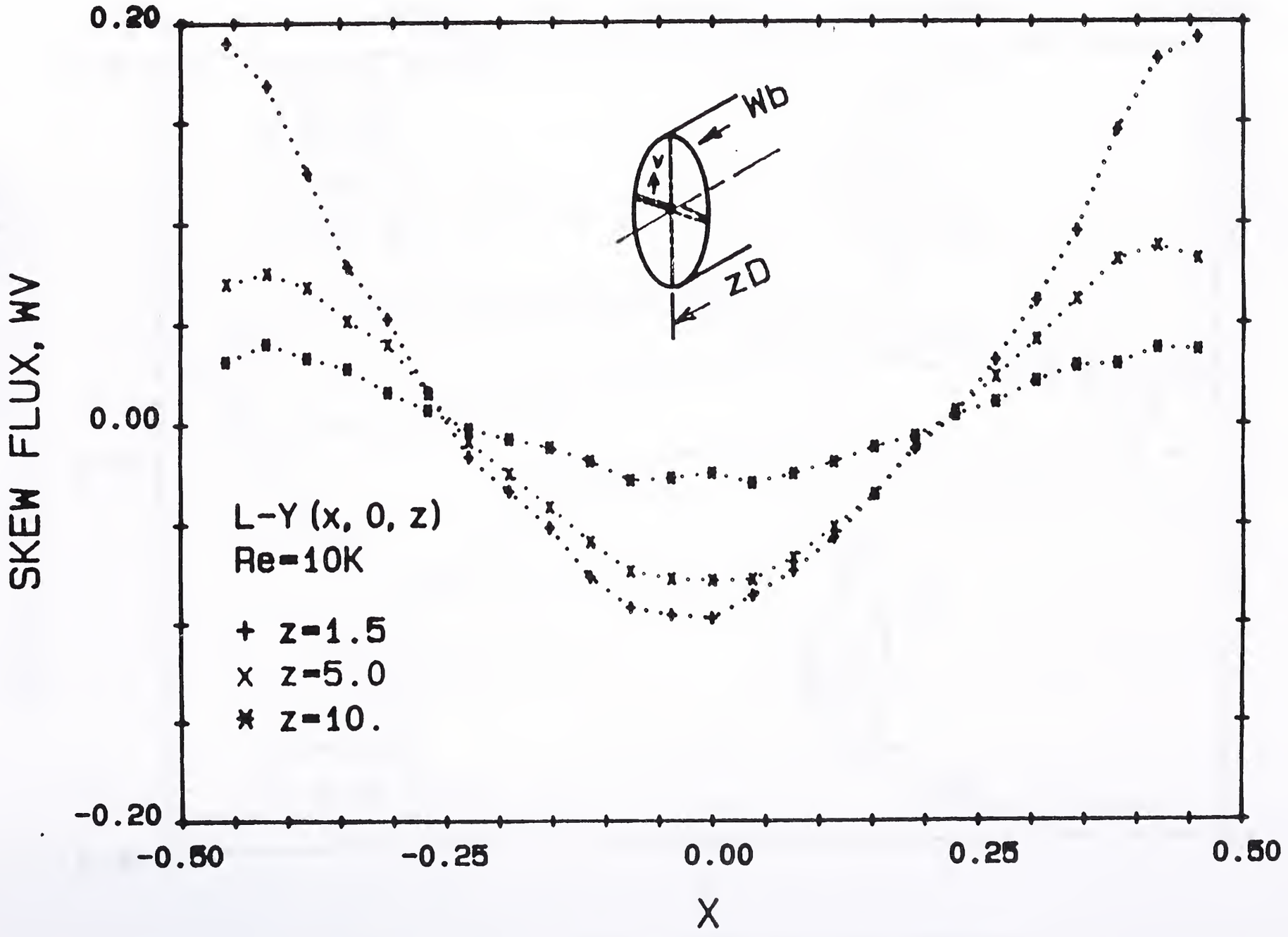


Fig. 36 (a) The horizontal profiles of skew flux for $Re = 10^4$

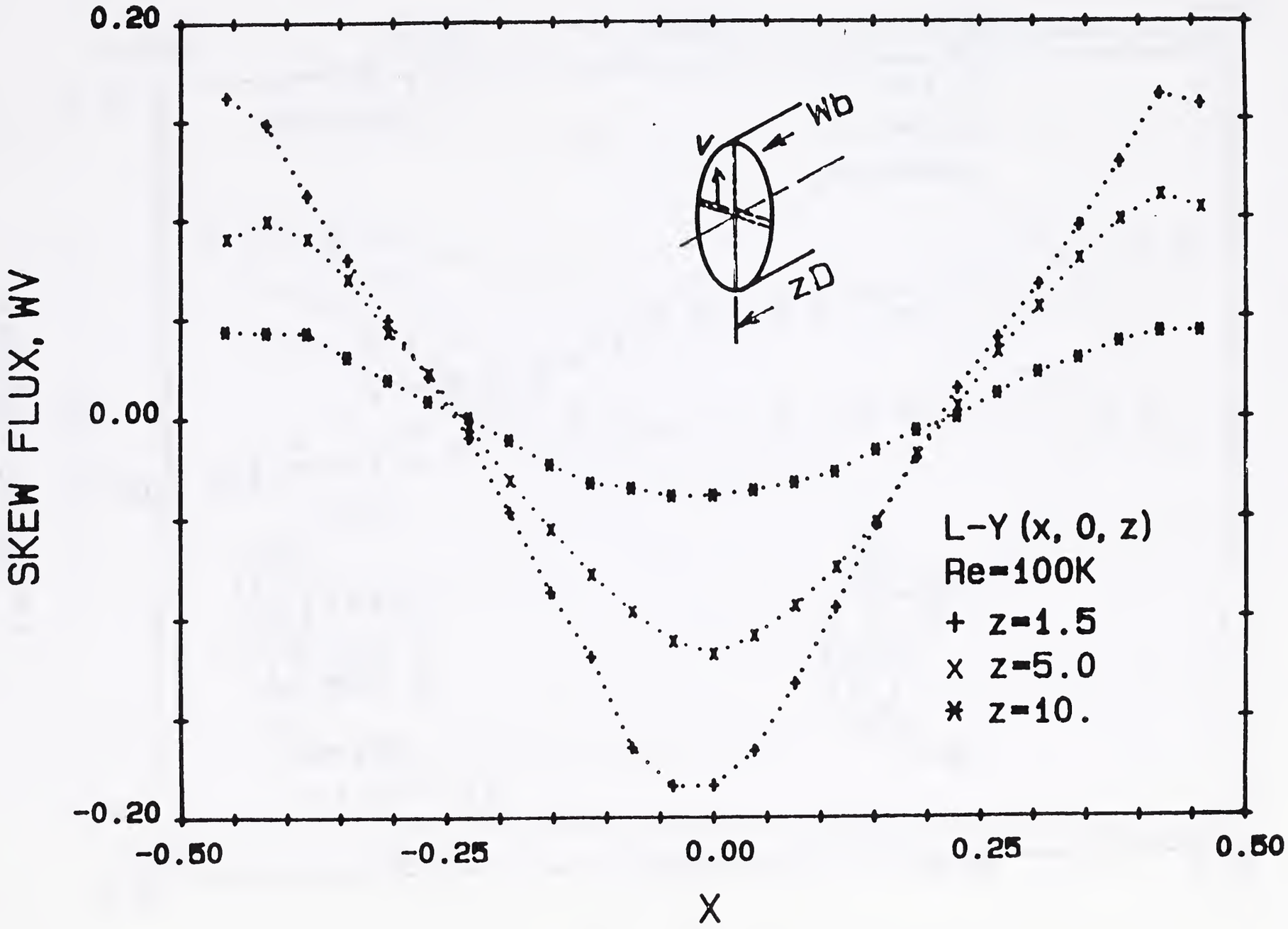


Fig. 36 (b) The horizontal profiles of skew flux for $Re = 10^6$

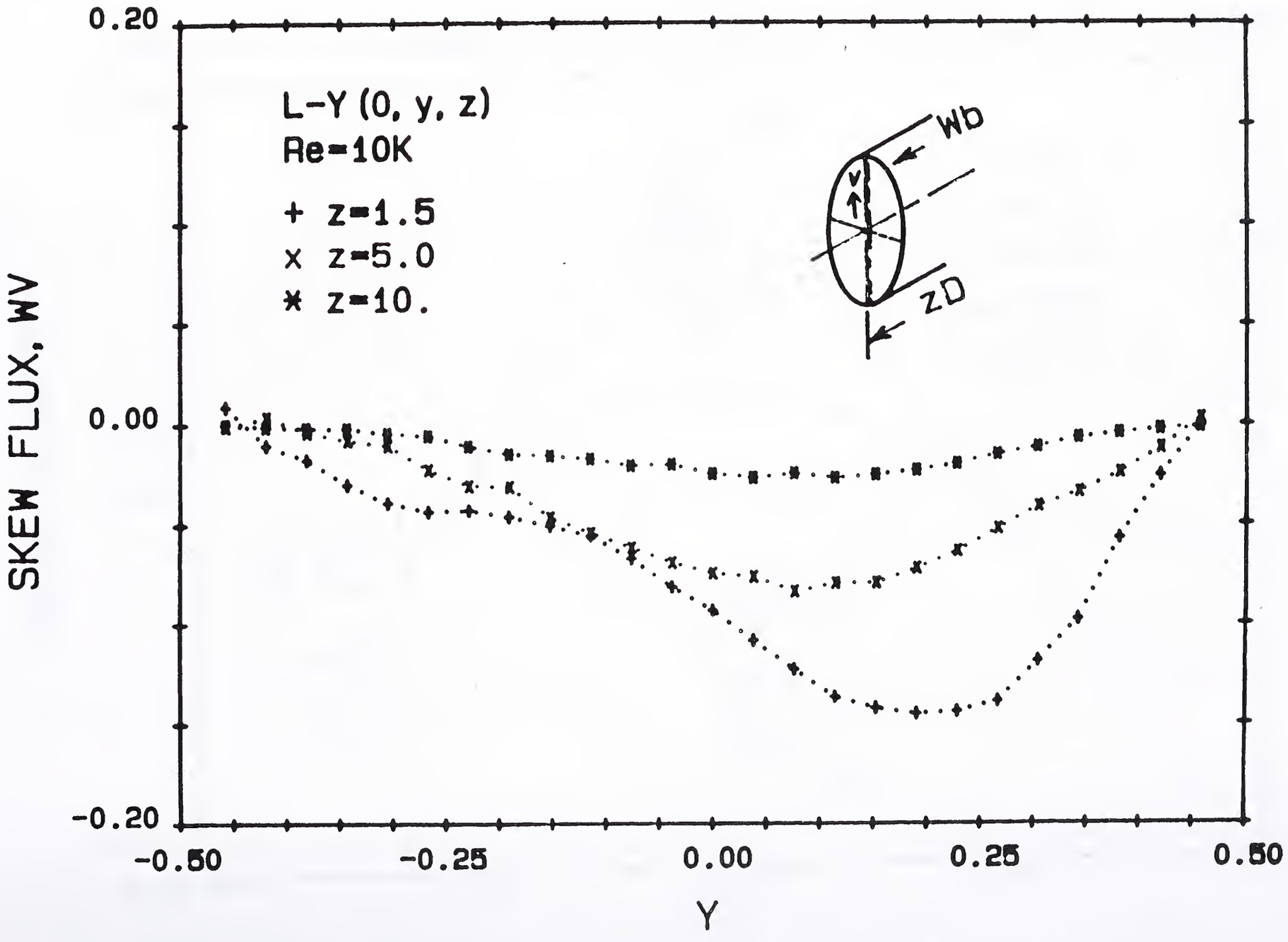


Fig. 37 (a) The vertical profiles of skew flux for $Re = 10^4$

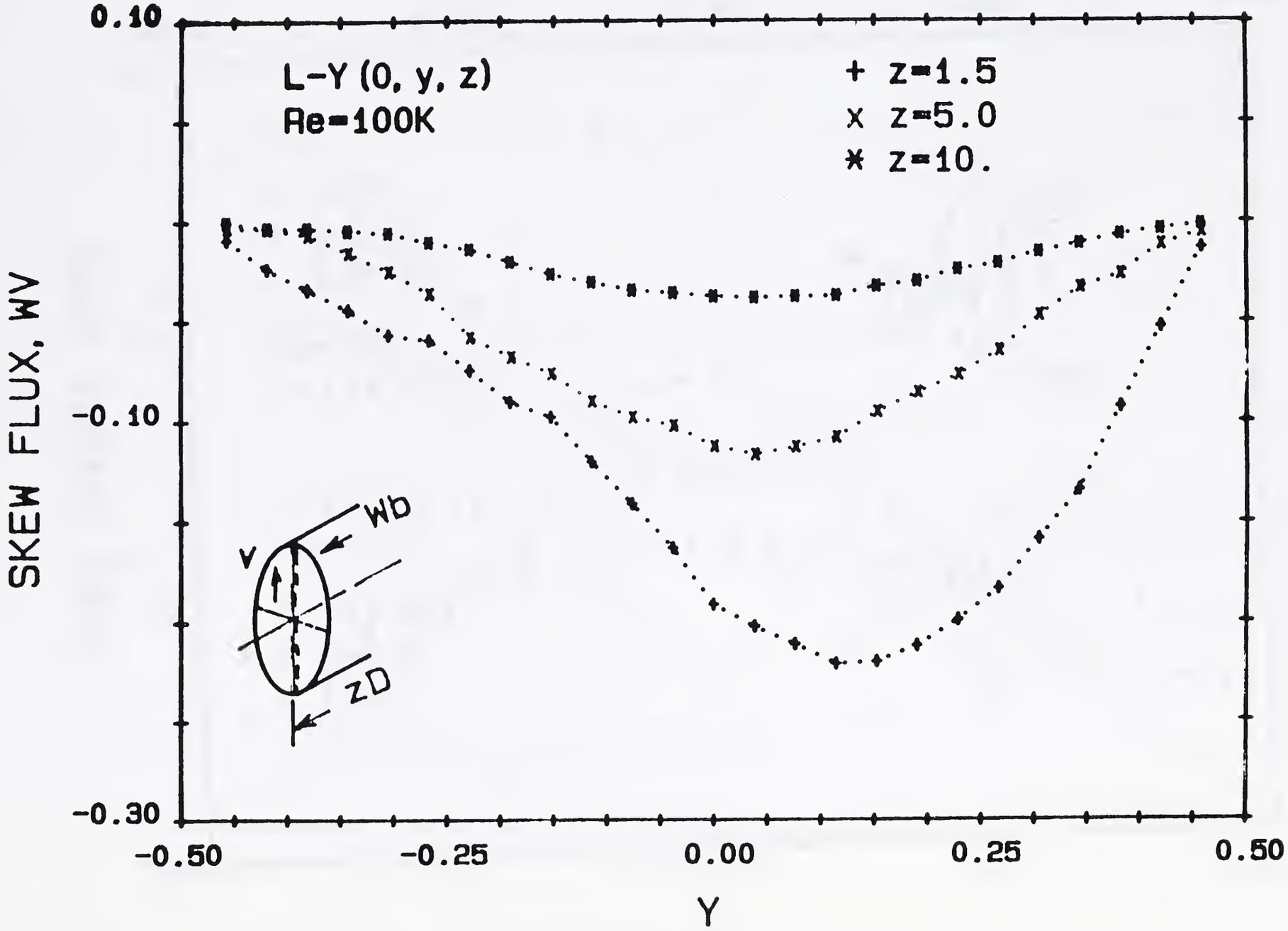


Fig. 37 (b) The vertical profiles of skew flux for $Re = 10^6$

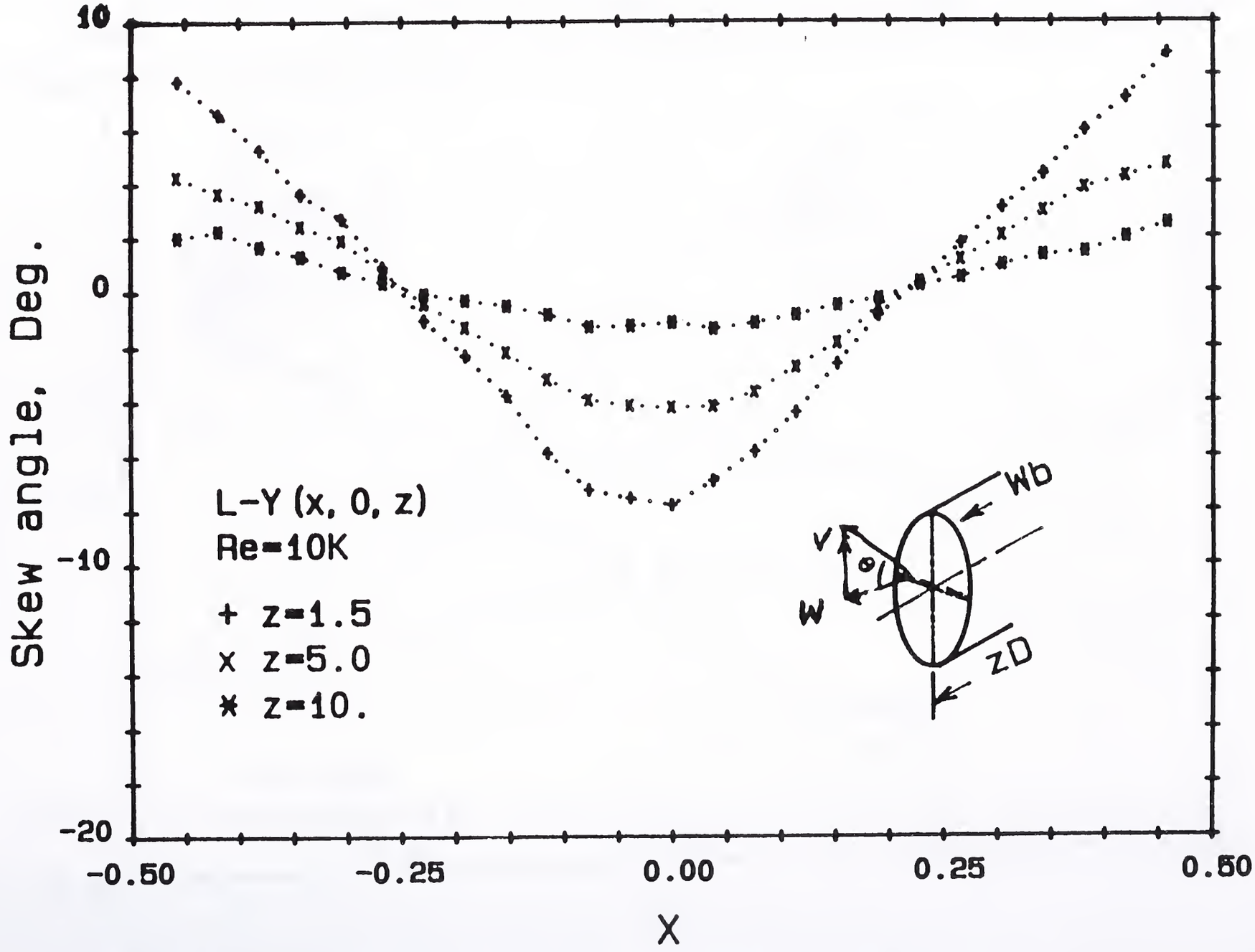


Fig. 38 (a) The horizontal profiles of skew angle for $Re = 10^4$

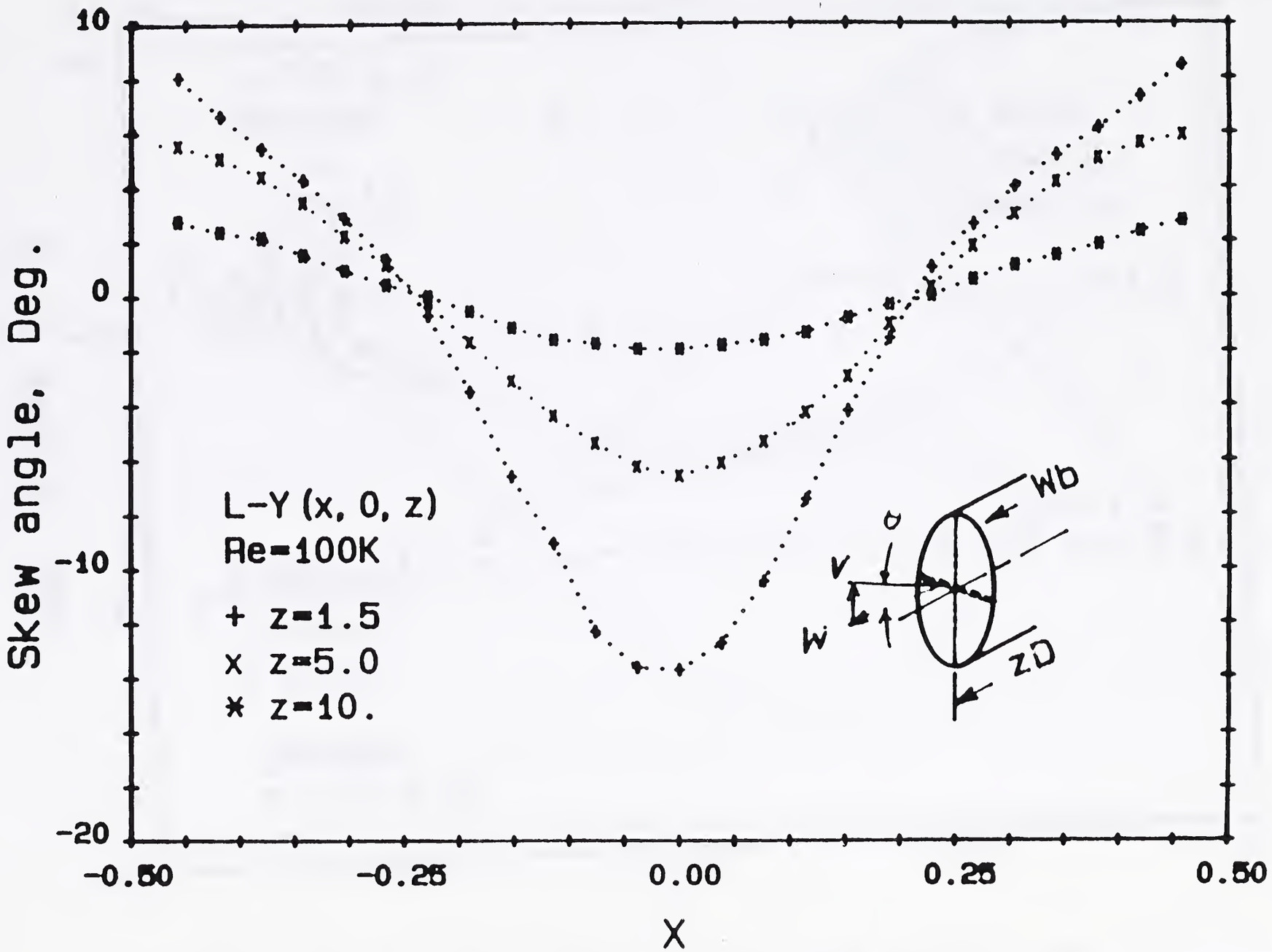


Fig. 38 (b) The horizontal profiles of skew angle for $Re = 10^6$

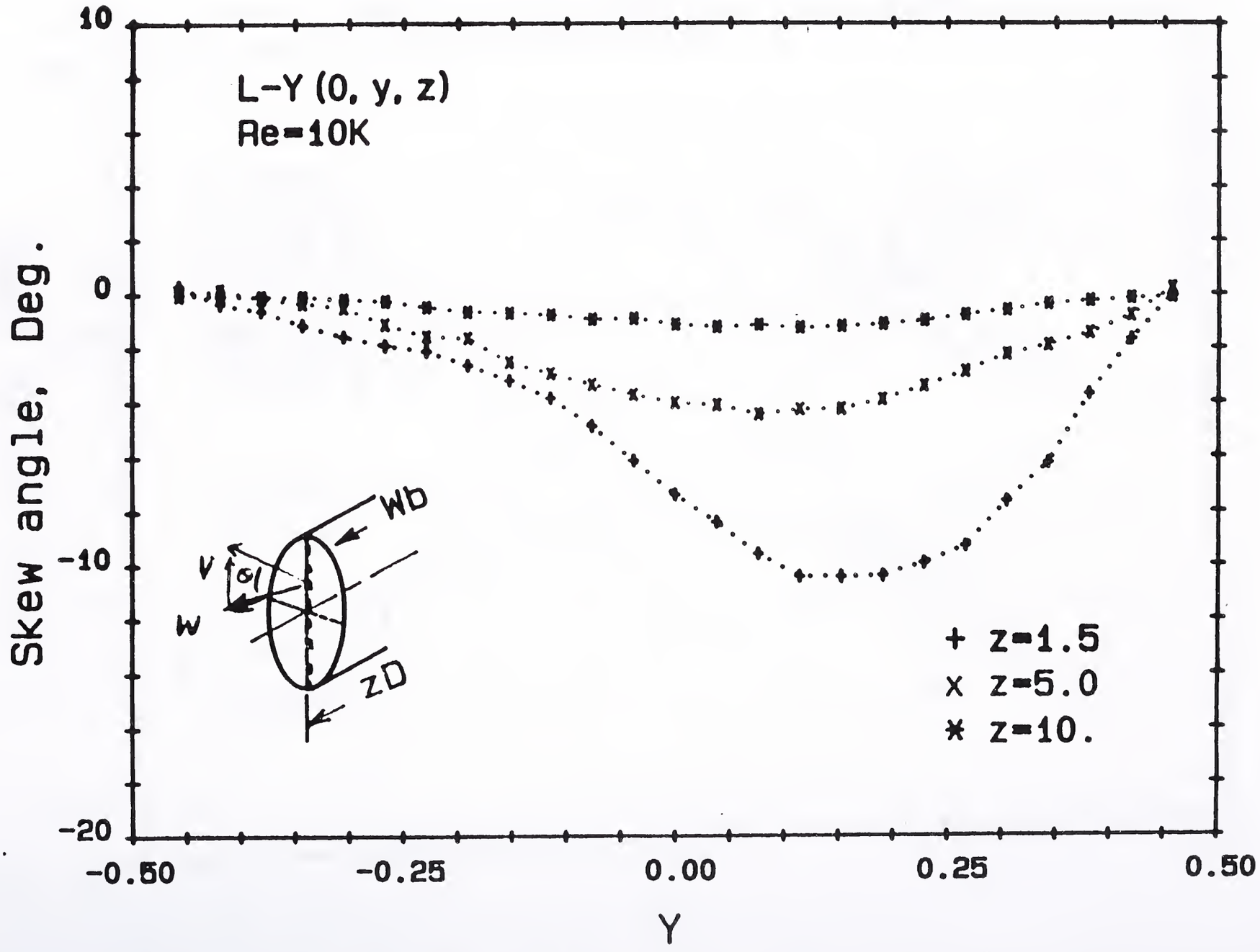


Fig. 39 (a) The vertical profiles of skew angle for $Re = 10^4$

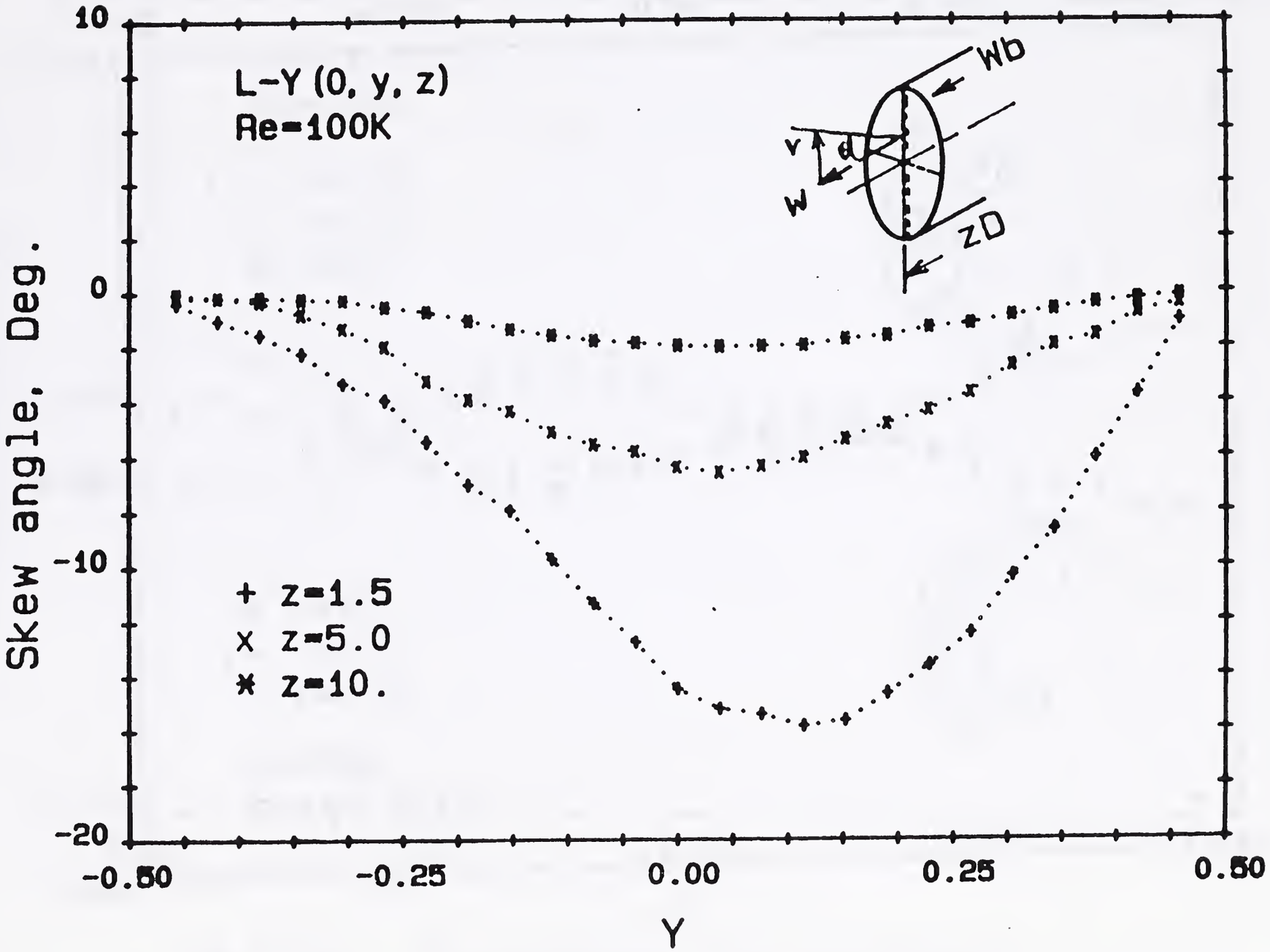


Fig. 39 (b) The vertical profiles of skew angle for Re = 10^6

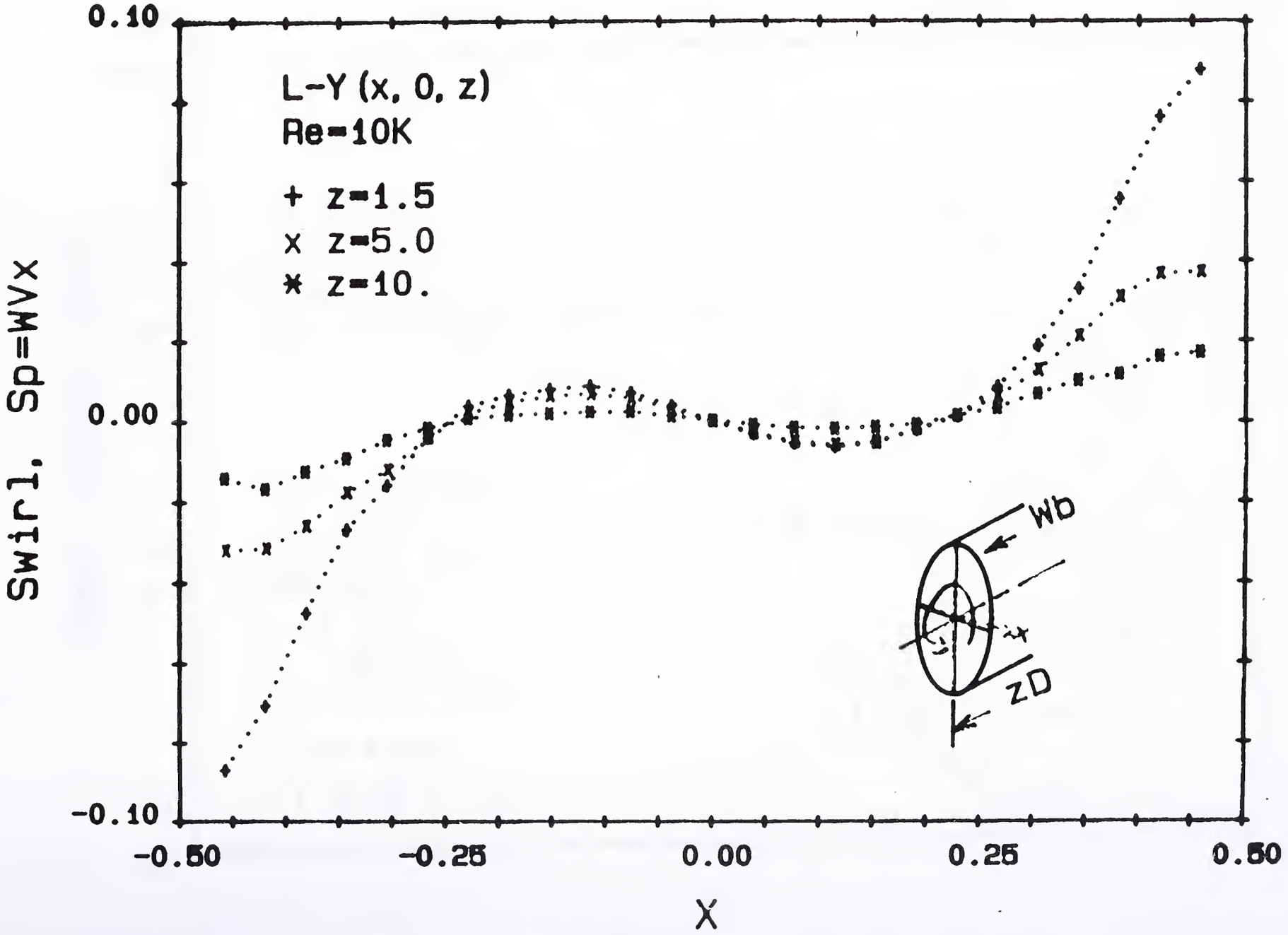


Fig. 40 (a) The distributions of the swirl intensity about the pipe centerline for Re = 10^4

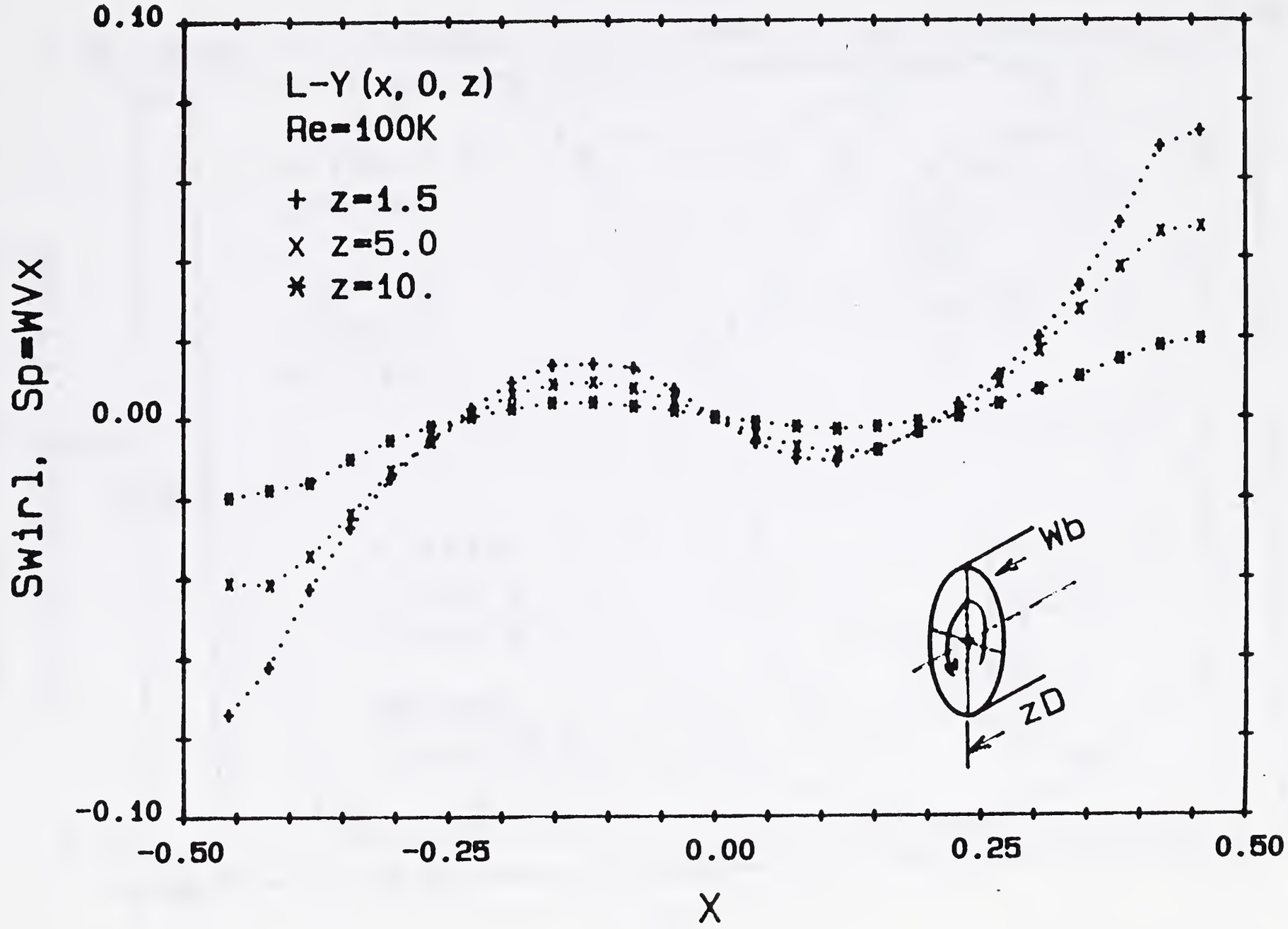


Fig. 40 (b) The distributions of the swirl intensity about the pipe centerline for $Re = 10^5$

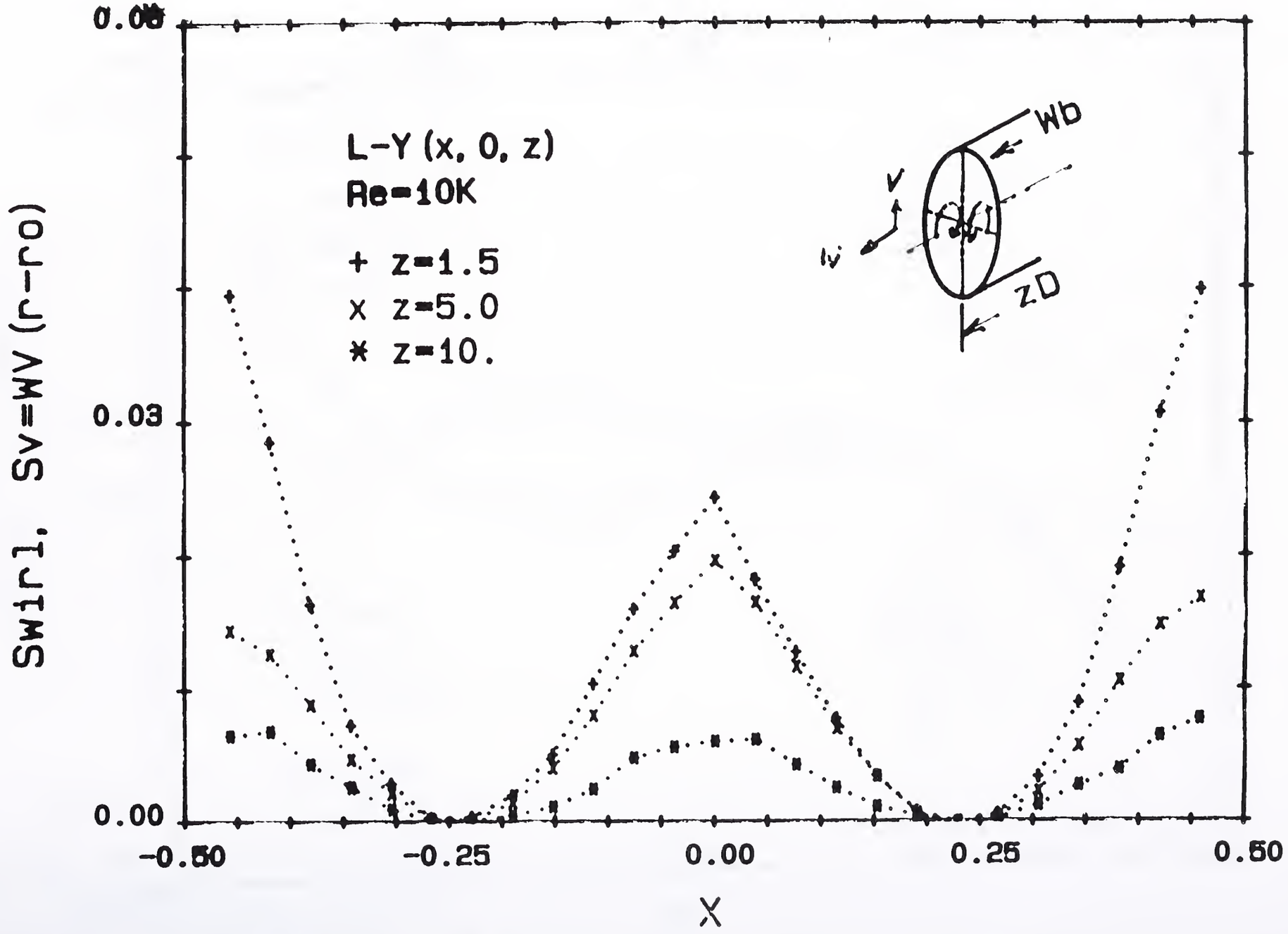


Fig. 41 (a) The distributions of the swirl intensity about the hypothesized vortex centers for $Re = 10^4$

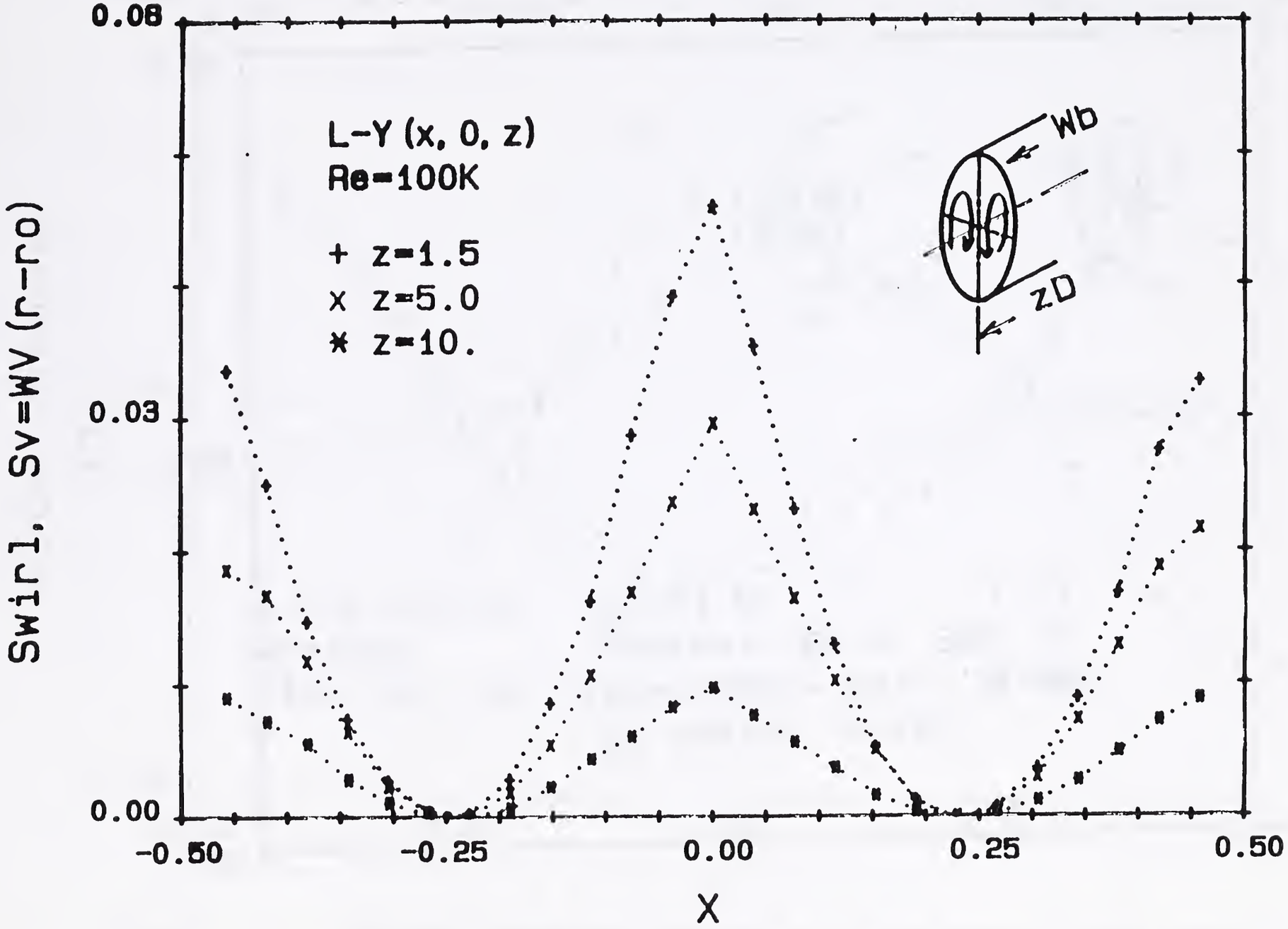


Fig. 41 (b) The distributions of the swirl intensity about the hypothesized vortex centers for $Re = 10^5$

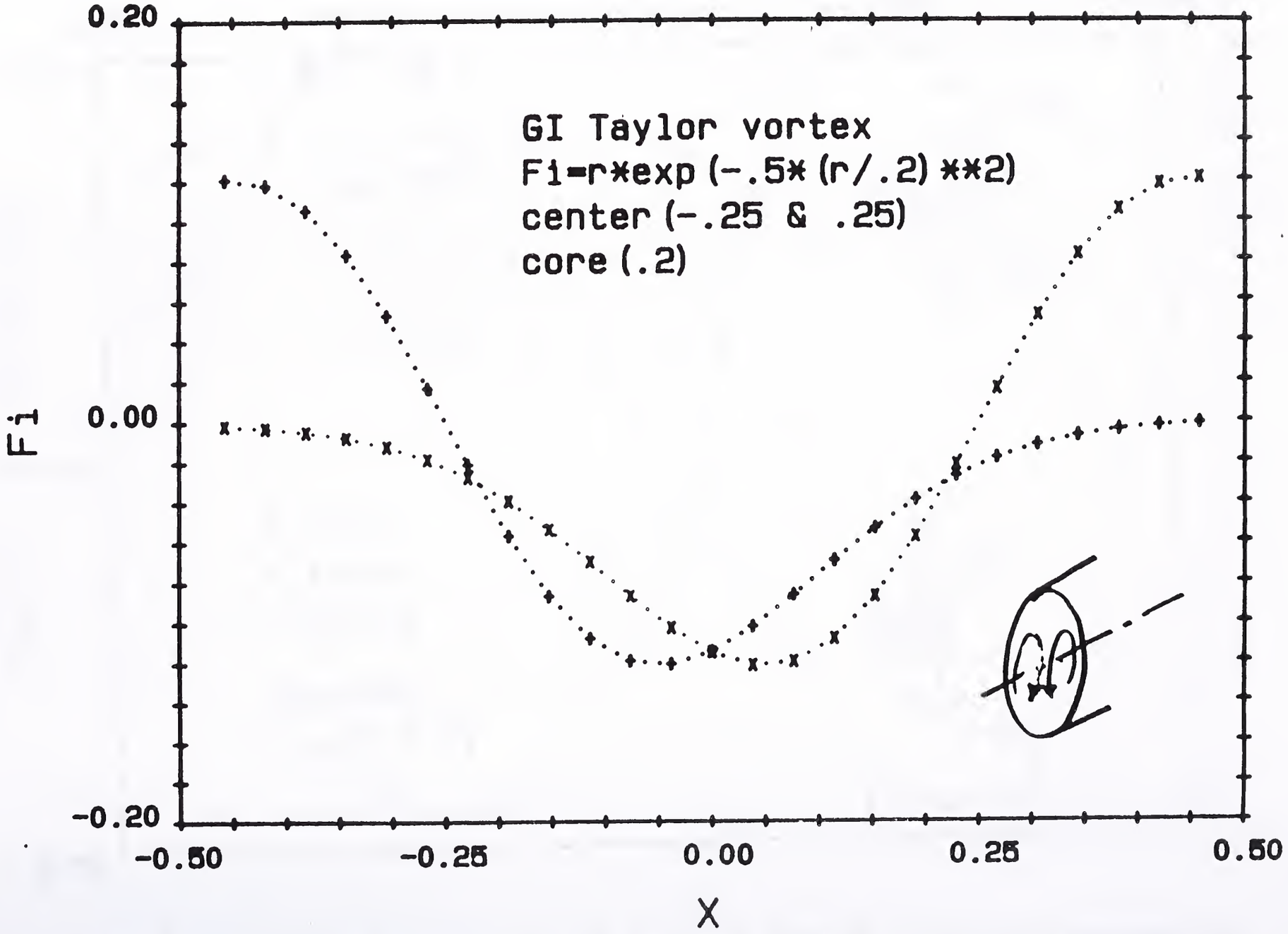


Fig. 42 Taylor vortex velocity distribution based on the hypothesized parameters

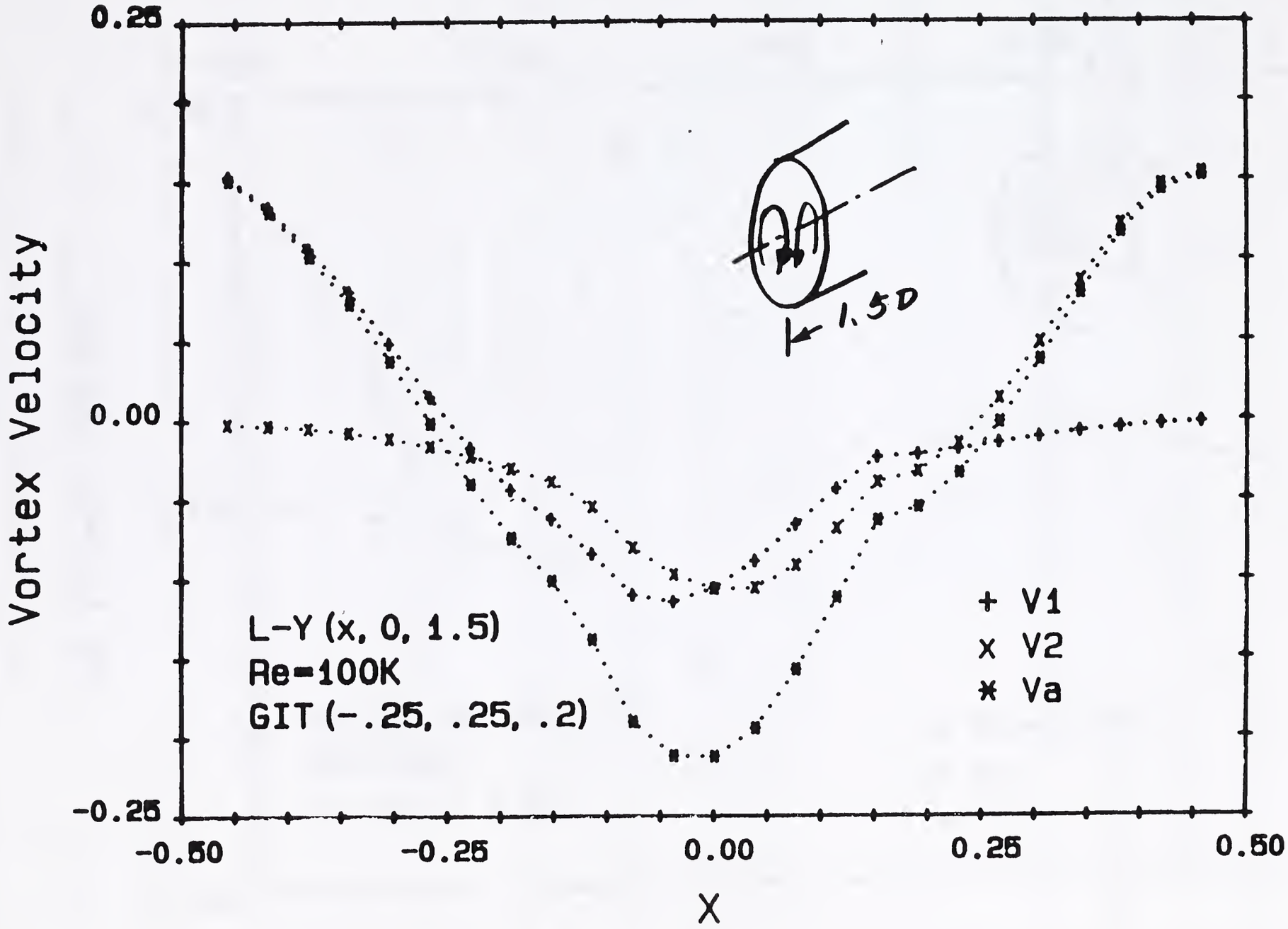


Fig. 43 Velocity distribution obtained by fitting data to Taylor vortex model for $Z = 1.5$ and $Re = 10^5$

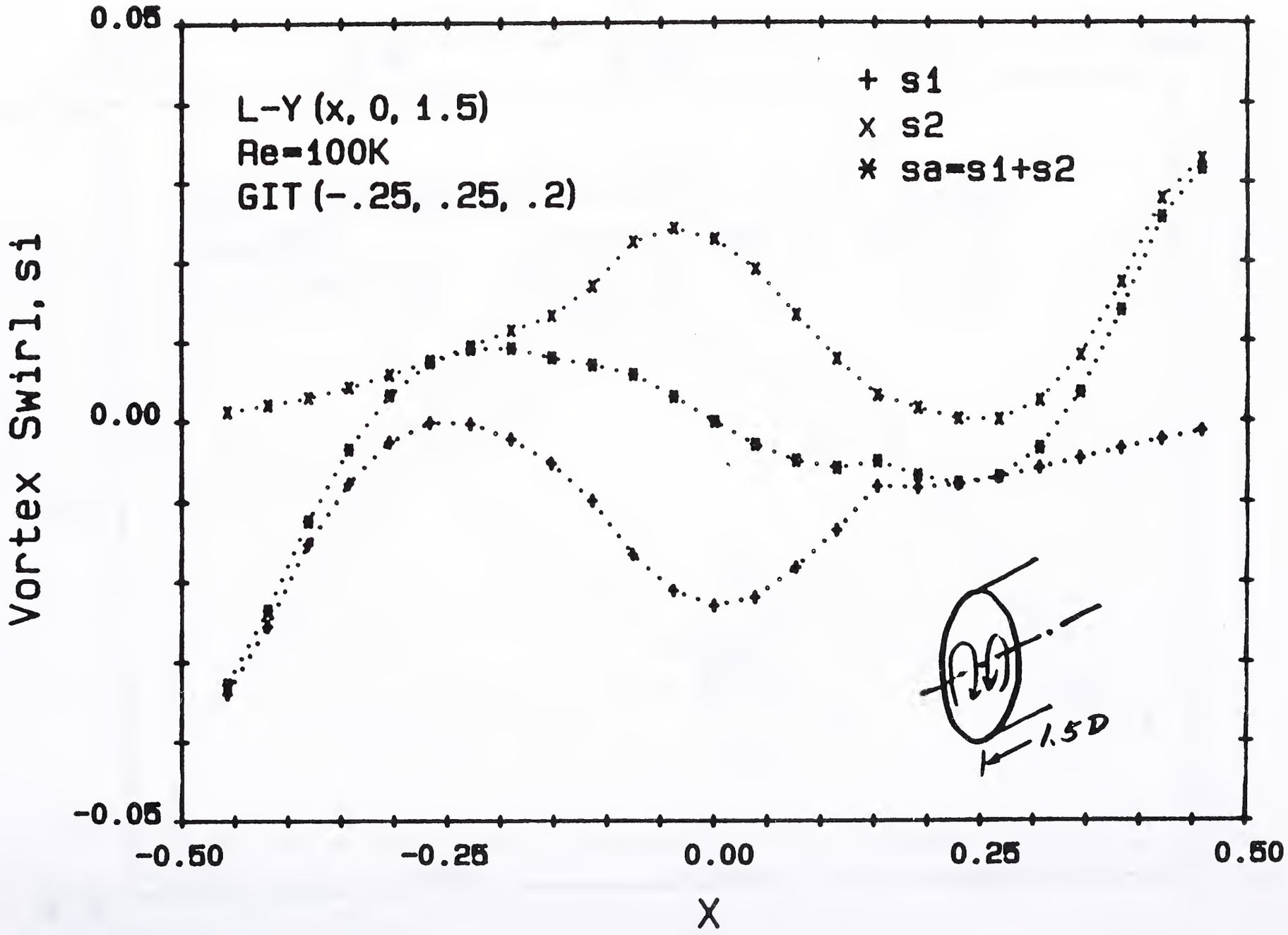


Fig. 44 Swirl intensity distribution based on the Taylor vortex model

NBS-114A (REV. 2-8C)

U.S. DEPT. OF COMM. **BIBLIOGRAPHIC DATA SHEET** (See instructions)	1. PUBLICATION OR REPORT NO. NISTIR 88-3898	2. Performing Organ. Report No.	3. Publication Date NOVEMBER 1988

4. TITLE AND SUBTITLE

NBS Industry - Government Consortium Research Program on Flowmeter Installation Effects Semi Annual Report: 1987 II

5. AUTHOR(S)

G.E. Mattingly and T.T. Yeh

6. PERFORMING ORGANIZATION (If joint or other than NBS, see instructions)

NATIONAL BUREAU OF STANDARDS
DEPARTMENT OF COMMERCE
WASHINGTON, D.C. 20234

7. Contract/Grant No.

8. Type of Report & Period Covered

9. SPONSORING ORGANIZATION NAME AND COMPLETE ADDRESS (Street, City, State, ZIP)

10. SUPPLEMENTARY NOTES

☐ Document describes a computer program; SF-185, FIPS Software Summary, is attached.

11. ABSTRACT (A 200-word or less factual summary of most significant information. If document includes a significant bibliography or literature survey, mention it here)

This report presents results produced in 1987 in a consortium-sponsored research program on Flowmeter Installation Effects. This project is a collaborative one that is supported by an industry-government consortium that meets twice yearly to review and discuss results and to plan subsequent phases of the work. This report contains the results and conclusions of the recent meeting of this consortium at NBS-G on Feb. 17, 1988.

The objective of this research program is to produce improved flowmeter performance when meters are installed in "non-ideal" conditions. This objective is being attained via a stategy to (A) measure, understand, and quantify the "non-ideal" pipeflows from such pipeline elements as elbows, reducers, valves, or combinations of these, (B) for selected types of flowmeters, correlate meter factor "shifts" relative to the features of these "non-ideal" installations, and (C) disseminate the resulting technology through appropriate channels such as publishing our results in pertinent journals and upgrading "paper" standards for flow measurement.

Specific results included in this report include:

1. the distributions of the mean and the turbulence velocities in the axial and vertical directions in both the (closely coupled) elbows-out-of-plane piping configuration and the "spaced" version of this arrangement,
2. the pressure loss measurements for both of the elbow-out-of-plane configuration and
3. the velocity distributions produced by the single elbow piping configuration.

12. KEY WORDS (Six to twelve entries; alphabetical order; capitalize only proper names; and separate key words by semicolons)

Flowmeter; Installation effects; pipeflow; Secondary flows; Swirl

13. AVAILABILITY

☒ Unlimited

☐ For Official Distribution. Do Not Release to NTIS

☐ Order From Superintendent of Documents, U.S. Government Printing Office, Washington, D.C. 20402.

☒ Order From National Technical Information Service (NTIS), Springfield, VA. 22161

14. NO. OF PRINTED PAGES

82

15. Price

$13.95